NIST-GCR-95-669

TURBULENT FLAME SPREAD ON VERTICAL CORNER WALLS

Cheng Qian
University of Kentucky
Department of Mechanical Engineering
Lexington, KY 40506-0108

March 1995
Issued April 1995

U.S. Department of Commerce
Ronald H. Brown, *Secretary*
Technology Administration
Mary L. Good, *Under Secretary for Technology*
National Institute of Standards and Technology
Arati Prabhakar, *Director*

Notice

This report was prepared for the Building and Fire Research Laboratory of the National Institute of Standards and Technology under grant number 60NANB3D1443. The statement and conclusions contained in this report are those of the authors and do not necessarily reflect the views of the National Institute of Standards and Technology or the Building and Fire Research Laboratory.

FINAL REPORT

submitted to

Building and Fire Research Laboratory
National Institute of Standards and Technology
Gaithersburg, MD 20899

Institution:	University of Kentucky
Grant No.:	60NANB3D1443
Grant Title:	Fire Spread along the Vertical Corner Wall, Part II: Effects of Ceiling on Spread Rate
Principal Investigator:	Kozo Saito Professor of Mechanical Engineering University of Kentucky Lexington, KY 40506–0108 Tel: (606) 257–1685
NIST Scientific Officers:	Dr. Walter Jones and Dr. Henry Mitler

(25 March 1995)

TURBULENT FLAME SPREAD ON VERTICAL CORNER WALLS

DISSERTATION

A dissertation submitted in partial fulfillment of the
requirement for the degree of Doctor of Philosophy
at The University of Kentucky

by
Cheng Qian
Beijing, China
Director: Dr. Kozo Saito, Professor of Mechanical Engineering
Lexington, Kentucky
1995

ABSTRACT OF DISSERTATION

TURBULENT FLAME SPREAD ON VERTICAL CORNER WALLS

Fire science is a rapidly growing research area. The motivation of fire research is to reduce fire loss and the cost of fire protection. Fire research is devoted to better understanding and prediction of fires. Flame spread is one of the most important phenomena in fire study because the spread rate is the measure of fire growth. In reality, flames are nearly all turbulent due to the large scale of building fires. Turbulent flame spread along vertical corner walls has the fastest spread rate among building fires. Because of the complex geometrical configuration and strong unsteady properties, the conventional instrumentations encounter great limitations. Therefore, there is relatively little data directly bearing on corner fire spreads. In this study, attention is given to the corner fire spread mechanism and the flame spread behavior. Infrared(IR) radiometry and image analysis techniques have been developed in this study to measure flame spread rate on large areas with high resolution and frequency. In addition to the flame spread measurement, the fire-induced flow was studied by flow visualization, and the total incident heat flux to the wall surface from the flame was measured by Gardon-type heat flux meters. Based on these experimental studies, a thermal model for corner fire spread has been successfully developed.

The burning wall temperature measurement through flames using an IR imaging technique has been studied both theoretically and experimentally. For most materials, the constant emissivity 1.0 can be used to determine the pyrolysis front temperature due to soot deposition on the surface. The flame effect consists of band emissions mostly from excited CO_2 and H_2O and a continuous emission from soot particles. The effects of the band emissions can be eliminated by a bandpass filter ($10.6 \pm 0.5\ \mu m$), and the soot particle effects can be neglected ($\varepsilon < 0.03$) for wall fires due to the small optical depth. Two-dimensional flame spread rate and the area of pyrolysis zone can be obtained by the IR imaging technique.

The pulsation of the flame can induce air puffing in a comparatively large area around the plume by pressure transmission. A non-symmetric fire configuration can produce a concentrate vortex in its plume. The vortex with a very strong axial flow may greatly enhance combustion. M-shaped pyrolysis front formation occurred for the flame spread along the vertical corner wall regardless of the effects of ignition mode, solid phase conduction heat loss, and fire induced cooling; it is primarily due to the flame displacement effect near the wall corner. The vertical flame spread rate increases as the ignition length increases, up to 20 cm, while the horizontal spread rate is almost constant. A similarity model has been developed to successfully simulate the progressing M-shaped pyrolysis front.

Flame heights for both flat wall and corner wall fires are primarily proportional to the elapsed time to the 1.3 power, even the flame on the corner wall is almost twice as high as the flame on the flat wall. The flame spread rate is essentially proportional to the pyrolysis height, but the upward spread rate for the corner fires is about three times higher than that for a same scale vertical flat wall fire. The high spread rate is mainly attributed to a strong fire-induced flow that enhances the heat convection and radiation to the walls. Transient heat flux distribution has been modeled as an exponential function of time and height. In spite of the neglecting lateral heat diffusion, one-dimensional conduction model provided 90% agreement with experiments in pyrolysis height prediction.

Author's Name

Date

Acknowledgments

This project would not have been possible without the funding from Building & Fire Research Laboratory, National Institute of Standards and Technology (NIST). I wish to acknowledge Dr. Henry Miter, Dr. Ken Steckler and Dr. Walter Jones for their guidance in this research program.

I would like to thank Dr. Kozo Saito for serving as my Ph.D. advisor. Dr. Saito emphasized the importance of observation in experiments and thought the observation is the source of imagination and successful modeling. He reinforce the faith of science from Einstein:"the most incomprehensible thing about the universe is that it is comprehensible.... imagination is more important than knowledge." I feel this is right today when I recall my research experience. Most of my significant experiments through my research were designed and carried out to prove my imagination. The faith of science he taught me will be beyond the research in this dissertation. Furthermore, Dr. Saito created the best academic environments I ever experienced in our research group. In this group, I felt the work challenging, interesting and was fully motivated.

I would like to express my appreciation to Dr. Louis C. Chow, Dr. C. J. Cremers, Dr. Peter A. Perry and Dr. Shiva N. Singh for serving on my Ph. D. committee. I also want to thank Dr. Dave Evans and Mr. Doug Walton for inviting me to join the NIST pool fire tests in Mobile, Alabama, Dr. Mary Delichatsios in Factory Mutual Research Cooperation for inviting me to join the flame spread tests in Ottawa, Canada.

Thanks must go to my research partners Dr. H. Ishida, and Dr. M. Daikoku and my office mates (John Baker, Heng Ban, Samir Dey, Douglas Denger, Tashtoush Ghassan, Seog Shin Lee, Vijay Ramasamy). Many of the staff at Mechanical Engineering Department and

Office of International Affairs have my gratitude, especially Linda Railsback, Dale Hall, Sylvan Ferrell and Austin Pyle.

Finally, a special thanks to my wife, Liyan, and the rest of my family for their encouragement through the graduate school years.

Table of Contents

Appendix

List of Figures

List of Tables

1.0 INTRODUCTION

1.1 Fire Science

Mankind's concern with unwanted fires likely predates the first practical use of combustion in unrecorded history. Yet the science of fire protection has progressed more slowly than other aspects of combustion science. This state of affairs is due partially to the complexity of the problem and partially to the fact that the effort made is not enough. Fire science embraces many topics including: behavior of fire, toxicity of smoke, interaction of fire with people and the environment, fire hazard and risk analysis, fire detection and suppression, fire safety design, and fire regulation and investigation. An overall description of the fire science and its classification was provided by T. Hirano (1992).

There is reason to believe that today's rapid technological advances intensify problems of unwanted fires. Hosts of new processes and new combustible materials are emerging and finding their way into widespread use. New living and working environments are being explored with fire safety concerns like subway system, air transportation system, and space station. Too often these innovations and developments become commonplace before their fire hazards are properly understood. Therefore, there is an immediate need for more extensive study of the fire science.

In the United States, most of the fires are residential fires, and most of the fire deaths occur in residential fires, but most of the property loss occurs in industry and commercial fires. The costs of fire safety and fire losses exceed $128 billion in the last year, reported in 1994 Project Summaries of Building & Fire Research Laboratory (BFRL), National Institute of Standards and Technology (NIST). What is a fire? As a general definition in fire science, a fire may be taken to be a combustion of fuel with the oxygen in the air, thereby involving heat transfer and fluid flow (Williams, F. A., 1982). What is the fuel ? Most materials can serve as fuels under certain conditions. Even steel will burn under suitable conditions. Carbon dioxide, water and sand are examples of materials that cannot burn.

Many different properties of fuels have bearing on their fire hazards. One is their ease of ignition. Even if its heat release rate is low, a material that can be easily ignited may pose a severe fire hazard. Another relevant property is the heat of combustion, materials with high heats of combustion are effective in sustaining fires. A detailed discussion of the physical and chemical aspects of a fire was provided by the leading authority of the field, F. A. Williams (1982).

As one of the most important phenomena, flame spread, or fire growth, is a dynamic or comprehensive property of fire hazard. Materials that are easily ignited and have high heats of combustion may spread flames rapidly and thereby be extremely dangerous. From a fire safety point of view, the most basic phenomena that we need to understand for the prediction and prevention of a fire will be the flame spread over combustible solid surfaces, such as walls, floors and ceilings. Therefore, testing and modeling the flame spread become an important part in fire research. Development of fire prediction models are also important to evaluate the fire hazard in buildings(Emmons et al., 1978).

1.2 Flame Spread Phenomena

Flame spread measures fire propagation or fire growth. It concerns the involvement of additional fuel in a fire. Flame spread rate represents the rate at which new fuel begins to burn. For example, in flame spread over the upper surface of a flat combustible material initially ignited along one edge, the local spread rate is the local horizontal velocity at which the boundary of the burning area moves over virgin fuel. Spread rates are important because they determine the time available for responding to a fire and thereby affect strategies for fire suppression. Flame spread tests on different materials are also performed as standard tests to assess material's flammability.

In practical case, the fire circumstances and fuel material properties are so different that there are many different kinds of flame spreads. Recently, a complete review on flame spread research was provided by T. Hirano and K. Saito (1994), which covered flame spread over solids, large scale spread through discrete fuels, and scale modeling techniques applied to flame spread study. This review summarized recent experimental findings from 162 papers and reports. As a conclusion, experimental observation and instrumentation were emphasized as the way to develop a better understanding of flame spread: the observation in experiments is the source of imagination and successful modeling. This philosophy is also the guideline for the research in this dissertation.

Fist of all, let us look at the process by which condensed-phase solid fuels burn. Heat is released in the exothermic combustion of gaseous fuels which are transformed from solids by pyrolysis. Some of the heat is transferred back to the condensed phase to cause the pyrolysis of the primary fuel. The pyrolysis is an endothermic process which releases the gaseous combustibles to burn. Thus, the heat transfer from the gaseous flame to the condensed fuel usually is an essential process to sustain a flame spread. In practical case, many parameters influence the spread process such as ambient air flow, external radiation, flame configuration, flame temperature, oxygen concentration, gravity, and heat loss effect, etc.

In building fires, fire can spread over floor carpets, along wall linings, even under ceilings. Among these flame spreads, the flame spread on a vertical wall and vertical corner walls is more hazardous, since fires tend to develop much faster on vertical surface than horizontal surface due to gravity. Much effort has been expended during the last twenty years (Orlaff, 1975; Ahmad and Faeth, 1979; Delichatsios, 1983; and Saito, et al., 1985) in predicting flame spread and burring intensities on vertical flat walls. These studies have found a one-dimensional spread rate model based on a two-dimensional fire plume is applicable with reasonable accuracy. But there is, surprisingly, little research on corner fire spread due to its complexity. This is primarily because the modeling of upward flame spread along the vertical corner walls requires additional consideration due to the two-dimensional (vertical and horizontal) nature of flame spread and the transient three-dimensional fire-induced flow. Furthermore, wall flame in building fires is usually turbulent due to the large scale of the building structure.

For a corner wall configuration, flames extend above the pyrolyzing section provide the heat for pyrolysis by radiation and convection. Above the flame tip, heat is transferred to the wall mainly by convection. The radiation property of the flame depends on the fuel property and combustion conditions. The flame height and flame geometry can be determined by natural convection flow and combustion process. Complex mechanisms of flame spread along corner walls make theoretical modeling difficult based on the available knowledge. And the two-dimensional corner fire spread is so rapid and accelerative that somewhat sophisticated methods are required for measuring the spread rate. Therefore, the experimental studies of corner fires were proposed using a 1/2 scale room corner model and IR imaging technique, which is the one of the most advanced temperature measurement techniques. This unique technology developed in our laboratory can measure the transient temperature distributions on a large burning area with a very high resolution and frequency without flame interference.

1.3 IR Imaging System

Energy is emitted by all objects having a temperature greater than absolute zero. The laws of radiation originated by Stefan-Boltsmann, Wien, Plank, and others establish definite and precise relationships between the object's temperature, composition and the radiation it emits. These law permits measurement of the temperature of an object by measuring the energy it emits, particularly the radiation in the infrared portion of the spectrum of emitted radiation. Generally, infrared radiation is defined as longer than 0.7 micron, extending to several hundred microns. In practice, 0.5 to 20 micron band is usually used for IR temperature measurement.

The infrared imaging system, which has been developed and applied to fire research is based on infrared thermography, video technique and image processing. Thermography is the process of generating a thermogram by using an infrared camera. A thermogram is a digital video image which maps the apparent temperature of the scene. A thermal imaging radiometer is a device which produces thermograms and measures quantitatively the thermal radiation within a definite waveband incident upon it. Based on the radiation measurements, the infrared imaging system can produce temperature information, and conduct subsequent calculation by imaging analysis.

To perform accurate temperature measurements, a thermal imaging radiometer incorporates a blackbody reference source that is viewed periodically by the detector for calibration. It uses lens and windows that transmit infrared wavelengths of electromagnetic energy which is going to be measured. Optical filters are used in this system to tailor the spectral response of thermal imaging radiometer to optimize measurement of specific materials including gases and flames.

The performance of a thermal imaging system is measured in a way that shows the total quantity of useful output information in a unit of time. This includes a combination of the thermal sensitivity, the scan speed, and the image resolution. Other features include system dynamic range, spectral band sensitivity, calibration and accuracy. These features will be explained in Chapter 3 with the development of experiment technique.

1.4 Objectives and Scope of This Study

The motivation of this study is to develop an advanced IR imaging technique for fire research application, understand the mechanism of fire spread along the vertical corner walls and develop a model to predict the spread rate. Specific objectives are:

1. To develop the infrared imaging technique, which can measure transient temperature at large area with high resolution, for the application in fire research. Investigate radiation properties of flames and fuels. Measure flame spread rate by spectrally resolved infrared emission measurement and infrared imaging analysis.

2. To study fire-induced flow along the vertically oriented corner walls, because fire plumes confined by corner walls have very complex flow patterns and vortex properties which determine the flame height and flame shape.

3. To measure and model heat transfer rate and distribution from the flame and the plume to wall surface, and analyze heat transfer mode inside the wall. The effects of floor and ceiling on heat transfer distribution, further on pyrolysis geometry will be examined.

4. To characterize flame spread on PMMA corner walls. Determine flame shape, pyrolysis geometry, and controlling parameters for this fire scenario; Measure flame height, spread rate and analyze flame spread mechanisms.

5. Based on the above study results, using heat transfer theory, develop a theoretical model to predict the fire-growth rate along corner walls which are made of common construction materials.

2.0 LITERATURE REVIEW AND THEORETICAL CONSIDERATION

2.1 Introduction

Before proceeding to analyze and report the experimental results, it is necessary to establish a theoretical basis for analysis and model development. Current progress of predicting upward turbulent flame spread is reviewed, in the hope of locating some of the obstacles to the theoretical understanding. Flame spread phenomenon includes three major components: preheating unburned fuel, pyrolyzing combustible material, and burning gaseous fuel. These three parts are connected by heat transfer, flow dynamics and other transport phenomena. This flame spread mechanism is depicted in Figure 2-1.

Flame spread problems started with experimental study of the mechanisms of small laminar flame spreading over solid combustibles. Experimental techniques in the study of flame spread were explained by Fernandez-Pello and Williams (1976). These include video and still photographs for flame morphology, thermocouple measurement of solid phase and gas phase temperatures, interferometric temperature measurements, radiometer measurements, gas sampling and analysis by gas chromotography, particle tract photography and LDV. Lastrina et al. (1971), Park (1972) and Hirano et al. (1974) conducted experiments to measure velocity and temperature profiles in laminar flame spread.

The spread of a laminar diffusion flame was formulated by deRis (1969). He described the burning process as: "The hot flame heats the unburned fuel bed, which subsequently vaporizes. The resulting fuel vapor reacts with the oxygen supplied by the incoming air, thereby producing the heat that maintains the flame spread process." Upward laminar flame spread with external radiation effects was studied by Fernanadez-Pello (1977), Annamala and Sibulkin (1979). Although laminar flame spreads are well understood, turbulent flame spreads still lack both an accepted conceptual framework and a body of reliable fundamental measurements.

In fire research, nearly all flames are turbulent due to the large scale of building fires. Because of the theoretical difficulties of turbulent flame modeling, an empirical heat transfer parameter Ø was introduced in turbulent flame-spread formulation (Sibulkin and Kim, 1977; Quintiere and Harkleroad, 1984). To develop a better understanding of turbulent wall flames, the fire plume from a steady wall fire and the heat transfer from the plume to the wall has been thoroughly studied by T. Ahmad and G. M. Faeth (1978). In this study, the wall fire was simulated by steady burning of wicks soaked with methanol, ethanol or 1-propanol. Measurements were made for burning rates in the pyrolysis zone, heat flux to the wall in the wall plume above the pyrolysis zone, and profiles of mean velocity, temperature and concentrations in all regions of the flow. These measurements were compared with solutions of the boundary layer equations. Significant contributions were made to the understanding of wall-fire structures by this study. Similar steady wall heat flux from a CH_4 line burner was also measured by Hasemi (1984). In Quintiere and Harkleroad's study (1986), the steady wall heat fluxes were measured using six different solid materials. They found the wall heat flux distributions are roughly correlated in term of distance divided by flame height. These models are applicable to some fire spread circumstances, but for corner fire spread additional considerations are required due to transient and three-dimensional nature. Therefore, the transient heat flux measurement and modeling are proposed in this study.

The energy balance on burning surface with gasification was formulated by L. Orloff, J. deRis and G. H. Markstein (1974). The heat loss to the interior solid fuel for a free burning vertical wall and its effects on the estimation of the heat of gasification have been studied by Kulkarni and Kim (1990) using PMMA. Theoretically, the transient conduction problem for a semi-infinite solid exposed to a specified heat flux was solved by Carslaw and

Jaegerfor (1959). This solution with the thermal theory of flame spreading, that the rate of flame spreading is equal to the rate at which the fuel ahead of the flame can be heated to pyrolysis temperature, is the base for most of the analytic approaches. A relevant and complete formulation of turbulent flame spread was given by Saito, Quintiere and William (1985). In their study, normal regression was introduced for gasification, flame height was correlated with energy release rate, and heat flux distribution was assumed to be uniform up to the visible flame height. Based on these assumptions, a linear integral equation was derived for the spread rate.

All the above studies are about the flame spread on flat vertical wall, but some principles and results are also applicable to the corner wall fires. Therefore, some fundamental elements of flame spread will be discussed in order understand the corner fire spread.

2.2 Flame Structure on Vertical Walls

The wall plume is the chemically reacting flow induced by a fire and is confined plume by the wall surfaces with mass addition in the boundary layer at the wall. The study of wall plume is of fundamental importance in understanding confined plumes, since it combines plume behavior and wall boundary layer effects. The wall plume also has practical significance for the problems of flame spread on vertical surface and preheating of unburned fuel elements in a fire environment. On this topic, Ahmad and Faeth (1978, 1979) have made a significant contribution in considering a turbulent wall fire consisting of a chemically reacting flow above a fire located at the base of a vertical wall. Based on their results, the fire plume over the vertical wall can be distinguished as four major regions, shown in Fig 3-2. The characteristics of each region are as follows:

Region 1. Pyrolysis Zone: In this region, the surface material is decomposing to provide combustible gases. The fire extends over the pyrolyzing surface, oxidizing a portion of fuel gases. Heat feed back from the fire to the surface sustains the decomposition process by providing energy of gasification of the fuel, as well as energy to compensate for heat losses from the pyrolysis zone, so that temperature can be maintained high enough (>T_p) for significant pyrolysis to occur.

Region 2. Combustion Plume (flame): Oxidation of all the fuel produced in the pyrolysis zone is completed in the combustion plume; however, pyrolysis does not occur at the wall surface and no additional fuel is produced. Heat transfer from the flame to the surface completes preheating the wall material to the point at which pyrolysis will occur. In the height of the combustion plume, radiation could be the major portion of heat transfer due to the attachment of the flame to the wall surface.

Region 3. Strongly Buoyant Plume: Although no additional combustion occurs in this region, gas temperatures are high. Therefore, variable-property effects are important in this region. Heat transfer from the plume to the wall continues the preheating process.

Region 4. Weakly Buoyant Region: This is the upmost region of the flow, where entrainment of ambient gases has cooled the plume. Variable properties and radiation are not significant, except for treatment of buoyant forces.

In Fig. 3-2, there are three cases corresponding to different scales of the fire, or from an early stage to a late stage of flame spread. In case (a), the transition from laminar to turbulent flow takes place in the non-combustion region and the entire flame is laminar. In case (b), the transition occurs in the combusting portion of the plume, and the flame is partly turbulent. In case (c), transition takes place near the leading edge of the pyrolysis zone and the flame is largely turbulent. In this study, the case (c), turbulent flame spread, is mainly considered because of the large scale of room fires.

2.3 Energy Balance on Burning Surface and Interior Heat Transfer

An analysis of energy balance on the burning surface was provided by Orloff et al (1974). The burning rate is controlled by the net surface heat flux available for fuel vaporization. With the origin of the coordinate system fixed to the regressing surface, the principal energy flux components to the surface are: (1) radiation from the flame, sometime with external radiation; (2) convection from the flame and the plume; (3) sensible energy carried to the surface by the solid PMMA. The energy flux components from the surface are: (1) outward radiation, or reradiation; (2) conduction into the PMMA interior; (3) radiation into the PMMA interior; (4) sensible enthalpy carried by the PMMA vapors away from the surface; and finally (5) reflection of flame radiation (Figure 2-3). Therefore,

$$\begin{aligned}&\dot{q}''_{rad}(flame - surface) + \dot{q}''_{con}(flame - surface) + \dot{m}''\int_{T_\infty}^{T_p} C_s dT \\ &= \dot{q}''(reradiation) - k_s\frac{\partial T}{\partial y} + \dot{q}''_{rad}(surface - interior) \\ &+ \dot{m}''\left[L_p + \int_{T_\infty}^{T_p} C_s dT\right] + \dot{q}''(reflecton)\end{aligned} \tag{2-1}$$

where L_p is the energy required to vaporize unit mass of fuel at temperature T_p. For steady burning of an infinitely thick slab the sensible enthalpy carried to the surface by the solid exactly equals the conduction plus radiation into the solid interior. Thus, eliminating these terms for steady burning, the energy balance becomes

$$\begin{aligned}&\dot{q}''_{rad}(flame - surface) + \dot{q}''_{con}(flame - surface) \\ &= \dot{q}''(reradiation) + \dot{m}''\left[L_p + \int_{T_\infty}^{T_p} C_s dT\right]\end{aligned} \tag{2-2}$$

where the surface reflection is also ignored, consistent with the indicated unit emissivity.

2.4 Solid-Fuel Gasification

The degradation of solid materials is a complex process. It involves flame heat transfer, fuel pyrolysis, charring and transient thermal effects. Although specific models have been developed, they are limited to classes of materials. Test apparatus, such as the Cone Calorimeter, can provide one of the means for dynamically measuring the mass loss and energy release of solid materials, but the interpretation of the data is limited by the lack of a simple model. A solid fuel gasification model has been developed by Quintiere (1992). The heat and mass transfer processes were displayed in Figure 2-4. The conservation of energy in the pyrolysis plane in this figure is given by

$$-k\frac{\partial T}{\partial x}\bigg|_{x=0} = \dot{q}_w{}'' - \dot{m}'' \Delta \mathrm{H}_g \tag{2-3}$$

and then

$$\dot{m}'' = \frac{\dot{q}'' + k\frac{\partial T}{\partial x}\Big|_{x=o}}{\Delta \mathrm{H}_g} , \tag{2-4}$$

where the ΔH_g is the heat of gasification of the solid fuel. Figure 2-5 depicts the behavior of the burning rate over time as gasification occurs after time zero. For non-charring materials, the surface temperature approximately remains constant T_p. At the beginning, the heat energy storage affects the gasification rate, providing the solid is thick so there is no significant back side influence. As time increases, for thermally thick material ($x \to \infty$), the conduction term in equation (2-4) will approach a constant value, causing a constant gasification rate. For charring fuel, the char layer will be produced after burning. This layer will reduce heat flux to the gasification plane, therefore, reduce the gasification rate.

2.5 Flame Height Correlations

During upward flame spread, heat transfer will occur by radiation and conduction from the flame. The heat-transfer rate on the surface adjacent to the luminous flame is munch greater than the post flame zone (Saito, K., Quintiere, J., and Williams, F. A., 1986). Thus the flame height is an important characteristics length in consideration of heat transfer. A definition for the flame height can be derived by assuming that the reaction zone ends when the fuel is completely consumed (Quintiere and Harkleroad, 1986). In this expression, the entrainment rate of oxygen primarily controls the flame height. This can be expressed as:

$$\int_0^{x_f} Y_{ox,\infty}(\rho v)_{y\rightarrow\infty}dx = \lambda r\dot{m}, \tag{2-5}$$

where x_f is the flame height, r is the stoichiometric oxygen to fuel ratio, $\dot{m}$ is the fuel supply rate and λ is the mixing factor which depends on the fluid dynamics of the flame. The value, x_f can be solved with a two-dimensional fire-induced flow for an idealized line fuel source wall-fire (Quintiere, J., and Harkleroad, M., 1986). It follows that

$$x_f = \left(\frac{1.5\varepsilon\dot{E}'}{\rho_\infty Y_{ox,\infty}\Delta H_{ox}aC_e u_o}\right)^{\frac{2}{3}} \quad . \tag{2-6}$$

Delichatsios (1984) finds, for turbulent wall flames,

$$x_f = 4.2\left(\frac{\dot{E}'}{\rho_o C_p T_o\sqrt{g}}\right)^{\frac{2}{3}}, \tag{2-7}$$

where $\dot{E}'$ is the energy release rate per unit width. Equations (2-6) and (2-7) are functionally similar. The major conclusion from the flame height analysis is that the flame height is proportional to the energy release rate to the exponent of 2/3. If the gasification rate is constant due to the constant heat flux in the pyrolysis zone, the heat release rate will proportional to the pyrolysis height, i. e.,

$$x_f \propto \dot{E}'^{\frac{2}{3}} \propto x_p^{\frac{2}{3}} \quad . \tag{2-8}$$

This result will be used to test the model developed later in this study.

2.6 Thermal Model for Flame Spread

Typically, a fire ignited on the bottom of a vertical corner wall spreads upwardly and laterally. The flame spread rate is defined as the velocity of the pyrolysis front on the pyrolyzing material. Upward spread along continuous fuels is unsteady and extremely rapid due to gravity. During upward spread, flames bathe the unignited surface, grow in size and soon become turbulent. Theory (Saito, Quintiere and Williams, 1985) shows that for infinitely thick materials upward spread is perpetually accelerative, while the horizontal spread is relatively slow and approaches a steady state.

In this thermal model, the process of flame spread is assumed as the pyrolysis front reaches a point P exactly when the surface temperature of the material at that point just reaches the ignition temperature T_{ig}, the same as the pyrolysis temperature T_p. Other assumptions include: the ignition temperature, T_{ig}, is well defined; the lateral heat diffusion can be neglected inside the wall; the thermophysical properties, ρ, c, and k of the material are independent of the temperature; and the material is inert. Under these conditions, a thermally thick wall can be treated as a semi-infinite slab, initially at the temperature of T_o subjected to the net heat flux of $\dot{q}''(x,y,t)$. Then it can be shown (Carslaw, 1959) the surface temperature is given by

$$T_s(x,y,t) = T_o + \frac{1}{\sqrt{\pi k \rho c}} \int_0^t \frac{\dot{q}''(x,y,\tau)d\tau}{\sqrt{t-\tau}} \quad . \tag{2-9}$$

Let $T_s = T_{ig}$, and rearrange this equation, the pyrolysis front can be represented as

$$\int_0^t \frac{\dot{q}''(x,y,\tau)d\tau}{\sqrt{t-\tau}} - \sqrt{\pi k\rho c}(T_{ig} - T_O) = 0 \; . \tag{2-10}$$

This is the pyrolysis front equation. To solve this equation, the wall heat flux has to be measured and modeled. For one-dimensional flame spread over the vertical flat wall, a constant heat flux model may be applied (K. Saito, J. Quintere and F. Williams, 1985), i.e., $\dot{q}'' =$ constant ≈ 2.5 W/cm² for $0 < x < x_f$ and $\dot{q}'' = 0$ otherwise. If this approximation is employed to equation (2-10), the upward spread velocity of the pyrolysis front is

$$V_p = \frac{4\dot{q}''^2 (x_f - x_p)}{\pi k\rho c\left(T_p - T_a\right)^2} = \frac{x_f - x_p}{\tau} \; , \tag{2-11}$$

where $\tau = \dfrac{\pi k\rho c\left(T_p - T_a\right)^2}{4\dot{q}''^2}$, the characteristic ignition time for spread depends fuel properties, the ambient temperature and the level of heat flux to the wall from the flame.

This model is applicable to most upward flame spreads with fine accuracy (D. Baroudi and M. Kokkala, 1992). But in the case of flame spread along corner walls, the modification of this model is needed due to a much stronger transient process with variable heat flux and rapid growth of flame height. In this study, the corner wall heat flux is proposed as a power function of height and time. This heat flux model will be introduced into equation (2-10), its applicability will be tested herein from the experimental data. Lateral heat diffusion and backside effects will be analyzed to validate the thermally thick assumption and the one-dimensional heat transfer model for flame spread.

3.0 INFRARED IMAGING SYSTEM AND APPLICATION TO FIRE RESEARCH

3.1 Introduction

This part of the study demonstrates that the infrared imaging technique, which is based on infrared radiometry and image processing, is one of the most useful means for measuring transient temperature distribution on a large burning surface. This technique is particularly useful for the measurement of flame spread rate on solid surface, where the conventional thermocouple and visual observation fail due to the complexity of implementation and the inherent ambiguity of visual observations by interferences from flames, respectively.

During flame spread, the transient infrared thermal image of the burning surface can be abtained through flames by the IR system with a narrow band pass filter, which eliminates the interference of the flame radiation. An image processing software has been developed to conduct gray level analysis of the recorded thermal images. The temperature distribution at any moment can be obtained and the spread rate of an isotherm, that is corresponding to the pyrolysis boundary, can be deduced in any direction. In this chapter, the theory of infrared radiometry and the infrared system performance will be explained first, and then the principle of image processing will be introduced. At last, the theoretical analysis of the filtering technique will be given, and some experiments conducted to prove this technology will be described.

To investigate the effects of band emissions and soot particles, tests were conducted using methane-air diffusion (yellow) flames, and a 10 cm diameter hexane pool flame (sooty yellow). To investigate the effects of emissivity of materials on infrared imaging temperature, five different materials, black painted Marinite board (non-combustible), white cardboard (combustible), black cardboard (combustible), transparent PMMA (combustible) and black PMMA (combustible) were employed.

3.2 Theory for Infrared Imaging Radiometry and System Performance

A Model 600 IR Imaging Radiometer from Inframatrics was used for this study (Fig. 3-1). This system is designed for accurate real-time analysis of static or dynamic thermal patterns. This high performance system combines superior image quality and thermal sensitivity with true temperature measurement display, digital remote control, automatic emittance and background correction. An electronics block diagram is shown in Figure 3-2. Other notable features include an 8:1 continuous electro-optical (E-O) zoom and built-in spectral band-pass filters. The system's detailed specifications are listed in Appendix 4-1. In this study the IR system was used with a VCR to record the thermal events in either color or black and white images for later analysis on playback. An image processing system has been developed based on an IBM PC with an image board (HRT-512-8) for higher resolution thermal image processing. The image processing flow-chart is shown in Fig. 3-3.

The IR imaging radiometer responses to the sum of the emitted, reflected and transmitted energies coming from the object of interest. The combination of the energies is called target radiosity. To obtain the target temperature, the emitted energy must be extracted by subtracting the reflected and transmitted energies from the incoming radiosity. The result must be scaled up by the emittance to obtain the blackbody equivalent value. This value can then be converted to temperature by querying the calibration lookup table with the software of the system. The resultant temperature is displayed on the monitor. In all internal calibration of the system, the graybody approximation is assumed. For a graybody the emittance, reflectance and transmittance are constant for all wavelengths within the waveband over which the instrument measures (Inframtrics, Manual of 600, 1988). Also, the temperature extraction algorithm is written for opaque targets since they comprise the majority of cases. So using this system for temperature measurement of opaque objects requires the knowledge of background temperature and target emittance. Both parameters can be measured using this system. The performance of a thermal imaging system is measured in a way that shows the total quantity of useful output information in a unit of time. This includes a combination of the thermal sensitivity, the scan speed, and the image resolution. Other major considerations include system dynamic range, spectral band selection, calibration and accuracy. The IR imaging system's performance will be introduced briefly.

3.2.1 Thermal Sensitivity

Thermal energy is given off by objects in individual bursts known as photons, much the same as the visible light. The timing between these busts is random. When very small samples of an object's radiation are made, the random emission of the photons is visible as a variation in intensity, or thermal noise. Noise in the thermal image looks the same as the "snow" that is seen when a television camera operates in extremely low light. Both are caused by random noise of photons from either the scene or the light sensitive element in the camera. A thermal imaging system is characterized by a noise equivalent temperature difference, the temperature difference between two objects that results in a signal equal to the random background noise of the camera. Averaging of multiple image data points reduces this noise level by the square root of the number of samples averaged. Well-designed instruments will average measurement points to reduce this noise. Noise is only significant when operating on the most sensitive ranges, viewing low thermal contrast targets. The noise equivalent temperature difference is less than 0.20 °C under ambient temperature of 30 °C (3-12 μm).

3.2.2 Scan Speed

The rate at which complete thermal images are updated by a particular mechanical scanner is the scan speed of the system. The rate at which television images are updated on the monitor is the frame rate and is defined by the television industry standards. Low scan speeds offer low acoustic noise and low cost as advantages, but result in the image that distorts severely when the scene moves. In addition, low frame rates (below about 50 Hz) on non-TV compatible systems cause an annoying flicker in the display. Extremely low frame rate (slow scan) systems offer high thermal and spatial sensitivity but are very difficult to focus and point. The scan speeds of the 600 system are 8 KHz horizontal and 60 Hz vertical. The output rates are 15,750 Hz horizontal and 60 Hz vertical.

3.2.3 Spatial Resolution-Slit Response Function and Instantaneous Field of View(IFOV)

Spatial resolution is a measure of the thermal imaging system's ability to detect and accurately measure the temperature of small objects, where "small" is defined relative to the size of the total image. Resolution is very important for a measurement system since the accuracy of the temperature measurement at each point of the image depends on the degree of resolution, even beyond that which appears sharp to the eye. Resolution is normally determined by the characteristics of the scanner with its optics scanning mechanism and detector. Typically an infrared system will detect the radiation at the scanner using a detector of finite size, thereby limiting the resolution. The electronics subsequently digitizes the image into picture elements (pixels), smaller than the detector samples. In this way, the digitization does not reduce the system performance. Note that a 256 by 256 pixel image does not usually contain nearly as many true spatial resolution elements, or detector samples.

The three-dimensional plot in Figure 3-4 shows the response of a typical electro-optical imaging system to a point source of illumination. As an example, this might show the relative response of a thermal imaging radiometer to a small, very hot object at a great distance. The vertical axis represents temperature and the X, Y axes represent horizontal and vertical dimensions on the video image detector. Notice that, due to the small object size, the response of the system to the object is less than 100%. As the object becomes large, the response gradually approaches 100% and the measurement becomes more accurate. There is no particular point where the object measurement is 100% accurate, but rather there is continuous curve of response versus object size.

It is convenient to characterize a thermal imaging system by the relative response to vertical slit target of various widths. The curve of this response is called a slit response function (SRF), and is useful in determining the amount of error or required correction factor for a target that can be approximated by one or more slit shape. Figure 3-5 shows typical SRF curve. The measured radiance of an object whose SRF is known as a function of the object radiosity and the average surroundings radiosity. An approximate equation in the temperature form is:

$$T_{\text{apparent}} = (\text{SRF})\, T_{\text{object}} + (1 - \text{SRF})\, T_{\text{surround}} \;.$$

The error between apparent and true temperature is greater when a large difference exists between the object and surrounding temperatures. The instantaneous field of view (IFOV) is defined as the ratio of the detector size to the effective system focal length. Thus, a 0.0254 mm x 0.0254 mm (0.001" x 0.001") image detector cell with 12.7 mm (0.5") focal length would have a 2 mr (milliradian) IFOV. The system 50% SRF and IFOV should be about the same, with the IFOV being somewhat larger.

Regardless of how one specifies resolution, it should be considered in context of the total image as well. a wide field of view (FOV) with good resolution is much more desirable than a narrow FOV with the same resolution. A measure of this is the total number of resolution elements per image. To find the total, divided the horizontal FOV by the resolution element size and multiply the result by the number of infrared lines per image. For example, a scanner which has a 2 mr 50% SRF, 20 degree horizontal FOV and 200 IR lines per image generates almost 35,000 resolution elements per image. Note that the scanning mechanism determines the number of IR lines per image.

3.2.4 Dynamic Range

Dynamic range specifies the ability of a thermal imaging system to resolve the fine temperature differences while simultaneously imaging large temperature spans. Dynamic range can be expressed as the number of gray shades, or digital levels of intensity, used to encode the thermal image, much like the number of gradations on a thermometer. The dynamic range of our system is 7 bit, 128 levels.

3.2.5 Spectral Band Selection

The earth's atmosphere absorbs radiated energy in the infrared except for two wavelength regions called the atmospheric windows (see Figure 3-6). Typically, it is the water vapor in the atmosphere that absorbs the majority of the infrared energy over much of the spectral band. Some gases absorb as well, but generally at only one or a few narrow spectral lines (Inframetrics, Model 600 Manual, 1988). The atmospheric windows allow radiometric measurements with minimal losses. The long wave region, 8-14 μm, is exceptionally free of absorption except with very high atmospheric water content. The short-wave region, 3-5 μm, has relatively high transmission, but usually requires compensation when high accuracy measurements are to be made at path lengths greater than one meter.

Modern thermal imaging radiometers are available with 8-14 μm (longwave), 3-5 μm (shortwave), or 3-14 μm (broadband) spectral response. Instruments are also available which detect and image short and long wavebands independently and simultaneously.

These are often called two color systems. The spectral relative response of the 600 system is shown in Figure 3-6.

3.2.6 Calibration and Accuracy

Thermal imaging systems measure radiation within a certain spectral band and must convert radiant intensity to temperature by the use of a measured calibration curve. Due to variations in system spectral response, every system has a unique calibration curve. The basic calibration curves for modern thermal imaging radiometers are measured at the factory and stored in a read-only memory, along with any special curves for installed optical filters.

The error in measurement of the system can be divided into a random error (precision) and a fixed error (bias). The purpose of instrument calibration is to remove the bias and define the precision. But the changes in detector sensitivity, which are usually resulted from the change of the detector temperature, optics transmission and electronic drift will cause the instrument to go out of calibration over a period of time. Typically, a liquid nitrogen cooled instrument's accuracy is plus or minus 2% to 5% of the temperature reading. In the context of versatility and all the other measurement uncertainties confronting the user, these accuracies are quite reasonable.

3.3 Image Processing

A software has been developed to calculate and display transient temperature distributions and deduce the movement rate of a specific contour from thermal images. A flow chart of the image processing system is shown in Figure 3-7. The video signal was digitized into 8 bit gray levels and stored for subsequent analysis. In image analysis, a smoothing operation was performed first to remove noise in the image. And then the distorted infrared image due to inclined projection was corrected to $\phi = \theta = 90^o$ using a coordinate transformation (see Figure 3-8). Finally, contour tracing was applied to obtain isothermal lines. The pyrolysis front is defined as a specific contour with the temperature of pyrolysis.

3.3.1 Image Data Compression

The image data compression technique was applied to reduce the number of bits required to store or transmit images without any appreciable loss of information. In general, data compression algorithms fall into two categories (Jain, 1981). The first category reduces data size by information related to redundancy, non-randomness, and predictability of images. The second category, called transform coding, performs transformations on the image and preserves certain properties.

The usefulness of a compression algorithm not only depends on its compression ratio but also on the resulting distribution and complexity of implementation. Therefore, a simple error-free coding algorithm with an average compression ratio of 2.5 was utilized. This algorithm reduces data size using 4 bits to store image variation. It is easy to implement and offers fast processing because bit manipulation is not required.

The image pixels are converted into 7 bits by setting the least significant bit to zero. This operation does not degrade the image quality due to its low resolution. The first pixel is stored in one byte as raw data, and the others can be stored in raw data or compression formats. If the difference between the current pixel number and that of its predecessor is within ±6, the difference is recorded as a nibble (4 bits) with the least significant bit set to one. Otherwise, one byte of raw data is recorded. If more than two consecutive pixels have the same intensity, they are presented by two nibbles in which one is the number of pixels and the other is used for identification. The least significant bit is used to distinguish the raw data from the compression format. If the ripple caused by digitization of the image is smoothed, the compression ratio can be further improved. The encoding and the disk storage time for a 200 x 170 image is 2 seconds. This simple compression scheme greatly enhances the system's capability to process a long sequence of images.

3.4 Wall Temperature Measurement through Flames

A room corner model with a steady gas burner was used to develop the IR technique. The infrared camera was located away from the fire source to acquire the Wall_1 temperature passing through the flame and the Wall_2 temperature without passing through the flame. This can be done by placing the infrared camera close to the Wall_2 plane to provide a large ϕ, shown in Figure 3-9. Using the infrared camera under this setting, two different images can be obtained simultaneously from the Wall_1 and the Wall_2. Then both images were transformed into two separate two-dimensional images.

Typically, the fire-heated wall temperature (<600K) is considerably lower than the average flame temperature (1100-1200K) determined from the measured (axial and radial) temperature profiles for sooty laminar hydrocarbon-air diffusion flames (Megaridis et al, 1982). At Wall_1 the IR camera detects the flame temperature instead of the wall temperature. The flame effect consists of band emissions from excited gas molecules and a continuous emission from soot particles. The band emissions are mostly from CO_2 and H_2O, and both have a "window" between 10 and 11 μm where they have negligible emissions at high temperature (Katto, Y., 1977). If a band pass filter whose band pass width is in the above wave length range were applied with the IR camera, the effects due to CO_2 and H_2O would be eliminated.

To evaluate the flame interference due to the soot particle radiation, the effects of flame temperature and optical depth on the emissivity of the flame were investigated. Exploratory tests on the wall fires (Saito, K. et al., 1985) proved that the visible yellow flame thickness is about 5 cm over the entire flame length. In addition, the soot particles exist only in the thin layer of the high temperature region (Saito, K., Williams, F. A., and Gordon, A. S., 1987), and they are not uniformly distributed across the flame thickness normal to the wall surface. Therefore, an effective optical depth will be smaller than the visible flame thickness. Assuming the optical depth L as the flame thickness (5.0 cm) or one half of the flame thickness (2.5 cm), the flame emissivity (ε) can be estimated using $\beta = 0.8\ \mathrm{m}^{-1}$ based on the assumption that the radiative property of a typical wall fire, such as from Beer's law, $\varepsilon = 1 - \exp(-\kappa\beta L)$. By this approach, an average flame emissivity, $\varepsilon = 0.04$ for $L = 5$ cm and $\varepsilon = 0.02$ for $L = 2.5$ cm, was obtained, where $\kappa\beta$ for PMMA is equal to those of hexane flames (Yumoto, T. J., 1971) since both flames have approximately the same sooting tendency (Daikoku, M. et al, 1992).

Next , calculations were made to estimate the relative importance of the radiation effect from particles to that from the fire heated walls, which will be pyrolyzing surfaces if the walls are combustible. Employing a pyrolysis temperature of 600 K for flammable materials , a plot was made of (radiation from the wall) / (radiation from the soot particles) as a function of the flame emissivity for the intermediate flame temperature 1100 and 1200 K, shown in Figure 3-9 and 3-10. This plot also contains the effect of four different band pass filters on the above radiation fraction. These results indicate that if the flame emissivity is less than 0.03 ($\varepsilon < 0.03$) for 1100 K and less than 0.02 ($\varepsilon<0.02$) for 1200 K, the radiation from soot particles will become approximately one order magnitude smaller than that from the wall. Furthermore, the optical depth dependence on wavelength leads to a low emissivity at long wavelength. Therefore, the above estimation indicates that the infrared imaging technique can measure the burning surface temperature through flames with a minor flame interference. When the flame emissivity: $0.05 < \varepsilon < 0.10$, this approach might work depending on the optical-depth dependence of the flame on wavelength. However, for the flames with $\varepsilon > 0.1$, this technique will fail.

To experimentally prove the above conclusions, the infrared camera was located to facilitate comparison of temperature profiles on Wall_1 measured through the flame to those on Wall_2 measured without passing through the flame. Four different narrow band pass filters (5.0, 6.0, 8.0 and 10.6 μm with band pass width ± 0.5 μm) were employed to eliminate the effects of the flame interferences. The comparison of temperature profiles measured by the IR camera through the flame and without the flame are shown in Figure 3-11. The temperature profiles from both sides of the wall should agree if the two walls are symmetrically heated by the flame and the filters could successfully remove the effects of the flame. These results reveal that temperature profiles using open lens and the 5.0, 6.0, 8.0 μm band pass filters were largely distorted by the flame interferences (Figure 3-11 a, c, d, e). But that obtained with the 10.6 μm band-pass filter shows hardly any effects from the flame, resulting in good agreement with the temperature profiles on $Wall_2$.

To further demonstrate the filter effects, four different color infrared images are shown in Figure 3-12 (a), (b), (c) and (d). The top two infrared images were obtained using a blue methane-air premixed flame, and the bottom two infrared images were obtained using a sooty hexane pool flame. The burner heat release rate of 18 kW was used for methane flame, and approximate flame height for the hexane pool flame was about 40 cm. The results (a) and (c) were obtained after the wall temperature achieved a steady state condition. The image (b) was obtained one second after the burner was turned off, and the image (d) was obtained in four seconds after the pool flame was quenched. The infrared images (a) - (c) and (b) - (d) are in good agreement demonstrating that the infrared imaging system can measure the wall temperature through the flame, and without the flame interference. Based on the IR thermal images obtained, three-dimensional perspective projections were obtained by gray level analysis, shown in Figures 3-13 and 3-14. The transient isothermal lines obtained by contour tracing are shown in Figure 3-15.

3.5 Flame Spread Measurement Using the Infrared Imaging Technique

In this section, several experiments will be introduced to prove the capability of the IR imaging system in temperature measurement. The experimental samples include charring and non-charring materials. Some experiments were conducted at laboratory scales as benchmark tests or as system calibration, and some others were performed at large scale to evaluate the system for the application to urban and wildland fires.

3.5.1 PMMA Flat Wall Experiment

In the first series of experiments, PMMA was selected because it is non-charforming and has been used by many fire researchers as a benchmark material. To prove the IR technique, upward flame spread tests on a vertically oriented PMMA surface were performed with the thermocouple and IR measurements at the same time. A propane burner was used to ignited the sample. After a sustained spread was achieved, the burner was turned off. During flame spread, the surface temperature was measured by the IR camera with a band pass filter and by 0.07 mm diameter thermocouples, simultaneously. Temperature histories at one reference point in the middle of the sample are shown in Figure 3-16. It can be seen that the temperature keeps increasing until it reaches the maximum value, at which the significant pyrolysis is assumed to occur, it is at this moment that the pyrolysis front is crossing the reference point. The pyrolysis temperature was determined by the thermocouple as 370 °C, corresponding to 329 °C determined by the IR camera. Therefore, in IR imaging flame spread measurement, the 329 °C isotherm can be defined as the pyrolysis front, or the boundary of the pyrolysis region. This conclusion was confirmed by visual observation in some experimental runs with a simple geometry case.

In the pyrolysis region, the thermocouple measured temperature and the IR measured temperature are in very good agreement. What causes the difference between the two measurements in preheating and onset of the pyrolysis? The major cause may be the physical change of the PMMA surface. The thermocouple reading is very sensitive to the way of imbedding and the structure change of the material. In the preheating process, the

PMMA surface softens, melts and forms fine bubbles, affecting the relative location of the thermocouple bead to the original surface. In addition, the deposition of soot on the sample surface also may affect thermocouple readings. The above effects may cause higher temperature reading by exposing the bead to the combustion gas stream whose temperature is higher than the solid, after the original surface recedes; while it may cause a lower reading due to the coverage of the bead with PMMA melts and bulbs.

3.5.2 Flame Spread on Card-Board Corner-Wall

In the second series of experiments, card board(char-forming material) corner walls were designed. One wall surface was black and the other white, both had the same dimensions(1.2 m high x 0.2 m wide x 0.002 m thick). The card board was chosen to test the effect of char-forming during pyrolysis on infrared imaging; and two different colored card boards were used to study the emissivity effects. The samples were simultaneously ignited at the bottom by a propane torch and the temporal wall temperature distributions were obtained using the IR camera with the 10.6 μm band-pass filter.

The two samples exhibited very similar temperature distributions and from which the spread rates for both vertical and horizontal directions were obtained to be the same. The almost same temperature distributions of the two samples may be attributed to the fact that the char is formed on the surface in the pyrolysis zone, and hence the emissivity is the same regardless of the cardboard type. Four infrared images obtained in 10 second intervals are shown in Figure 3-17. In this test, a video camera was also employed to record flame behavior to investigate an alternative use for spread rate measurement. However, the burning area boundary is hardly to be identified from these video images, see Figure 3-17 bottom. Through the above experiments, the merits of the infrared imaging technique can be seen in the following three areas: (1) it is capable of obtaining of a temporal and two-dimensional pyrolysis front; (2) it is suitable to charring and non-charring materials, and is affected little by the change of the sample surface structure; (3) little sample preparation is required.

3.5.3 Flame Spread on Large-Scale Plywood with External Radiation

In this experiment, the IR imaging technique was applied to the large-scale flame-spread measurement for the first time. Since flame spread rate and heat transfer increase with scale, upward flame spread accelerates quickly as the size of the burning materials increase. However, most of the data available for validating upward fire spread models is limited primarily to 1.2 m heights or less and to non-charring materials such as PMMA. In 1992, Factory Mutual Research Corporation(FMC) and the National Research Council Canada (NRCC) initiated a joint research project of large scale flame spreads on charring materials, plywood board. Our laboratory was invited to joint the flame spread test to measure spread rate using IR imaging system. This experiment was conducted at NRCC fire test facility in suburban Ottawa.

A schematic of the experimental setup was shown in Figure 3-18. The 0.61 m wide x 2.4 m high specimens were mounted in a specimen holder which consisted of a steel frame, a balance mechanism, a load cell and a steel supporting structure. Two 0.3 m wide x 2.4 m high Marinite boards were positioned on the both sides of the specimen. A water cooled radiation shield was located at the base of the specimen holder. This shield was used to protect the holder and the load cell assembly, and also minimize the convection flow from the floor to the low portion of the specimen. A large scale (1.5 MW) radiant panel was used to provide radiant exposures to the test specimens. This panel was constructed using 40 commercial premixed gas-fired (propane) radiant heaters with porous ceramic tiles used in the front face of the burners. The heaters were mounted in two vertical arrays to provide a flat radiant area of 3.6 m high by 2.7 m wide. The radiant flux density produced by this radiant panel depends on the gas supply rate and the distance of the panel from the specimen. For these tests, the supply rate was maintained constant and the radiant flux was varied by changing the distance between the specimen and the panel. A direct photograph of the flame spread and the surface temperature of the burning area were displayed in Figure 3-19.

The IR camera with a 10.6 ± 0.5 μm band-pass filter can measure the burning surface temperature eliminating the interference from the flame. To detect the pyrolysis region, the pyrolysis temperature had to be determined by a calibration test. In this test, during flame spread the surface temperature history at a center point of the sample was measured by a thermocouple and the IR camera simultaneously. These results were plotted in Figure 3-20. Even we can not believe the thermocouple reading is the real temperature because of the surface structure changing during preheating, but we can determine the pyrolysis front is crossing the measurement point when the temperature increases sharply. Therefore, a nominal pyrolysis temperature by the IR camera was determined as 310 °C, see Figure 3-20. Then, the pyrolysis temperature was used to trace the pyrolysis front using the isothermal mode of the IR imaging system. The IR thermal images at different moments are shown in Figure 3-21. In these images the pyrolysis fronts were highlighted by white spots. The pyrolysis height was measured as a function of time under different external radiation levels, and shown in Figure 3-22.

3.6 Measurements of Flame Temperature in Pool Fires

Another application of this IR system is the flame temperature measurement in large-scale pool-fires where the conventional thermocouple technique has limitations. Combustion as a tool to mitigate oil spills on the ocean surface turns out to be more feasible compared to other possible means by converting rapidly large quantities of oil into its primary combustion products, carbon dioxide and water with small percentage of unburned residue and other byproducts (Evens et al, 1992). However, it is difficult to establish an effective combustion method which has a high burning rate and produces only environmentally acceptable emissions, mainly because the structure of large-scale crude oil fires is not well understood. To investigate the nature of the large-scale pool fires, the Building and Fire Research Laboratory at the National Institute of Standards and Technology (NIST) conducted a series of pool fire experiments to characterize the radiation emission and smoke yields from large-scale crude oil fires (Koseki, et al., 1994). These experiment were performed using different diameter pools in order to establish effective correlations among these different pool fires. In November 1994, our laboratory was invited to joint the NIST pool fire test in Mobil Alabama using our unique IR imaging technique to measure the flame temperature.

A schematic of the experiment layout and a direct photograph of the pool fire test are shown in Figure 3-24. The pool was 15m x 15m, and diesel oil was used as the fuel. The infrared camera was located 121.5 m from the center of the pool with the field of view(FOV) 15 degree vertical x 20 degree horizontal to cover the whole image of the flame and plume. Continuous thermal images (60 frames per second) were obtained by the IR imaging system and recorded on a video tape for later analysis. The images of flame structure and temperature distribution for some moments were printed out and shown in Figure 3-25. These results show that the flame is not a continuous body, consisting of 3 to 4 huge “fire balls” due to a strong pulsation of the flame. The measured average flame temperature was around 1000 to 1200 °C.

4.0 STATIONARY CORNER-FIRE EXPERIMENT

4.1 Introduction

To understand the heat transfer from the flame to the corner walls, a room corner model, which is the half scale of the NIST prototype room fire model, was designed and built in the Combustion and Fire Research Laboratory. A steady gas burner was used to simulate the fire source. The combustion heat is transferred to the wall surface in large part by convection and radiation. Therefore the study of the fire-induced flow in the corner walls is necessary since the flow patterns not only affect the heat convection directly, but also affect the radiation by dominating the flame height and geometry. In the first part of this study, a series of flow visualization experiments were performed to investigate the structure of the fire-induced flow. And then the direct measurements of wall heat flux and wall surface temperature were conducted. In these measurements a special attention was paid to the ceiling effect on heat transfer, because in the previous experimental observation, Williamson et al (1984) found as the flame extending to the ceiling from a corner fire, it runs along the intersection of the ceiling and the walls. It is also shown by Mitler and Steckler (1993) that the presence of a ceiling will strongly affect how a flame spreads along corner walls, especially in the late stages of the corner fire.

The fire-induced flow confined by the corner walls is a chemically reacting flow with the characteristics of the turbulent fire plume and the complicated corner wall boundary effect. The accurate flow field measurements are not simple because of the lack of analytical relations to use for calculation and reduction of experimental data. Frequently, the flow may be altered as a result of probes that are inserted to measure the pressure, velocity, and temperature profiles, so that the experimenter is uncertain about the effect that has been measured. Flow visualization by optical methods may be more accurate when it is properly conducted with the minimum disturbance to the flow field. In some instances, the flow visualization technique may be more feasible than point by point measurements, while in other cases it may serve only to furnish qualitative information regarding the overall flow behavior. In the past study, smoke streak lines were used to visualize flow patterns; a sporadic occurrence of a concentrate vortex was observed along the corner (Daikoku, et al, 1991). In the present experiment, instantaneous stream lines were visualized by particle tracking method, which can lead to a quantitative measurement using particle image velocimetry (PIV) technique. Some typical flow patterns were obtained corresponding to the specific gas burner locations. The wall surface temperature distribution and the heat flux distribution to the wall were measured under this steady condition. Under the ceiling influence, a bottle-neck pattern was found for both temperature and heat flux distributions. These results were found very helpful to understand the pyrolysis geometry in later flame spread study.

4.2 Visualization of Fire-induced Flow along Corner Walls

4.2.1 Experimental Method

A schematic of the experimental apparatus is shown in Fig. 4-1. The walls were made of two centimeter thick Marinite boards (non-combustible/heat insulating material) which are backed up by 1.5 centimeter thick particle boards for heat insulation, and fixed on a steel frame. The corner wall model is 1.6 m high, 1.0 m wide and 1.0 m deep. The exit dimension of the gas burner is 0.15 x 0.15 m. The floor was lifted to the same level as the burner exit to eliminate flow disturbances by the burner's edges. To obtain a clear visualization image, a blue propane-air premixed flame was used. The burner can provide combustion heat up to 22.5 kW. In preliminary tests, it was found that the heat release rate is a weak parameter to influence the fire-induced flow patterns. Hence these experiments were performed at the constant heat release rate of 6.0 kW with different stand-off distances (x,y) as shown in figure 4-1.

The 50% intermittent flame height that is defined as continuous flame height is about 0.25 m. Ambient air was seeded with a few micron diameter magnesium oxide (MgO) particles. These particles can float in the air for several minutes following the flow faithfully. Flow visualization experiments were conducted in a quiescent surroundings to ensure the minimum disturbance from the draft. The laser beam from a 5 Watt argon-ion laser device was converted to a laser sheet by a cylindrical lens. The laser sheet can be set to slice the plume region of the fire vertically and horizontally. Tracing particles were illuminated by the laser sheet and the instantaneous flow stream lines were visualized and recorded by a still camera with a shutter speed of 1/8 s.

4.2.2 Results and Discussion

(a) Puffing Motion in Fire-induced Flow

First, the flow visualization was applied to a vertical section cross the fire plume about 0.5 meter range. Except the basic flow patterns, photographs presented in Figure 4-2 (a) - (d) clearly show the puffing motion in buoyant plumes and in the surroundings. Photographs (a) to (c) were taken under the same conditions at different moments. From these picture, we can see the significant fluctuation in velocity field.

As is well known, the transition of a laminar flame to a turbulent flame occurs with increasing the scale and velocity of the flame. Meanwhile, the luminous fire pillar of the buoyancy-controlled flame begins to oscillate. This oscillation is produced by the aerodynamic instability due to the interaction between the plume and the surrounding air (Ishida, H. 1992). The effect of flame oscillation on air entrainment and mixing processes are notable in the side view photographs in Fig. 4-2 (a), (b), (c) and (f). It is also found that these effects exist in a wide range, larger than 1.0 meter for this test. The air flow already becomes distorted with the oscillation in velocities before it enters into the plume, even it is far away from the fire plume. Hence, the turbulent fluctuations generated in the plume boundary area are not only carried away in down stream by convection but transferred in horizontal direction; and not only directly in adjacent layer of fluid by diffusion, but over a great distance. This phenomenon is so-called "long range action" of the turbulence (Abramovich, G. N. 1979). The turbulent long range action was also found in transverse direction, and it becomes important in reverse direction in a low speed flow field, like the fire-induced flow. The mechanism of long-range action is the transmission of the pressure pulse over distance, therefore it is not sensitive to the direction.

(b) Vortical Structures and Major Flow Patterns

Swirl formation was found to be another important feature in the fire-induced flow along the vertical corner walls. At a non-symmetric location respect to the walls, the gas burner can induce a large swirl around the flame which could change the entrainment rate tremendously. By the experimental observation, three major flow patterns can be identified. They are a quarter free plume pattern (Figure 4-3), single vortex pattern (Figure 4-4), and vortex couple pattern(4-5), corresponding to the zero stand-off distance, one side stand-off, and both side stand-off three different burner locations, respectively.

A photograph in Fig. 4-3 shows the instantaneous stream lines in a horizontal plane as the burner is just in the corner. A flow pattern sketch was also provided in this figure. The vertical flow pattern can be seen in Fig. 4-2(a) - (c), which is similar to that of the flow field induced by a turbulent jet from a floor (Dike, 1982). Because the corner walls exist, and the burner's two edges are flush with the wall surfaces, the plume will attach itself to the walls. This plume in the corner can be thought as a quarter of a total free plume. The entrainment rate of a fire plume confined by the corner walls will be a quarter of that of a free plume if the effects of wall boundary layer can be neglected. When the burner is moved away from the walls, a couple of vortex tubes were found at two edges of the burner, this couple vortex flow pattern is shown in Fig. 4-5. The breakdown of vortex couple occurred quickly after it was produced because of the interference between two vortex cores. When the burner is flush with one-side wall and stand-off from the other, one vortex tube becomes stronger and dominates the induced current in the corner, this single vortex flow pattern is shown in the Fig. 4-4. A side part of the flame is detached from the main body by the axial flow of the vortex. The vortex tube can last much longer than the vortex couple, and it decays gradually.

4.3 Measurements of Wall Heat Flux and Temperature

The objective of this experiment is to develop an understanding of the heat transfer mechanism, and the effects of ceiling on the heat transfer process. The room corner model introduced before was used in two configurations: with ceiling and without ceiling. In this study, the burner heat release rate was set at 18 kW, the corner walls were preheated by the burner, and the measurements were conducted after a steady state was achieved. Temperature distributions were measured by 0.1 mm diameter Chromel-Alumel thermocouples, the beads of which were imbedded 1.0 mm bellow the wall surface to eliminate the radiation heat loss and the hot gas interference. Total incident heat flux distribution on the wall was measured by water-cooled Gardon-guage heat flux meters. Both temperature and heat flux measurements were carried out at ninety nine locations. The measured heat flux distributions and the temperature contours are shown in Figures 4-6 and 4-7 for the cases with and without ceiling.

For both cases, with and without ceiling, from the heat flux distributions (figure 4-6), we found the maximum heat flux is at some area close to the corner above the burner. In the plume region the heat flux in the corner is lower than that on the wall. This heat flux pattern can be used to explain why the wall surface in the corner does not burn.

The ceiling effect is significant in this figure. In the upper region of the corner, the measured heat flux was greater when the ceiling was present. This is consistent with the measured resulting temperature distribution (Figure 4-7). The increase in heat flux may be resulted from the confining of the plume by the ceiling. However, the heat flux and the resulting temperature in the middle region of the corner were reduced by the introduction of the ceiling (Figures 4-6 and 4-7). That is probably because the pressure increase due to the presence of the ceiling lowers the flow velocity of the plume, which produce a decrease of the convective heat transfer to the wall surface.

4.4 Summary of the Stationary Corner-Fire Experiment

(1) The oscillation of the flame can induce air puffing in a relatively large area around the plume. The flame oscillation is caused by a pressure transmission which is enhanced by the presence of the wall boundaries.

(2) An non-symmetric location of the burner can produce a concentrate vortex at one side of the flame. The vortex with a very strong axial flow may enhance combustion rate significantly. Hence, for a transient flame spread process, the flame oscillation and vortex formation in the plume are critical elements to understand the turbulent entrainment and mixing process.

(3) Heat flux and temperature measurements conducted with and without ceiling demonstrate that the effects of the ceiling on the heat transfer to wall are quite significant.

5.0 EXPERIMENTS OF FLAME SPREAD ON CORNER WALLS

5.1 Introduction

Upward flame spread along a vertical wall is a typical process leading to the hazardous growth of an enclosure fire. Past studies, both experimental and theoretical, have focused on the upward flame spread over a vertical flat wall, where two-dimensional flame behavior is usually observed and a one-dimensional spread rate model is applicable with reasonable accuracy (Saito, et al, 1985; Mitler, 1990; Delichatsios, et al, 1994). The modeling of upward flame spread on a vertical corner wall, requires additional consideration due to the transient, three-dimensional nature of the fire induced flow, which leads to a complex convective and radiative heat transfer to the corner wall.

From their preliminary observation, Williamson et al (1991) reported a "T shape pattern" as one characteristic flame spread behavior in room corner fires under the effect of the ceiling. But the mechanisms of corner fire spread are not well understood, and there are very limit data available about this phenomenon. This circumstance is mainly due to that the experimental instrumentation is extremely difficult by conventional techniques because the large scale, complex geometry and strongly transient nature of corner fire spread. The motive of this part work is to quantitatively characterize the corner fires as to establish a reliable database for the model development of fire spread on vertical corner walls.

To develop prediction models, the detailed transient temperature distribution of the pyrolyzing wall surface must be measured accurately. Conventional thermocouple techniques, if applied, have limitations due to the complexity of implementation and the uncertainty of pyrolysis temperature. Visual observation techniques, which were previously applied for flame spread measurement (Orloff, L., 1975) can produce ambiguous results in the determination of the two-dimensional transient pyrolysis front location. To overcome the limitations associated with these conventional methods, IR radiometry, which is a non-contact temperature measurement, was applied with automated image analysis to obtain transient temperature distributions (Arakawa et al., 1993; Qian et al., 1994). A series of upward flame spread tests were conducted over vertically oriented PMMA corner walls. The progress rate of pyrolysis front was successfully measured using the IR camera. PMMA is selected as a bench-mark material in many fire studies primarily because it is an ashless burning solid, it does not yield very sooty flames. It is available in a form that does not drip very much, its surface temperature remains almost constant if it burns under zero or fixed external radiation heat flux, and more important, many of its properties have been thoroughly investigated.

5.2 Experimental Design

A schematic of the corner-wall flame spread test apparatus is shown in Figure 5-1. The room corner model with ceiling and floor is made of Marinite boards fixed on a steel frame. The dimension of the model is 1.6m high x 1.0m wide x 1.0m long. Polymethymetharylate board (PMMA, 12.7 mm thick) samples were flush mounted on the corner walls and the ceiling. Ignition was provided at the bottom of both side walls by a small propane torch. To prevent excess preheat of the virgin surfaces, the sample was covered by a Marinite board except at the ignition zone which is 30 mm high and its length is adjustable. When the cover was removed after the whole ignition zone was ignited, a sustained flame spread was achieved (see Fig. 5-2). The sample was assumed as thermally thick and no burn-out during flame spread. When the peak of pyrolysis front reached the top of the sample, the flame was extinguished by a sudden purge of CO_2.

During flame spread, the two-dimensional spreading pyrolysis front was detected by tracing the isothermal of T_{ig} using the automated IR imaging temperature measurement system. The principal assumption is that the pyrolysis front reaches a point exactly when the surface temperature at that point reaches the ignition temperature, T_{ig}. The infrared camera was located about 7.0 meters away from the burning walls, and it could acquire the whole thermal images of the walls and the ceiling with the FOV of 15 deg. vertical x 20 deg. horizontal. To avoid the flame interference, which includes radiation from solid soot particles and exited gas molecules, a $10.6\pm0.5\mu m$ band pass filter was used with the IR camera. The flame spread rates over materials most commonly used in buildings were found to be accurately measured by the IR camera system. The accuracy of the measurement associated with the determination of T_{ig} and the elimination of flame interference has been discussed in Chapter 3. During the test, the visible flame shape was simultaneously recorded by a video camera on a VHS tape, from which a time averaged visible flame height can be deduced. Based on the pyrolysis front measurements, total heat flux histories at those points along the trajectory of the peak of the pyrolysis front were measured by Gardon-type heat flux sensors, with automatic data recording and storage on a computer disc.

In this Chapter's work, PMMA corner wall and ceiling models were tested; two-dimensional flame spread rate, flame height and total heat flux histories from the flame to the wall surface were measured. Based on these measurements, a one-dimensional heat transfer model was applied to predict the vertical spread rate. Flame spread measurement results were correlated with time and compared with the above calculated results. An empirical model for the M-shaped pyrolysis front, which has practical significance, has also been developed.

5.3 Results and Discussion

A series of direct photographs recording the flame geometry during the corner fire spread are shown in Figure 5-2 (a) - (d). Their corresponding IR thermal images which display the pyrolysis region are shown in Figure 5-3 (a) - (d). From these pictures, we can see that most of the flame body is well developed turbulent flame. The general geometry develops from a triangle to a "T" type. The horizontal flame spread is much slower than the vertical flame spread. In the IR thermal images, the boundary of pyrolysis region has the pyrolysis temperature and is high lighted by fine white spots. We can see from these results the temperature inside the pyrolysis region is approximately uniform. A very interesting flame spread behavior found here is that the flame does not spread continuously, it jumps to the ceiling and the portion of the side wall that is adjacent to the ceiling (see Figure 5-3 (c)). In the following sections, some findings about controlling parameters, spread geometry, spread rate will be presented, some in-depth analysis will be provided to explain the thermal mechanisms of flame spread along corner walls.

5.3.1 Controlling Parameters of the Corner Fire

Typically, a fire ignited on a section of corner walls spreads vertically and horizontally. Different ignition methods correspond to various modes. In our previous study, it was found the unsymmetric one side ignition can produce more complex spread patterns. For the sake of simplicity, this study will deal with the symmetric line ignition mode along the bottom of the corner walls. When the PMMA corner walls were ignited at both sides symmetrically and the ignition height is fixed (30 mm, approximately minimum height for a sustained flame spread), the ignition length Y_0 will be the only controlling parameter for this simulated fire scenario. Therefore, the effects of Y_0 on flame spread were investigated first.

Four flame spread tests were performed with ignition lengths of 10, 30 and 40 cm. The height of all the samples is 100 cm. During the flame spread process, a "M-shaped" pyrolysis front, one peak on each side of the wall, was observed. The pyrolysis zone detected by the IR system on one-side wall is shown in Figure 5-2. The two most important features of this flame spread are the vertical flame spread at the peak and the horizontal spread at the bottom. The highest flame spread rate was achieved at the peak of the pyrolysis front. The pyrolysis height X_p and width Y_p were measured as a function of time for different ignition lengths, and plotted in Figure 5-4. From these results, we find the vertical spread rate increases with increasing of the ignition line length, but it tends to achieve a maximum value when the ignition reaches a critical length. To further confirm this conclusion and find the critical length, the time elapsed when the flame spreads to the top of the sample is plotted against the ignition length, shown in Figure 5-5. From this curve it can be seen the critical ignition length is about 20 cm. However, back to the results presented in Figure 5-3, it can be found that the horizontal flame spread rate is approximately constant and independent of the ignition length.

These corner fire spread characteristics can be well explained by the previous flow visualization. It was revealed in the flow visualization study that the vertical flame spread is a concurrent flow spread (in the direction of local gas flow) and the horizontal flame spread is an opposed flow spread (opposite to the local gas flow). The high vertical spread rate is mainly contributed to a strong fire-induced flow that enhances the heat transfer from the flame to the wall surface. There exists a critical ignition length (20 cm) beyond which the flame spread rate does not increase any more, probably because the fire-induced flow in the corner can not be enhanced any more by increasing the ignition length, or increasing the flame width. For the horizontal flame spread, two major factors dominating spread rate are radiation heat transfer and opposed flow cooling. With decreasing the ignition length, the pyrolysis front moving into the corner, radiation heat transfer increases due to the flame on the other side wall. But this increase could be offset by the increasing in opposed fire-induced flow, finally a constant flame spread rate was obtained.

5.3.2 Mechanisms of the M-shaped Pyrolysis Front Formation

Two pictures, which were taken after the corner fire was extinguished, clearly show the pyrolysis region geometry in Figure 5-6. It was found the pyrolysis front has one peak on each side of the wall, and the wall surface just inside of the corner does not burn. This special geometry was termed as "M-shaped pyrolysis front". It is always appeared regardless of the length of ignition (see Figure 5-6 a, b). Temporal 329°C contour (pyrolysis front) can be obtained from IR images shown in Fig 5-3. The infrared pyrolysis fronts at six different time periods were obtained from the IR images, are shown in Fig.7-8. In this figure, the formation of the M-shape pyrolysis front is evident and the spread rate in any direction can readily be deduced. If an attempt was made to duplicate the similar result by multi-point thermocouple measurement, the work would be extremely elaborate.

From the fire safety point of view, the prediction of the maximum upward spread rate is crucial. The mechanisms of the M-shape pyrolysis front formation, therefore, needs to be understood, since its peak spreads toward the ceiling with the maximum rate.

The four mechanisms, M-1 through M-4 considered below were experimentally examined using corner wall models composed of two duplicated pieces of PMMA wall, 1.6 m high x 0.3 m wide x 0.02 m thick, housed in the Figure 5-1 shown apparatus. In the following experiments, pyrolysis front shape was examined by both the IR technique and the CO_2 extinguishment method which was explained in the flame spread experiment section.

M-1 Effect of ignition mode: In the first series of experiments, a uniform line ignition was applied at the bottom of both corner walls by a propane torch, Figure 5-6 (a). In the second series of ignition experiments, a spot ignition was provided at the bottom corner, allowing the flame to spread horizontally and vertically, Figure 5-6 (b). In the third series of ignition experiments, a 30 cm long line ignition was provided at the bottom of one side wall, Figure 5-7. For all three cases, a very similar M-shape pyrolysis front was resulted. Interestingly, the height of pyrolysis region on the initially torch ignited wall is shorter than that on the unignited wall, resulting in the faster spread over the initially unignited wall. This may be attributed to the fact that for the initially unignited wall, enhanced convective heat transfer occurred through a steeper temperature gradient, which was formed near the initially unignited wall due to the closer distance between the flame and the wall. Visual observation and gas phase temperature measurements proved that to the case.

M-2 Effect of solid phase conduction heat loss: Based on the failure of the M-1 mechanism, heat conduction through the corner wall was thought to be the main reason for the M-shaped pyrolysis front formation. To test this mechanism, two different corner configurations as shown in Fig. 5-8 (case I and case II) were designed. In case I, two PMMA samples were glued together to form a solid corner; while in the case II, two PMMA samples were fixed to form a hollow corner. For case I a large conduction heat loss was expected through the solid corner wall; while for the case two, a minimal conduction loss was expected. In addition, two PMMA samples were fixed with a 5 mm distance between each sample with the intention to test the M-3 mechanism to be explained later. Flame spread tests were conducted using a uniform line ignition mode. If the M-2 mechanism is the principal reason for the M-shaped pyrolysis front formation, the pyrolysis front shape for cases I and II should be significantly different (the case II pyrolysis shape should be not like a M-shape). However, the two cases resulted in a very similar M-shape (Fig. 5-8) rejecting the above assumption.

M-3 Fire-induced Flow Cooling: The fire-induced air may be entrained through the bottom of the corner and it may flow along the corner. If a substantial amount of the air flow is entrained, a significant cooling effect could be expected. The possibility of this mechanism is certainly worth examining, since the previous flow visualization results (Qian and Saito, 1992) revealed a sporadic vortex formation along the corner. To examine this mechanism, the case III experiment (Fig. 5-8) was designed and performed using the line ignition mode. The intention of this experiment is to significantly reduce the fire-induced flow along the corner by separating the two samples by 5 mm, the distance sufficiently smaller than the distance between the corner and the pyrolysis front peak. Under these experimental conditions, a significant change in the pyrolysis front shape is expected, if M-3 is the principal mechanism. However, the M-shaped formation did not change very much. When the two walls are further separated, flame spread becomes similar to the single vertical wall case as is expected.

To further confirm the insignificance of the M-3 effect, a square piece of aluminum plate, 5 cm x 5 cm wide x 0.5 cm thick was placed in the corner halfway between the sample top and the bottom and perpendicular to the corner walls (see Figure 5-9). The aluminum piece is large enough to alter and stop the flow, yet small enough to cause an insignificant heat loss effect. An upward flame spread experiment was conducted using the same experimental technique mentioned earlier. Regardless of this effort, the formation of M-shape pyrolysis front appeared again.

M-4 Flame-displacement effect: Because of the unsuccessful trials with the mechanisms M-1 through M-3, the M-4 mechanism flame displacement effect, was finally considered. This mechanism is based on a large heat loss in the gas phase due to poor mixing of pyrolysis products and air forming a nonflammable (probably fuel rich mixture) layer between the corner and the flame. This layer is thick enough to be an effective insulation, so that the surface temperature in the corner can not reach pyrolysis temperature. Through a series of exploratory tests, it was found that the flame displacement distance, the distance between the maximum gas temperature location and the wall corner can be changed by changing the corner angle, θ. To further investigate this observation, four different corner angle models ($\theta = 45^{\circ}, 90^{\circ}, 135^{\circ}$, and 180°) were designed. Schematics of these models are shown in Fig. 5-10. Of particular interest is Fig. 5-10 (c), the $\theta = 135^\circ$ case, which resulted in no M-shape formation. The $\theta = 45^\circ$ case shows somewhat enhanced image of the M-shape, while $\theta = 180^\circ$ shows a parabolic shape pyrolysis front normally approximated as one-dimensional spread. To estimate the heat loss in the gas phase, the flame displacement distance, δ, was measured by traversing a 100 μm diameter alumel-chromel thermocouple normal to the corner. It was found the δ decreased with increasing θ. Heat flux distributions along the corner for the $\theta = 135^\circ$ model were measured by traversing a Gardon gauge heat flux meter: it was found that the heat flux just above the pyrolysis front was 0.7 W/cm^2 in agreement with the minimum heat flux that allows upward flame spread to occur (Saito et al., 1989). We also experimentally confirmed that the M-shaped formation occurred for at least cardboard, particle board and black coated PMMA, in addition to transparent PMMA, suggesting that the material properties are likely not important for the M-shaped formation.

5.3.3 Flame-Spread Rates and A Similarity Model for Pyrolysis Front

During flame spread, the maximum upward spread rate was achieved at the peak of the M-shaped pyrolysis front. It was found that with increasing the ignition length from a spot (about ϕ3 cm) to 20 cm, the vertical spread rate increased, while for 20 cm $< Y_o <$ 40 cm, the vertical spread rate remained constant. It is because the fire induced flow in the corner may not be enhanced further with increasing the width of the flame. To investigate the flame spread to the ceiling, a PMMA ceiling was added. Interestingly, it was found that the ceiling and the portions of vertical corner walls close to the ceiling were ignited before the upward spreading pyrolysis front reached that height. For the 160 cm high room corner model, when the upwardly spreading pyrolysis front reached the height of 140 cm, the top of the corner wall and part of the ceiling was already ignited allowing a simultaneous downward spread (see Figure 5-3 c).

This part of study will focus on the upward and lateral spread of the M-shaped pyrolysis front because this process includes most part of the corner fire spread, and is very important in the early stage of fire development. In the M-shaped pyrolysis front spread mode, vertical spread at the peak and horizontal spread at the base are critical aspects of the flame spread phenomena. Based on the previous flow visualization study on fire-induced flow along the corner walls, it can be shown that the vertical flame spread is a concurrent flow spread (in the direction of local gas flow) and horizontal flame spread is an opposed flow spread (opposite to the local gas flow). Therefore, their spread characteristics are discussed separately as follows.

(a) Vertical Flame Spread at the Peak

The peak heights of pyrolysis front, X_p, detected by the IR camera as a function of time for four ignition lengths ($Y_o = 10, 20, 30$ and 40 cm), are presented in Figure 5-12. The X_p and Y_o are depicted in Figure 5-1. There is a good agreement for the results from the three tests ($Y_o = 20, 30$, and 40) when $X_p > 20$ cm. By the observation, the disagreement in the region $X_p < 20$ cm corresponds to the transition from laminar to fully developed turbulent flames, and with the effects of ignition. We also found that X_p varies almost linearly with time for $X_p > 20$ cm in this log plane. This linear distribution suggests an exponentially increasing pyrolysis height as a function of time. A least-square logarithmic fit of the data for pyrolysis heights above $X_p = 20$ cm yields,

$$X_p = 0.00299t^{1.84}. \tag{5-1}$$

A power law correlation of the pyrolysis height with the spread time is obtained. To directly compare the corner-wall fire spread rate with the flat wall fire spread rate, the flame spread rate was calculated based on the measurement data. The flame spread rate is plot in Figure 5-13 with the similar scale to the flat wall fire spread rate from Orloff (1975). We found that for both cases, the spread rate was essentially proportional to the pyrolysis height, but the upward spread rate for the corner fires was about three times faster than that for the same scale vertical flat wall fire, i.e., $V_p = 0.0134\ X_p^{0.944}$ versus $V_p = 0.00441X_p^{0.964}$ (Orloff, L., deRis, J., and Markstein, G. H., 1975). The high spread rate is mainly because of a strong fire-induced flow that enhanced heat convection from the flame to the wall surface and an enhanced radiation from the flame to the walls.

(b) Horizontal Spread at the Base

From Quintiere and Harkleroad(1984) downward and lateral flame spread in air, on a vertical flat can be expressed as follows:

$$V_p = \frac{\phi}{(k\rho c)(T_{ig} - T_s)^2}. \qquad (5\text{-}2)$$

For the flame spread on a PMMA plate, the ignition temperature: $T_{ig} = 378$ °C, effective thermal inertia: $k\rho c = 1.02\ (\mathrm{kW/m^2K})^2\mathrm{s}$ and flame heat transfer parameter: $\phi = 14.4\ (\mathrm{kW})^2/\mathrm{m}^3$. In the corner-wall fire experimental, the horizontal flame spread rate was measured as: $U_p = 0.0113$ cm/s, see Figure 5-4. Using equation. 5-2 we can calculate the heat transfer parameter as: $\phi = 14.1(\mathrm{kW})^2/\mathrm{m}^3$. It can be seen the heat transfer parameters for these two cases result in very good agreement. As we already know the horizontal flame spread is an opposed flow spread, the opposed flow reduce the convection heat transfer to the preheat zone. However, the radiation heat transfer can be increased by the other side wall flame. Therefore, the reason of the similar heat transfer parameters is that the additional radiant heat flux from the other side wall and flame is offset by a stronger opposed flow confined by corner walls. It is also found a similar mechanism that causes the approximate constant lateral spread rate with increasing ignition length, i.e., with increasing the ignition length the radiation decreases and the opposed flow also becomes weaker. Hence, the width of the pyrolysis region as a function of time is given by a linear relation based on the constant spread rate assumption,

$$Y_p = 0.0113t + Y_o \, . \tag{5-3}$$

This relation will be applicable over the size range where the corner effect is important. It will be used to develop a similarity model of pyrolysis front on corner walls.

(c) The Similarity Model for Pyrolysis Fronts on Corner Walls

The location of spreading pyrolysis front measured by the IR camera as a function of time is shown in Fig. 5-11(a). To develop an empirical model, a similarity fit of the pyrolysis front is likely applicable and convenient. First, the data was normalized by the peak pyrolysis height, X_p, in vertical direction and by the base pyrolysis width, Y_p, in horizontal direction. These normalized pyrolysis fronts were shown in Figure 5-11(b). From this plot we found that the correlation of the normalized data is excellent for $X_p > 20$ cm. The normalized pyrolysis front was then fit by a fifth order polynomial with a correlation coefficient of 0.993.. Hence an empirical model for the pyrolysis front was obtained as:

$$\xi = 32.74\eta^5 - 107.24\eta^4 + 127.87\eta^3 - 67.30\eta^2 + 13.98\eta + 0.0203 \, , \tag{5-4}$$

$$\text{where} \quad \xi = \frac{x_p}{X_p} = \frac{x_p}{0.00299t^{1.84}} \quad \text{and} \quad \eta = \frac{y_p}{Y_p} = \frac{y_p}{0.0113t + Y_o} \, .$$

This is the equation : $f(x_p, y_p, t) = 0$. There are many applications of this equation. For example, calculate $V_p = dx_p/dt$ and $U_p = dy_p/dt$ to get the two-dimensional flame spread rate. Another application is to calculate the pyrolysis area. This result with a gasification model can provide a transient fire source model for the computer simulation of heat transfer and smoke movement in a building corner-wall fire. In previous numerical study (Quintiere, 1992), a rectangular pyrolysis region was applied because of the lack of experimental data. By this pyrolysis front similarity model, a great improvement can be made here.

5.3.4 Heat-Flux Measurement and Applicability of A One-dimensional Heat Transfer Model to Predict Spread Rate

A first step has been taken to characterize the heat transfer process in the preheat region, so that the upward flame spread rate might be predicted. Heat flux measurement was performed with a 160 cm high PMMA corner wall model with an ignition length of 20 cm on each side of corner wall bottom. Total heat flux histories were measured at five different heights along the trajectory of the pyrolysis peak, located by the IR imaging system. Figure 5-14 shows the measured incident total heat flux versus time and height from the floor. The t_f and t_p respectively correspond to the times when the flame tip and the pyrolysis front reach the measurement point. There is no significant increase in heat flux when the flame tip reaches the measurement point probably due to the flame pillar effect (Williamson et al., 1984), a kind of precursor flame which carries much less combustion energy than the main flame. A maximum heat flux of 3.25 W/cm^2 was achieved in the pyrolysis zone that is approximately 50-60% higher than the corresponding value in the vertical flat wall fires (Quintiere et al., 1986; Hasemi, 1986). In the past studies, heat flux measurements were usually performed under a steady state, the wall fire was simulated by steady burners (Ahmad and Faeth, 1978; Hasemi, 1986). This transient heat flux distribution was measured and published for the first time (Qian and Saito, 1994). Studies found the transient nature of heat flux distribution can not be ignored due to the high spread rate of corner fire.

Heat transfer in the solid phase PMMA includes heat conduction in the direction perpendicular to the wall surface to the PMMA inside and lateral heat diffusion, i.e., a transient three-dimensional heat conduction. However, the lateral heat diffusion can be neglected because the thermal conductivity of PMMA is very small and the temperature gradient in the lateral direction is much smaller then the gradient in the perpendicular direction. To confirm this assumption, a one-dimensional heat transfer model was applied with the measured heat flux as boundary condition to simulate the preheat process. If the calculated pyrolysis front agrees with the experimental result (Figure 5-12), the one-dimensional heat transfer model will be applicable, and the thermal model for flame spread on corner walls will be simplified significantly.

It can be shown (Carslaw, H. S., 1959) that the surface temperature of a semi-infinite slab initially at the uniform temperature T_o, subjected to a net heating flux $\dot{q}''$ (x,t) is given by

$$T_s(x,t) = T_o + \frac{1}{\sqrt{\pi k \rho c}} \int_0^t \frac{\dot{q}''(x,t)}{\sqrt{t - \tau}} d\tau . \tag{5-5}$$

By equation 5-5, let $T_s = T_p$, the time when the pyrolysis front reaches the heat flux measurement height can be calculated based on the measured incident heat flux history in the preheat period (from $t = 0$ to $t = t_p$). The heat flux history ($0 < t < t_p$) was fit by a third order polynomial, and then introduced into equation 5-5. In keeping with the approximate nature of the model, all the material properties of the fuel are taken as constant. The effective thermal inertia of PMMA: $k\rho c = 1.02$ $(kW/m^2K)^2s$ from Qintiere (1986). The pyrolysis temperature equals to 373 °C determined previously. The calculated pyrolysis heights versus time were plotted in Figure 5-15, compared with the measured data. It was found that the calculated pyrolysis height was about 10% lower than the experimental value. There are four effects we did not include in this model: lateral heat diffusions, reradiation at PMMA surface, variable properties with temperature and thermally thick assumption. These effects are likely contribute to this disagreement.

What kind of consequences can be resulted by these effects?

(a) The lateral heat diffusion includes vertical and horizontal heat conduction inside PMMA. The effect of the vertical conduction is not important since the temperature gradient is very small due to the long distance of preheat zone in this direction. The horizontal conduction is much more important than the vertical since there is a large temperature gradient and heat is conducted to both side of the pyrolysis peak. In general, the lateral heat diffusion has a cooling effect for preheating the virgin fuel. Therefore, if this effect is included in the calculation, equation 5-5 and the experiment will disagree more than 10%.

(b) Reradiation is the heat loss by radiation from the PMMA surface to the surroundings (the highest surface temperature is 646 K, the surrounding temperature is around 300 K). Obviously, neglect of this effect increases the spread rate.

(c) The thermal inertia $k\rho c$ of PMMA is a function of temperature. But the variation with temperature in the experimental range is very small. In previous studies (Quintere et al., 1986; Kulkarni et al., 1990; Mitler, 1990), it was shown that a constant value was acceptable.

(d) Finally, thermally thick assumption or semi-infinite model can make the calculation height lower than the experiment. When the experimental sample was 12.7 mm, and there was a gap between PMMA and Marinire board, conductive heat loss to PMMA is much less than a semi-infinite media. Because of this effect, the experimental spread rate because higher than the calculation regardless of the negative effects (1) - (3). This conclusion is also supported by Kulkarni's results (1990). In his study the conduction heat loss to the PMMA slab interior was measured. It was concluded that the thermally thick solid assumption is inappropriate in the early stage (first several hundred seconds) of the fire for combustion of PMMA slabs of the typically used thickness of 10 or 20 mm. Disagreement between the experiment and equation 5-5 is at most 10%, therefore, we can conclude that the one-dimensional heat transfer model is applicable in preheating process to predict flame spread along corner walls with a reasonable accuracy.

5.4 Summary of Experimental Results

(1) Infrared image analysis is an effective tool for studying phenomena associated with building fires. It can provide instantaneous measurement of two-dimensional transient wall temperature with high accuracy. The flame spread rate in any direction can be deduced. Temporal pyrolysis front shapes on burning PMMA, plywood, cardboard and other materials were successfully measured by the IR imaging technique.

(2) Total heat flux received on a PMMA sample surface was measured as a function of time for upwardly spreading fires at five different heights along the corner wall. The heat flux reaches its maximum value of 3.25 W/cm^2 and is approximately uniform in pyrolysis zone. The heat flux intensity is around 50-60% higher than the heat flux measured in the flat vertical wall fires.

(3) M-shaped pyrolysis front formation occurred for the upward flame spread along the corner wall regardless of the effects of ignition mode, solid phase conduction heat loss, and fire-induced flow cooling. The formation of M-shaped pyrolysis is primarily due to the flame displacement effect near the corner. The M-shaped pyrolysis fronts can be normalized and then fit by a polynomial with a very high correlation coefficient. We call this correlation a similarity model for 2-D pyrolysis front.

(4) A one-dimensional thermal model was found to be applicable to predict the maximum

upward spread rate of pyrolysis front with reasonable accuracy. The flame spread on vertical corner walls and the associated heat transfer mechanisms have been addressed experimentally and theoretically. For thermally thick solid fuels without burn-out, vertical and horizontal flame spread rates were correlated and a two-dimensional pyrolysis front model has been developed that holds in the pyrolysis height range from 20 to 140 cm. This model has practical significance since it can be provided as a fire source model for numerical simulation of room fires. To predict vertical flame spread, the one-dimension heat transfer model can provide an approximate solution within about 10 percent error.

6.0 EMPIRICAL MODEL FOR CORNER FLAME SPREAD

6.1 Introduction

Based on the obtained experimental results of the flame height, the flame spread rate and the heat flux, using a one-dimension heat transfer model which was approved in the last chapter, a thermal model for the corner fire spread will be developed in this chapter. The modeling of flame spread can be conceptually divided into two parts: (1) the determination of the flame spreading velocity v_p at a specified surface heat flux distribution $\dot{q}''(x,t)$; and (2) the modeling of $\dot{q}''(x,t)$ for a given flame spreading.

In the past studies (Saito et al., 1986; Delichatsios, 1987; Mitler, 1990), the heat flux distribution was assumed to be constant up to the flame height and then be zero beyond. Under this assumption, the transient nature of the heat flux only relies on the variation of the flame height with time. This assumption significantly simplifies the heat transfer analysis and was approved applicable to the flame spread on a flat wall with reasonable accuracy.

The circumstances are different for corner wall fires due to the triangle configuration of the flame (see Figure 5-2), the effects from the other side wall flame, and the much stronger fire-induced flow confined by a corner wall. The experimental measurement reveals that the heat flux from the flame to the wall surface varies strongly with both position and time, especially in the preheating period, see Figure 5-14. Hence, it is necessary to model the heat flux as a function of time and height.

In this chapter, an exponential function will be introduced to simulate the heat flux during the preheat period. An analytic solution for the upward flame spread can be obtained for variety of fuel materials, based on the heat flux model and the thermal flame spread model.

6.2 Power Law Correlations for Flame and Pyrolysis Heights

6.2.1 Power Law Relations and Their Limitations

The upward flame spread accelerates with time, in fact, the pyrolysis height and the flame height increase exponentially with time, displayed in the past studies (Orloff, deRis, and Markstein, 1974). Therefore, the flame height x_f and pyrolysis height x_p can be correlated with the spread time t by power law relations, and the power law relations between x_f , v_p and x_p can be deduced, theoretically. Orlloff et al. (1974) obtained the results: $x_f = 5.346x_p^{0.781}$ and $v_p = 0.00441x_p^{0.964}$ in their exploratory study of the flame spread on PMMA vertical flat wall, which have been referred by many researchers since they were published. In this study, by careful analysis we found that the power law relations meet a singularity problem when one relation is used to deduce another one by taking derivation. Generally, if we assume:

$$x_p = At^m, \tag{6-1}$$

then by the definition of the spread rate,

$$v_p = \frac{dx_p}{dt} = Amt^{m-1} = \frac{Am}{A^{\frac{m-1}{m}}} x_p^{\frac{m-1}{m}}. \tag{6-2}$$

If we correlate v_p and x_p directly from the experimental data, it can be obtained,

$$v_p = Bx_p^n. \tag{6-3}$$

Comparing equation 6-3 with equation 6-2, we get,

$$B = \frac{Am}{A^{\frac{m-1}{m}}},$$

and $$n = \frac{m-1}{m} \quad \text{or} \quad m = \frac{1}{1-n}.$$

We can see that these relations do not hold when n = 1. The exponent n could be 1, in fact, it is very close to the unit for the upward flame spread. For example, in the Orloff's results above: n = 0.964, resulted in the exponent m = 27.78 and then x_p is proportional to $t^{27.78}$. This result does not make sense, so this derivation should be avoided because there is a singular point at n = 1. The cause of this singularity is that the power law relation does not represent physics, is only a mathematical approximation. It also should be noted that the coefficient and the exponent in the power relation are only valid in the experimental range, or in the scales of common buildings.

6.2.2 Flame Height and Pyrolysis Height Correlations

Flame height is usually considered as a characteristic length for the heat transfer from the flame to the wall surface, since the scale of the luminous chemical reaction zone dominates radiation and convection. It has also been found that the heat flux somehow correlates with the height normalized by the flame height x/x_f (Hasemi, 1986; Quintere, 1986). Therefore, it is an important step to model the flame height for the heat flux modeling.

In flame spread tests, the flame height was recorded by a video camera and measured on playback screen. Results assembled from three tests with ignition lengths of 20, 30 and 40 cm for corner fires are shown in Figure 6-1. It was observed that the laminar-to-turbulent transition occurred as the flame height reached about 15 cm, and a fully developed turbulent flame was found over 25 cm. For the turbulent flame to the test scale of 160 cm, the flame height can be fit by a power law with the exponent of 1.310 and the correlation coefficient is 0.981. More interestingly, the flame height on a flat vertical wall of the similar scale, even almost 50% lower than the corner.fire flame, can also be fit by a power law with approximately the same exponent of 1.302 with the correlation coefficient of 0.983, see Figure 6-2. The flame height data for the flame spread on the flat wall was provided by Saito's experiments (1985). These analysis shows that the flame height for an upward turbulent flame spread, over the size range of interest here, can be represented by the general relation:

$$x_f = Ct^{1.3}. \tag{6-4}$$

The constant coefficient C is 0.094 for the corner fire, and is 0.051 for the flat wall fire. It will be shown later the power of 1.3 can result in an important simplification in analysis. This flame height model can be further confirmed by the following analysis. In the past studies, the flame height has been studied extensively due to its importance (Ahmad and Faeth, 1979; Delichatsos, 1984; Hasemi, 1986; Quintere and Harkleroad, 1986). The most representative result was given by Delichatsos as:

$$x_f = 4.2\left(\frac{\dot{Q}^2}{\rho_o^{\,2} C_p^{\,2} T_o^{\,2} g}\right)^{\frac{1}{3}}, \tag{6-5}$$

where $\dot{Q}$ is the heat release rate. If the assumption of a constant gasification rate is applied to the pyrolysis zone (see equation. 3-4 and Figure 3-2 for non-charring materials), then the total heat release rate is proportional to the area of pyrolysis. So, we have the relation,

$$x_f \propto \dot{Q}^{\frac{2}{3}} \propto A^{\frac{2}{3}} \approx \left(X_p Y_p\right)^{\frac{2}{3}}, \tag{6-6}$$

where the area of pyrolysis: $A = X_p Y_p$ since the pyrolysis zone can be approximated as a triangle. As it is shown in Figure 5-4 and by equation 5-3, the lateral spread is much slower than the vertical spread. Hence, we can assume Y_p constant compared with X_p in equation 6-6. Introduce Eq. 5-1: $X_p = 0.00299t^{1.84}$ into Eq. 6-6, we can obtain,

$$x_f \propto \left(X_p Y_p\right)^{\frac{2}{3}} \propto X_p^{\frac{2}{3}} \propto \left(t^{1.84}\right)^{\frac{2}{3}} \approx t^{1.23}. \tag{6-7}$$

A very good agreement can be seen between Eqs.6-4 and 6-7. This result supports the power of 1.3 in the flame height model.

6.3 Model of the Heat Flux from Flame to Wall Surface

The measured wall heat flux histories at five different locations are presented in Figure 5-14. These measurement points were distributed along the trajectory of the flame spread peak as indicated in Figure 5-1. In the preheat period, from $t = 0$ to $t = t_p$, the experimental results display increasing heat fluxes with time, and then the heat fluxes approach to a maximum and nearly constant value of 3.25 W/cm^2 when the pyrolysis occurs.

From the above results, spatial heat flux distributions at different moments, corresponding to the different flame heights, can be deduced. Based on the past studies, it was thought appropriate to scale the height x with the flame height x_f in considering the heat flux distribution. Such an analysis was performed by Hasemi (1984) for CH_4 line burner fires against a wall with the heat released rate ranging from 10 to 100 kW/m. Also he reprocessed the data of Ahmad and Faeth (1979) into this form, his results are shown in Figure 6-3. The same analysis of the steady burning of vertical walls, which were made of variety of materials, was performed by Quintiere (1986), his results are shown in Figure 6-4. This approach was used to process the corner wall heat flux data. The result was shown in Figure 6-5. There are some common and important characteristics in the above three results:

(1) The approach of x/x_f does significantly collapse the heat flux data for both flat wall and the corner wall fires. (2) These results are consistent regardless of the different fuels. (3) The levels of heat flux are similar for the flat wall fires, around 2.5 W/cm^2. For the corner wall fire, the heat flux can reach 3.25 W/cm^2. The higher heat flux value is believed due to the corner fire configuration, i.e., the additional radiation from the other side wall fire. These results display that the wall heat flux seems to have an approximately universal distribution when plotted with the distance normalized by the flame height (x/x_f). For the preheat period in the corner fire, that corresponding to the downward-extending leg in figure 6-5, the heat flux can be fit by a power relation: $\dot{q}''=0.822(x/x_f)^{-2.294} \approx 0.822(x/x_f)^{-2.3}$ with a correlation coefficient of 0.926 (see figure 6-5). In Mitler's study (1990), it was shown that the power law relation with the exponent of -2.3 holds for most of the flat wall fires. We also can see that the Hasemi's result with the power of -2.5 is very close to -2.3 in Figure 6-3. Therefore, in general the heat flux can be modeled by the relation:

$$\dot{q}'' = D\left(\frac{x}{x_f}\right)^{-2.3}. \qquad (6\text{-}8)$$

Introduce the flame height model Eq. 6-4 into Eq. 6-8, we have

$$\dot{q}'' = D\left(\frac{x}{Ct^{1.3}}\right)^{-2.3} = Ex^{-2.3}t^{2.99} \approx Ex^{-2.3}t^{3}\ , \qquad (6\text{-}9)$$

where C, D are constants, respectively determined by the flame height and the maximum heat flux, and $E = D/C^{-2.3}$. Equation 6-9 is the general form of heat flux distribution for the vertical flat wall and the vertical corner wall fires. The wall heat flux calculated by the model Eq. 6-9 was plotted against the experimental data obtained before (Figure 5-14) in Figure 6-6. From these plots, we can see the agreement is very good for medium heights (around x=75). In the beginning and the last phases, there are influences from the floor and the ceiling making the situation more complex. Considering the preheat history in the flame spread problem, however, the integration of the heat flux from this model versus time can be expected even better in agreement with the practical case.

6.4 A Thermal Model for the Flame Spread

The flame spread occurs as a consequence of heating of the unignited portion of the fuel to a temperature at which the vigorous pyrolysis begins. In general, we assume that the pyrolysis front reaches a point x_p exactly when the surface temperature at that height reaches the pyrolysis temperature of the wall material, T_p. If we assume that the thermophysical characteristics, k, ρ and c of the material are independent of temperature. A semi-infinite solid, the heat flux at $y = 0$ is a prescribed function of time and height $\dot{q}''(x,t)$, and the initial temperature is T_a, the ambient temperature. Then it can be shown (Carslaw and Jaeger, 1959) that the surface temperature T_s is given by

$$T_s(x,t) = T_a + \frac{1}{\sqrt{\pi k \rho c}} \int_0^t \frac{\dot{q}''(x,\tau)}{\sqrt{t-\tau}} d\tau . \tag{6-10}$$

Let T_s equal to T_p, x equal to x_p, the equation above can be written as:

$$\int_0^t \frac{\dot{q}''(x_p,\tau)}{\sqrt{t-\tau}} d\tau - \sqrt{\pi k \rho c}\left(T_p - T_a\right) = 0 \tag{6-11}$$

Equation 6-11 is the basis for the thermal model. Although this equation is practically useful, it has some limitations because a number of simplifying assumptions were made in this heat transfer model:

(1) The heat transfer in the preheat zone was modeled as one-dimensional heat transfer. The lateral heat transfer can be neglected due to the approximately uniform heat conduction in

the x direction, and a minor heat conduction in horizontal direction. This can be proved by the previous experimental study that revealed an almost constant surface temperature gradient in preheat zone(Qian and Saito, 1992). This simplification provides about 90% agreement with experimental results for vertical flame spread (Chapter 5). However, for other slower flame spreads the disagreement may be significant.

(2) This model is for semi-infinite slabs and may not be accurate for finite thickness slabs, particularly when it gets thinner. It was found the thermally thick assumption is inaccurate for the fire on the PMMA slabs of the typically used thickness of 10 or 20 mm (Kulkarni and Kim, 1990). Moreover, the value, kρc is a function of temperature for most of the fuel materials, however, it is difficult to obtain its functional relationship either by experiment or by theoretical analysis.

Introduce the heat flux model Eq. 6-9 into Eq. 6-11,

$$\int_0^t \frac{E x_p^{-2.3} \tau^3}{\sqrt{t-\tau}} d\tau - \sqrt{\pi k \rho c}\left(T_p - T_a\right) = 0, \qquad (6\text{-}12)$$

and then solve this equation for the pyrolysis height x_p as a function of time t and the fuel material properties, it was obtained

$$x_p = \left[\frac{E \int_0^t \frac{\tau^3}{\sqrt{t-\tau}} d\tau}{\sqrt{\pi k \rho c}\left(T_p - T_a\right)} \right]^{0.435}, \qquad (6\text{-}13)$$

where $\int_0^t \frac{\tau^3}{\sqrt{t-\tau}} d\tau = \frac{96}{105} t^{\frac{7}{2}}$ by an integral relation. At last, the predicted pyrolysis height by this model:

$$x_p = \frac{0.962D^{0.435}}{C^{0.566}(\pi k\rho c)^{0.217}(T_p - T_a)^{0.435}} t^{1.523} , \qquad (6\text{-}14)$$

where C and D are constants from the flame height model (Eq. 6-4) and the heat flux model (Eq. 6-8), and x_p is in centimeter and t in second.

For PMMA corner fire tests, $T_p = 376$ °C, $T_a = 20$ °C and $k\rho c = 0.0102$ $(W/cm^2K)^2s$. The calculated pyrolysis height can be obtained as:

$$x_p = 0.0136t^{1.526} . \qquad (6\text{-}15)$$

Equation 6-15 is compared to experimental results in Figure 6-7: very good agreement for the early period, poor agreement for the later period due to the failure of thermally thick assumption(Chapter 5).

The flame spread model includes three parts: flame height model, wall heat flux model and heat conduction model. It can be applied to calculate the time for a fire to spread from the floor to the ceiling and calculate the heat release rate of a corner fire with the similarity model for pyrolysis front (Eq. 5-4). And this model also provides a better understanding of the flame spread phenomenon. We can see how material properties and ambient conditions influence the flame spread rate in equation 6-14. The exponents 1.3 in the flame height correlation and 2.3 in the heat flux correlation are scale dependent, i.e., they only hold in the flame spread test scale. The constants C and D are largely fire configuration dependent.

7.0 SUMMARY AND CONCLUSIONS

7.1 Principal Conclusions

In this study, the infrared imaging system has been developed and successfully applied to the fire research. A stationary gas burner and large scale PMMA samples were utilized with a room corner model to simulate the room corner fires. The flame spread characteristics, fluid dynamics and heat transfer aspects of corner fires were investigated experimentally. A thermal model for the upward flame spread has been developed. The model includes three parts: the flame height model, the heat flux model and the heat conduction preheating model. The principal conclusions drawn from this study are presented as below:

(1) The Infrared Imaging Technique and Its Application to Fire Research

Infrared radiometry and image analysis are an effective tool in fire research associated with flame spread. The surface temperature measurement through flames using IR imaging technique has been addressed both theoretically and experimentally. For most materials, the constant emissivity 1.0 can be used to determine the pyrolysis front temperature due to soot deposition on the pyrolyzing material surface. The flame effect consists of band emissions mostly from excited CO_2 and H_2O and a continuous emission from soot particles. The effects of the band emissions can be eliminated by a bandpass filter ($10.6 \pm 0.5\ \mu m$), and the soot particle effect can be neglected ($\varepsilon < 0.03$) for wall fires due to the small optical depth and the medium sooting tendency. The remarkable feature of the IR imaging system is that it can measure temperature on a large area with high resolution, and high frequency. The target surface is not needed to be prepared. Two-dimensional flame spread rate, the area of pyrolysis zone and other information can be obtained by image processing from the IR thermal images. The IR imaging technique also can be used to measure the flame height and geometry from large scale pool fires.

Measurements that were difficult several years ago now can be made without excessive effort because of technological advances. The IR imaging system enables the corner fire spread mechanisms to be ascertained with high degree of confidence. If an attempt was made to duplicate the same measurement by thermocouples, the work would be not only extremely elaborate, but also may not be as accurate as IR results.

(2) The Fire-induced Flow and Ceiling Effects

The pulsation of the flame can induce air puffing in a relatively large area around the plume by a pressure transmission. A non-symmetric fire configuration can produce a concentrate vortex in its plume. The vortex with a very strong axial flow may enhance combustion largely. For a transient flame spread process, the flame pulsation and the vortex formation in the plume are important elements to understand the turbulent entrainment and mixing. Heat flux and temperature measurements conducted with and without ceiling demonstrate that the effects of the ceiling on the heat transfer to the wall are quite significant.

(3) M-shaped and T-shaped Pyrolysis Fronts

M-shaped pyrolysis front formation occurred for the flame spread along the vertical corner wall regardless of the effects of ignition mode, solid phase conduction heat loss, and fire induced cooling. It is primarily due to the flame displacement effect near the wall corner. With the ceiling effects, a jumping spread occurred as the ceiling and the intersection wall were ignited before the M-shaped pyrolysis front reached this area. After the flame tip reached the ceiling, the pyrolysis front became T-shaped by connecting the ceiling pyrolysis zone and the M-shaped pyrolysis front. The vertical flame spread rate increases with the increasing of ignition length up to 20 cm, while the horizontal spread remains almost constant. A similarity model has been developed to successfully simulate the progressing M-shaped pyrolysis fronts.

(4) The Spread Rate and The Power Law Correlation

Although the acceleration process of flame spread is not necessarily exponential, good approximation can be provided by the power law relations. Great care should be taken in the mathematical deduction of these empirical relations when the lack of the physics is evident. Flame height for the flat wall and the corner wall fires is primarily proportional to the elapsed time to the 1.3 power, even the flame on the corner wall is almost twice higher than the flame on the flat wall. This conclusion supports the previous findings that the flame height is proportional to the energy release rate to the 2/3 power. The flame spread rate is essentially proportional to the pyrolysis height, but the upward spread rate for the corner fires is about three times faster than that for the same scale vertical flat wall fire, i.e., $V_p = 0.0134\ X_p^{0.944}$ versus $V_p = 0.00441X_p^{0.964}$ (Orloff et al., 1975). The high spread rate is mainly due to a strong fire-induced flow that enhances the heat convection and radiation to the walls.

(5) Modeling Corner Wall Heat Flux

Transient heat fluxes tend to have an universal distribution when plotted with the vertical distance normalized by the instant flame height (x/xf). By correlating the experimental data, the heat flux in preheating period can be modeled as:

$$\dot{q}''(x,t) = E\left(\frac{t^3}{x^{23}}\right),$$

where E is a constant, depending on the maximum value of heat flux corresponding to the fire configuration. This formulation includes the steady state wall fire heat flux distribution model as a special case when the time, t is constant. Furthermore, the model considered here, with the variable, t, to the integer power 3, yields a simple integration for calculating temperature. This approach was less satisfactory in low and high positions on the corner wall where effects of the floor and the ceiling were observed. But the overall agreement with experiments is acceptable.

(6) Modeling Flame Spread along Corner Wall

Based on the thermally thick assumption, the transient heat conduction in solid fuel interior can be simulated by the one-dimensional conduction model in a semi-infinite solid, exposing to a variable heat flux. In spite of neglecting the lateral heat diffusion, this model provided 90% agreement with experiments in pyrolysis height prediction. Flame spreads much faster on the corner wall than on the flat wall, so that the one-dimensional heat conduction model is applicable to the corner fires. Substantial unsteadiness was observed in preheating of the solid fuel. Comparing the measured pyrolysis height with the prediction, the thickness of PMMA sample 12.7 mm was found to dissatisfy the thermally thick assumption. Applying the transient heat flux model to this heat conduction model, the pyrolysis height can be given by:

$$x_p = \frac{Ft^{1.523}}{(\pi k \rho c)^{0.217}(T_p - T_a)^{0.435}},$$

with $F = 0.962(D^{0.435}/C^{0.566})$, where the C and D are from flame the height and the heat flux correlations.

The results of this study hold for the turbulent room fires, while for the small scale fires where laminar flames dominate heat transfer and large wall fires where flame radiation dominate the heat flux, these correlations and models should begin to fail.

7.2 Future Research

Based on the findings from this study, the following areas are recommended for future research:

(1) The general flow structure induced by a spreading wall fire along corner walls with a ceiling should be investigated. This includes the flow structure study of fire plume at the intersection of the corner walls and the ceiling. The horizontal flame extensions were observed to have a distinct spiral structure. The formation of these vortices remains unclear.

(2) To further understand the detailed heat transfer mechanism, the measurement of heat flux distributions on the ceiling and intersection walls are needed. The radiation and the convection to the wall need to be measured separately in order to model both of them based on different mechanisms.

(3) Development of a numerical model to simulate the heat conduction process in solid phase is useful to understand the three-dimensional, unsteady heat transfer mechanism, and to further confirm the one-dimensional heat transfer model.

(4) Further theoretical work is needed to construct a three-dimensional model for predicting upward flame spread behavior along the vertical corner walls. This should include the development of a model to predict flame height. The interaction of the fire plume with the wall boundary layer needs to be investigated.

(5) Using the IR technique, which is capable of two-dimensional flame spread

measurements, the effects of sample width in the upward flame spread on a vertical flat wall can be investigated. The significant edge effects were observed from a parabolic pyrolysis front.

(6) From a fire safety point of view, it will be very useful to extend this research in order to study: (a) the unsymmetrically ignited corner fire spread, (b) the flame spread under a ceiling, and (c) the flame spread from the floor to a vertical wall, because actual room fires could occur under these conditions.

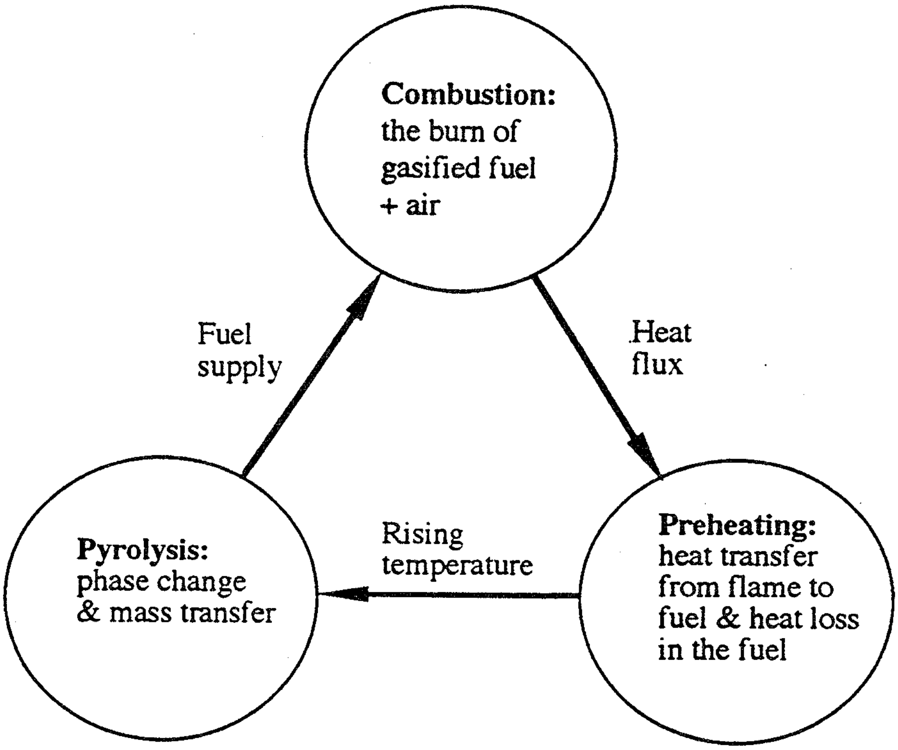

Figure 2-1 Depiction of the flame spread mechanism on solid fuel

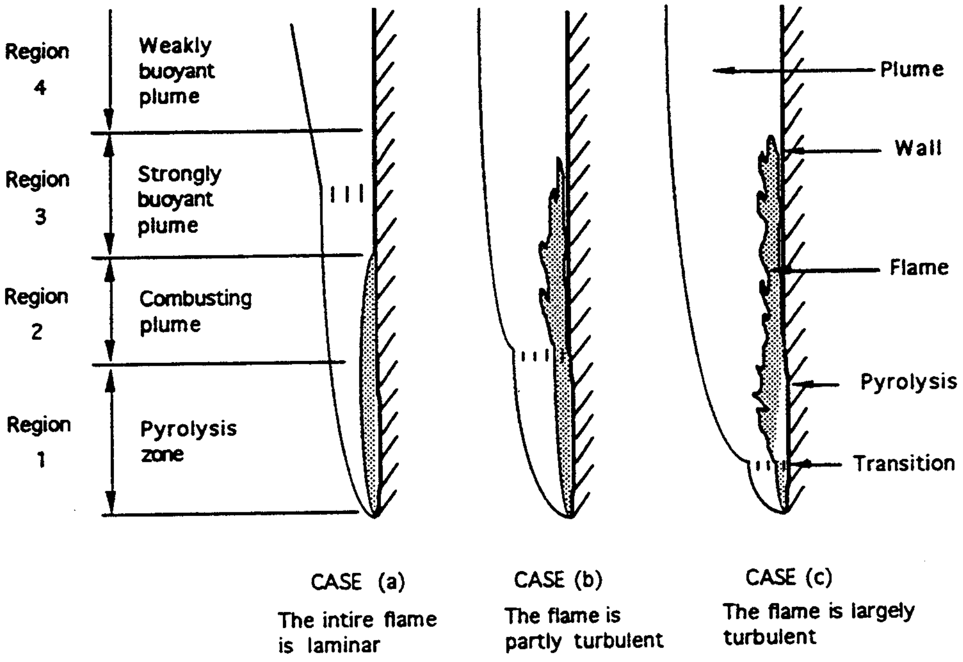

Fig. 2-2 Sketch of fires and plumes on vertical wall (modified from Ahmad)

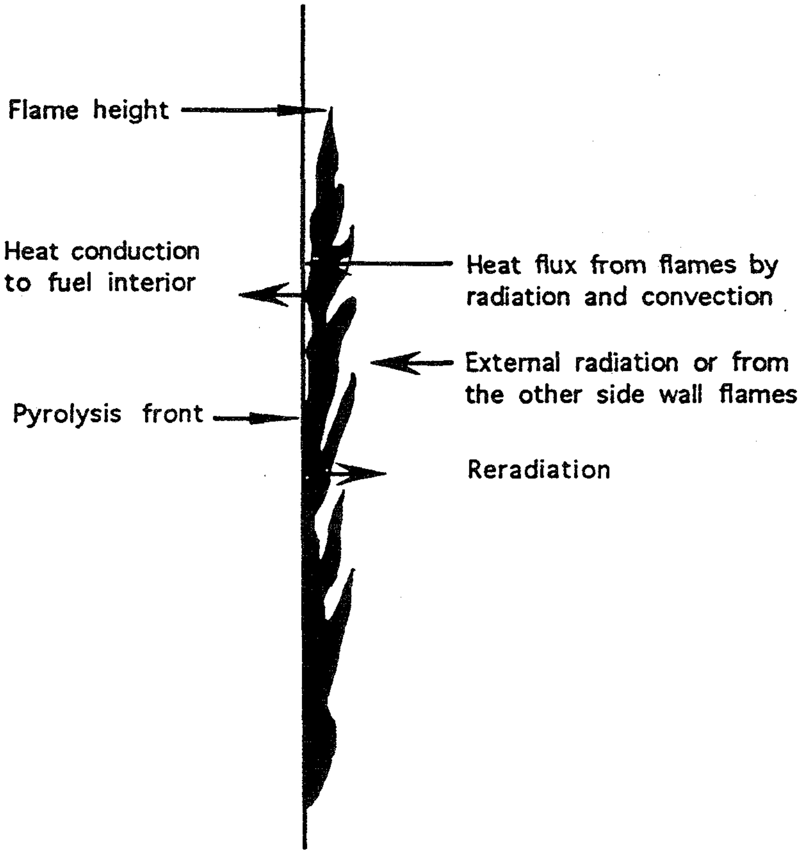

Figure 2-3 Cross section geometry of a fire on vertical wall or corner walls

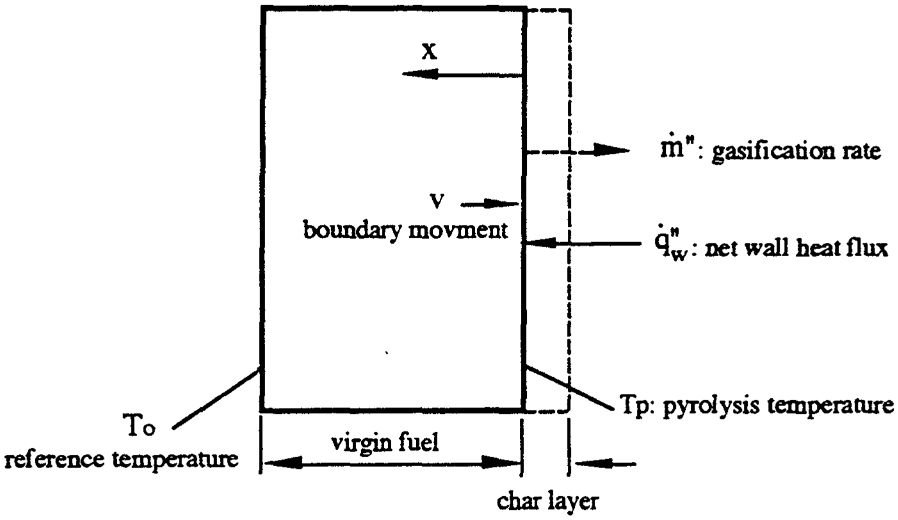

Figure 2-4 Solid fuel gasification, charing and heat transfer processes

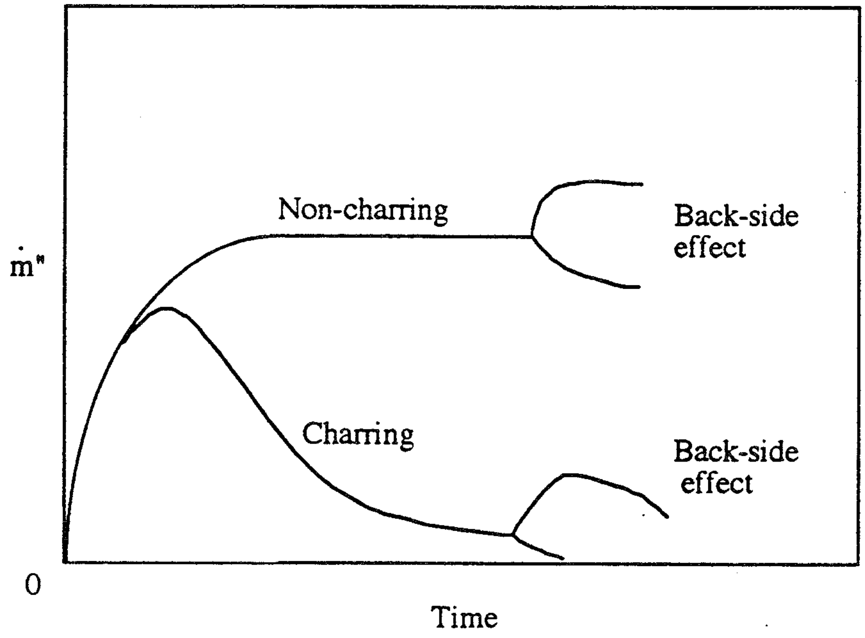

Figure 2-5 Qualitative description of gasification rates for charring and non-charring solid fuels (from J. Quintiere, 1992)

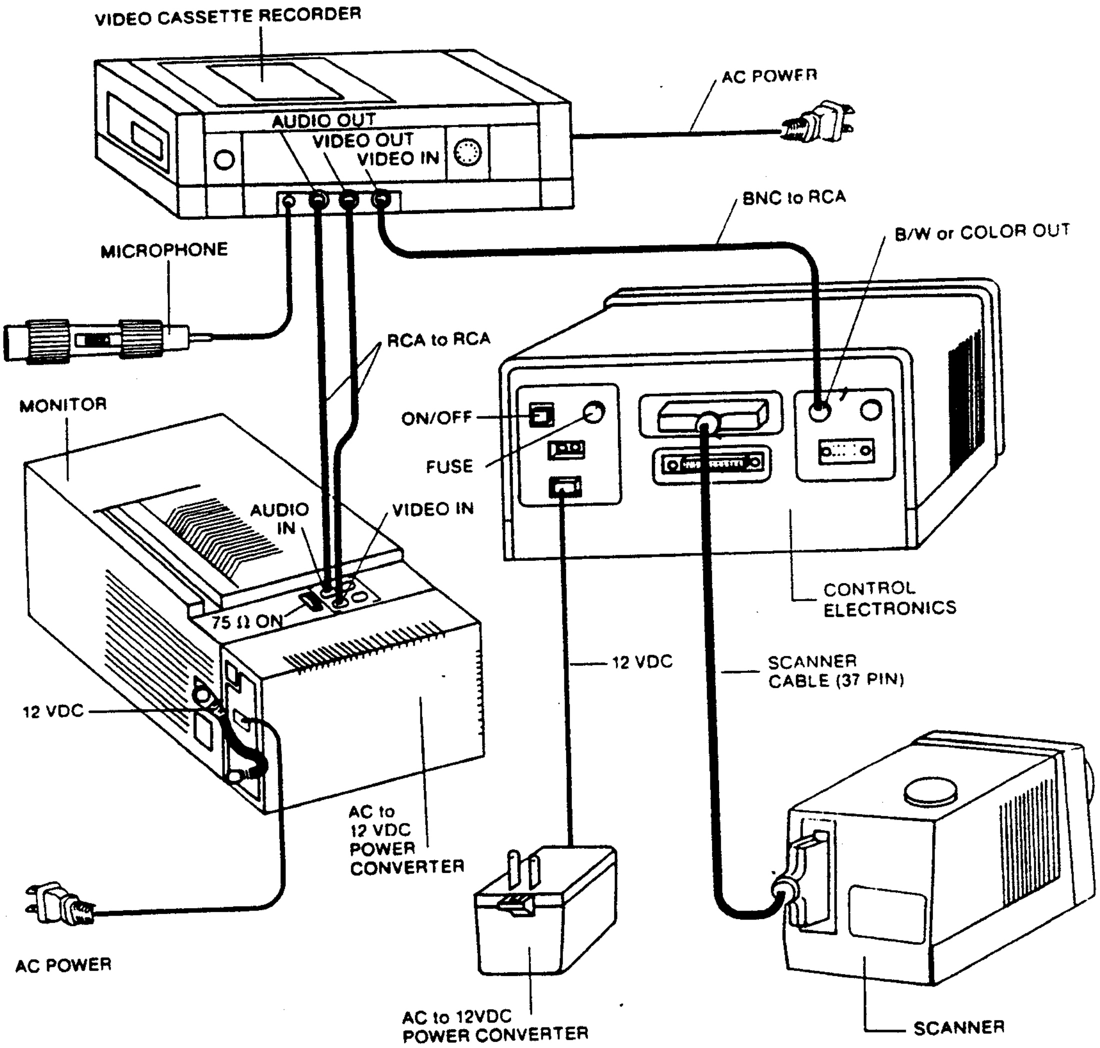

Figure 3-1 IR camera system 600 and electrical connections for thermal image recording

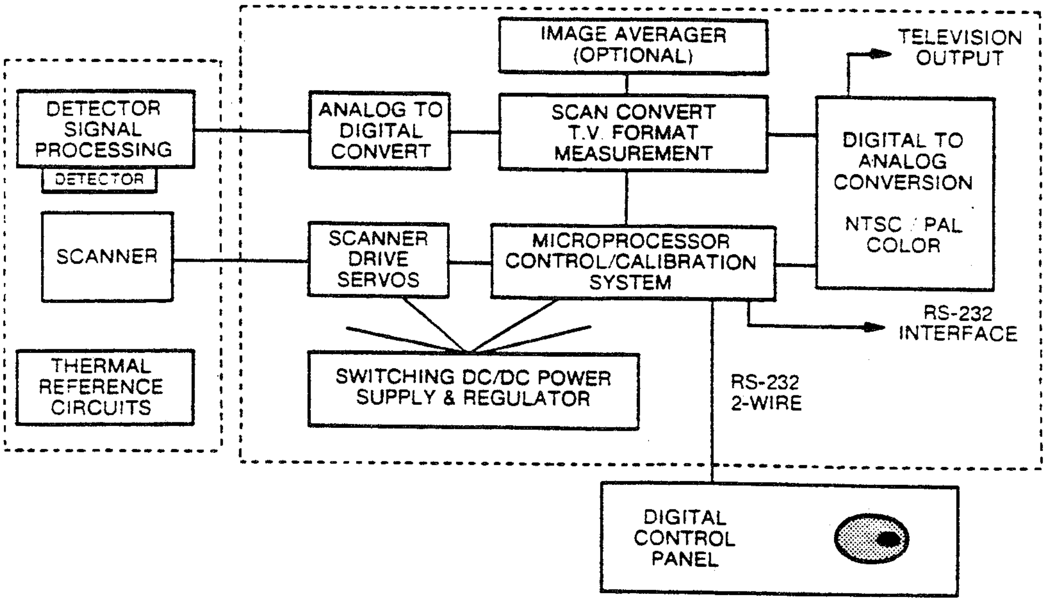

Figure 3-2 Electronics block diagram for infrared imaging system Model 600

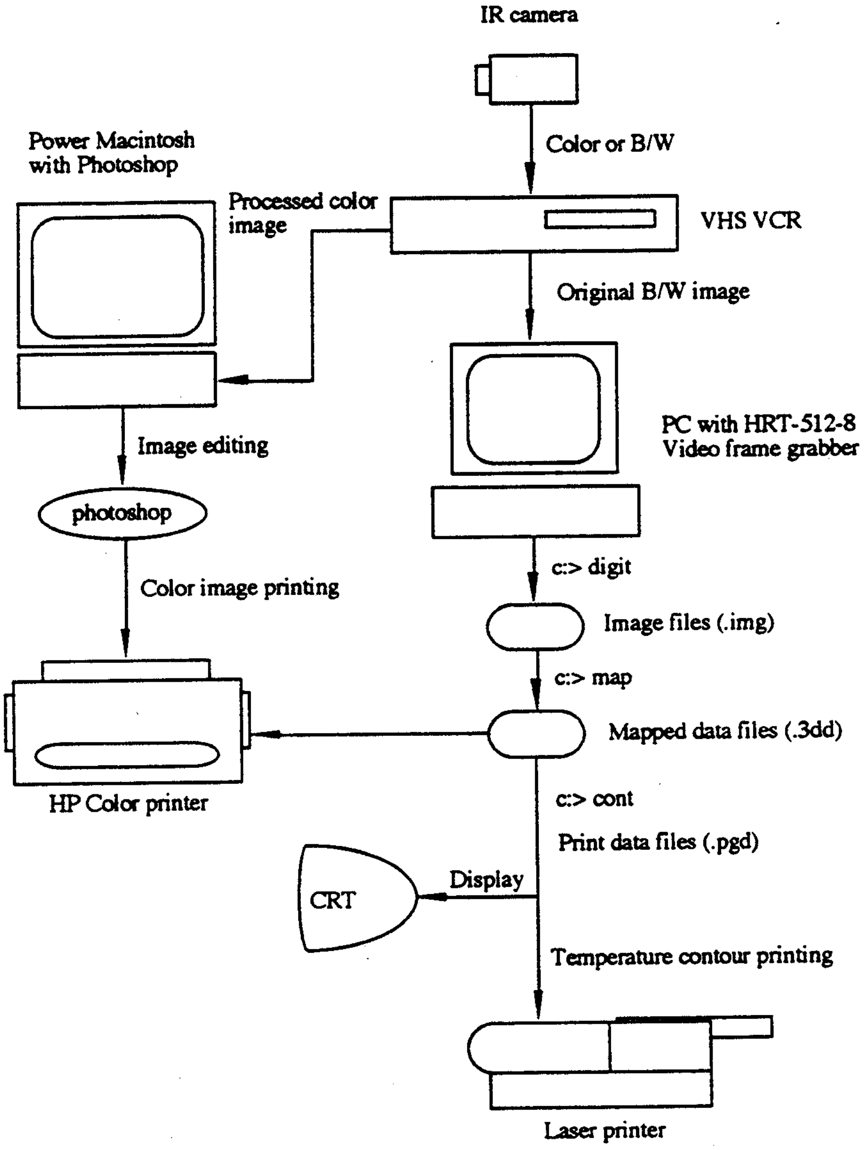

Figure 3-3 IR image processing system and procedure

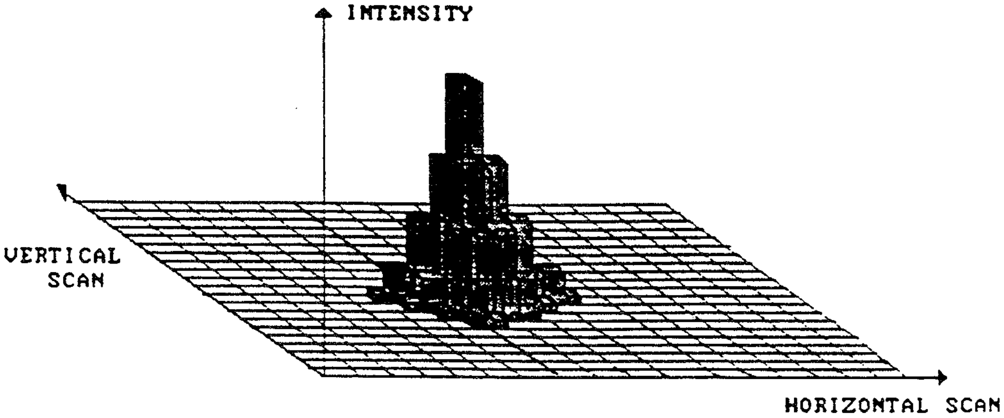

Figure 3-4. A typical electro-optical imaging system's reponse to a point source

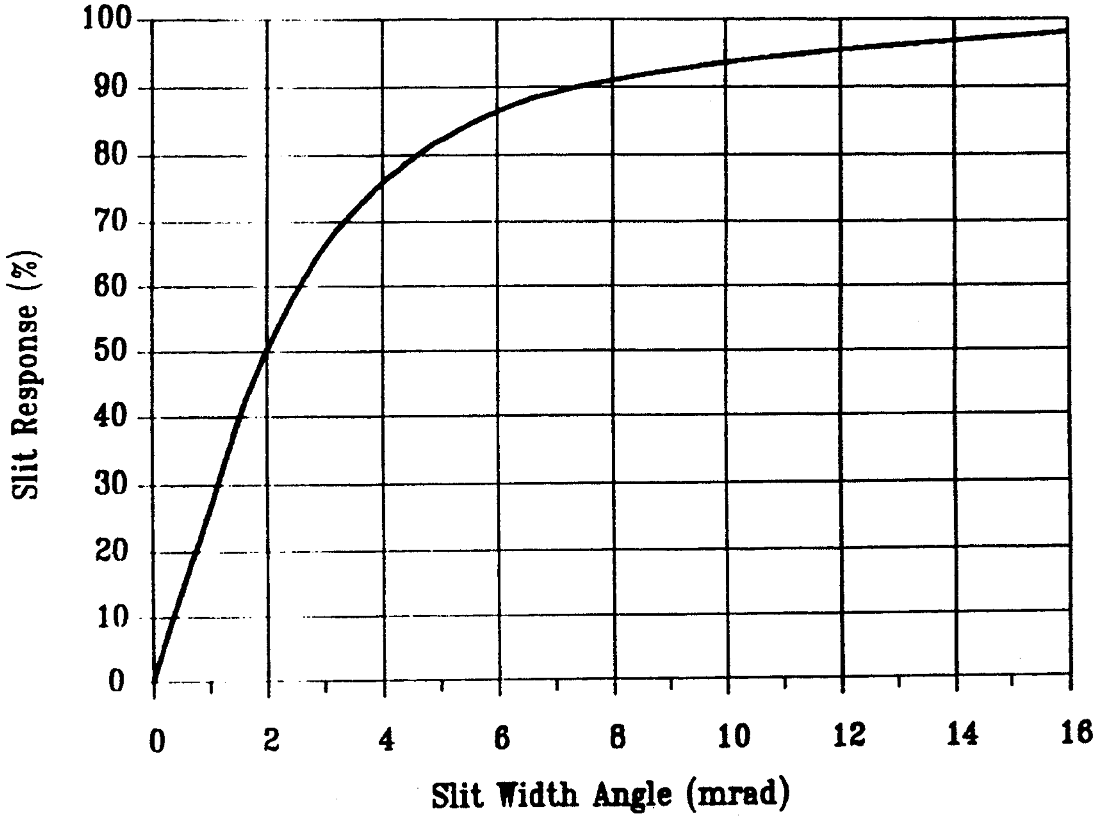

Figure 3-5 Typical slit response function

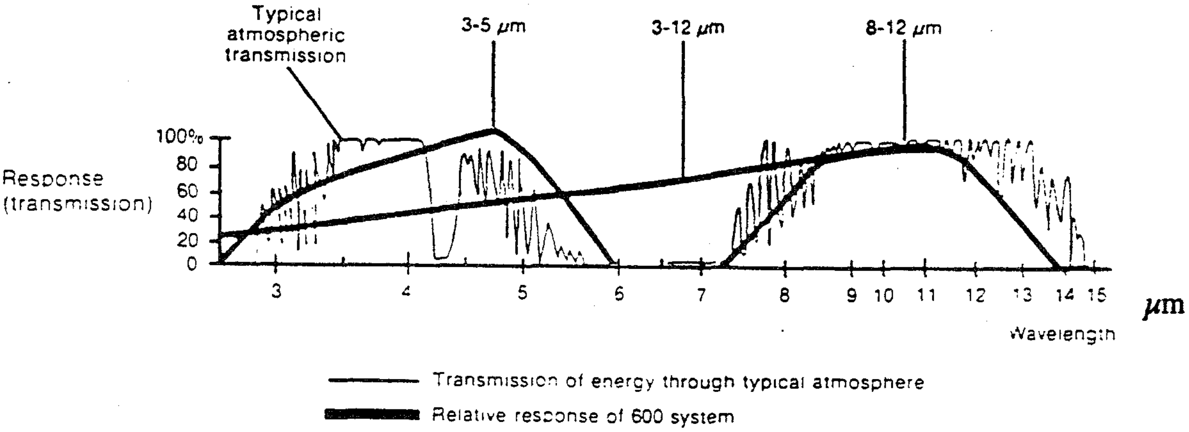

Figure 3-6 Atmospheric transmission and relative response of the model 600 infrared imaging system

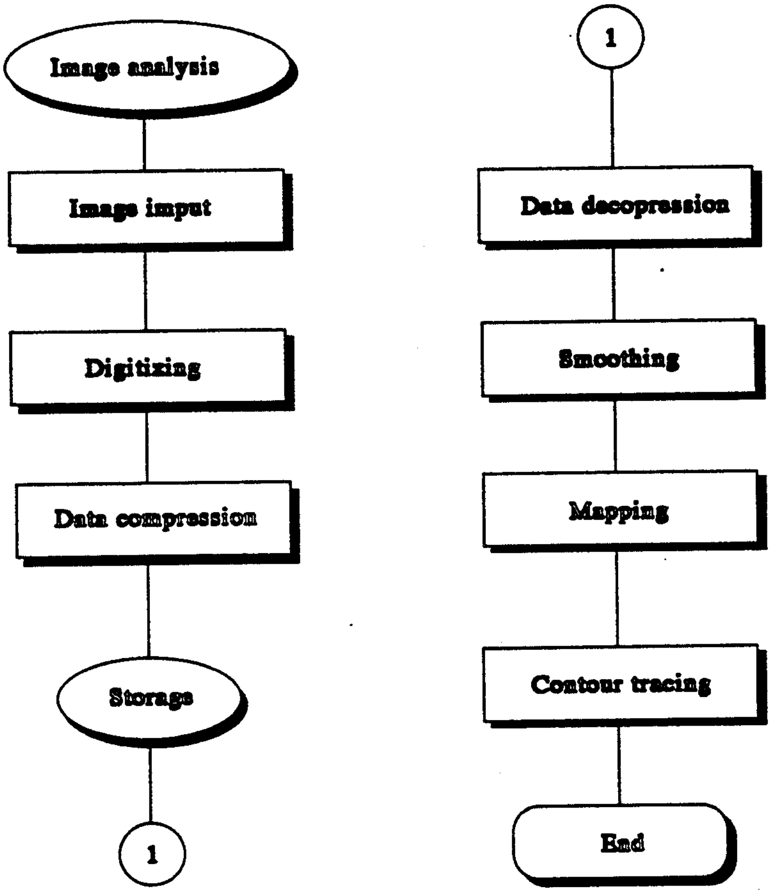

Figure 3-7 IR image analysis flow chart

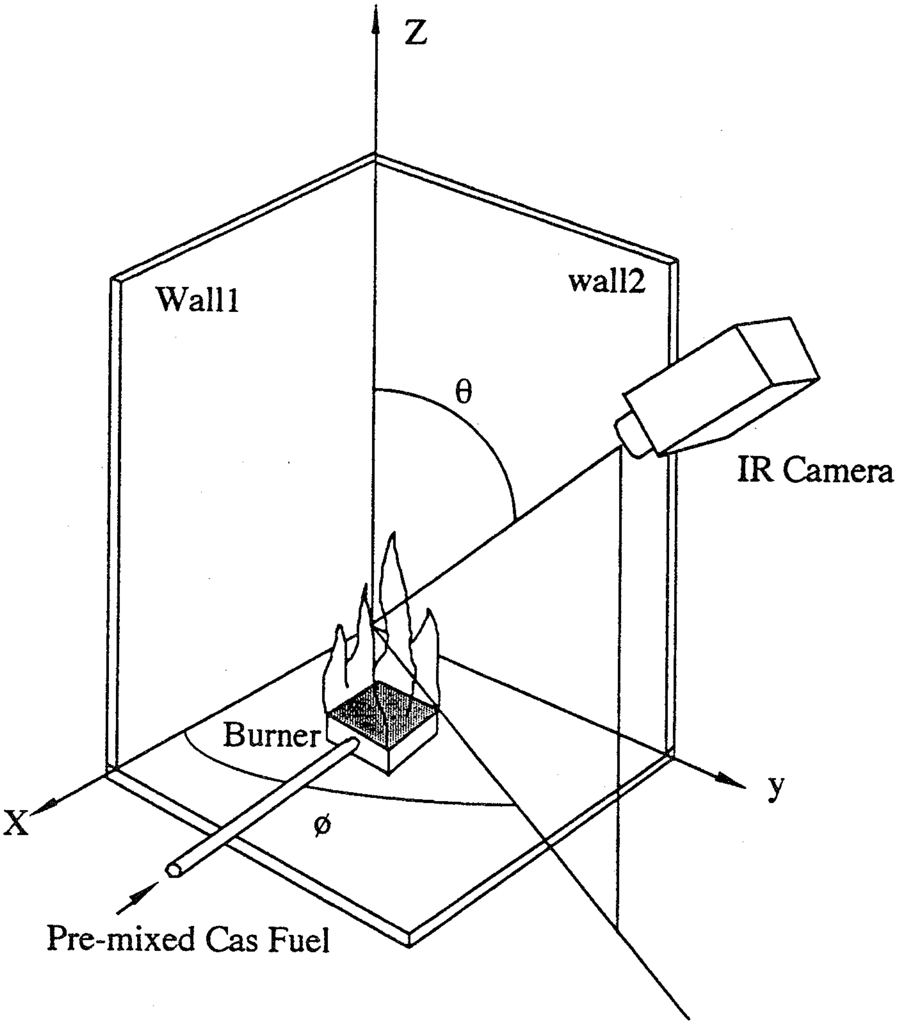

Figure 3-8 Schematic of the IR camera setup to get two thermal images through flame and without the flame at the same time

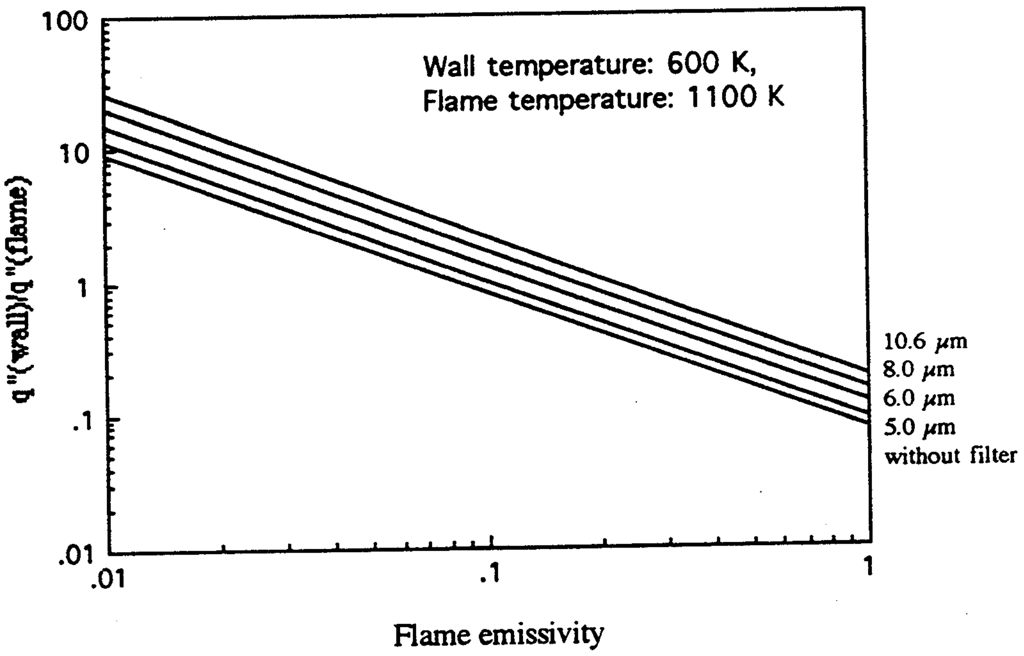

Figure 3-9 The ratio of wall radiation to flame radiation as a function of flame emissivity with band pass filter and without filter. Wall temperature: 600 K, flame temperature: 1100 K.

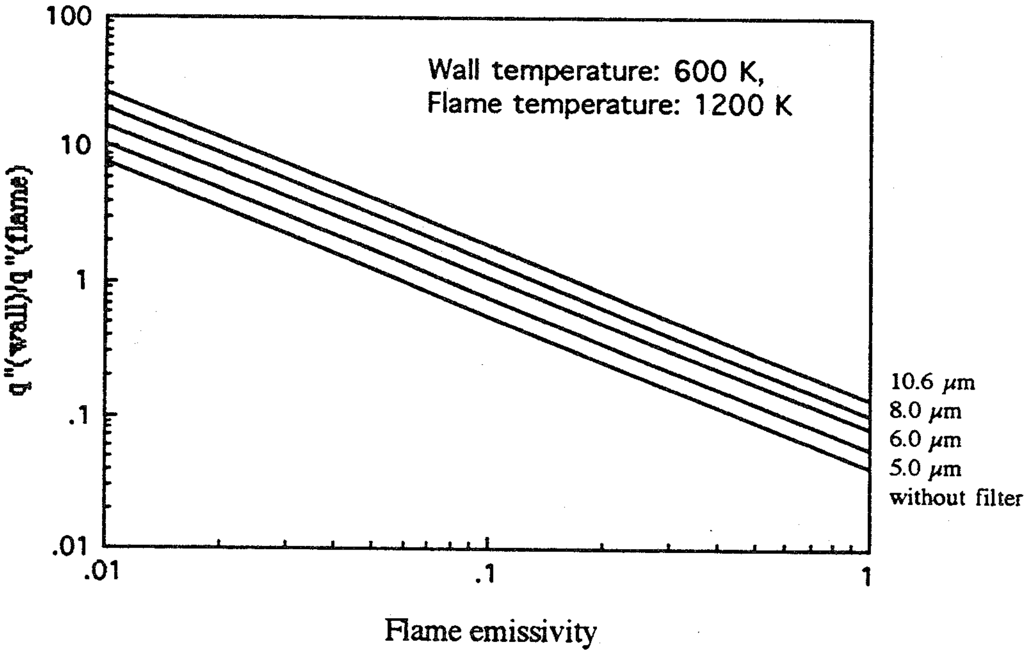

Figure 3-10 The ratio of wall radiation to flame radiation as a function of flame emissivity with band pass filters and without filter. Wall temperature: 600 K, flame temperature: 1200 K.

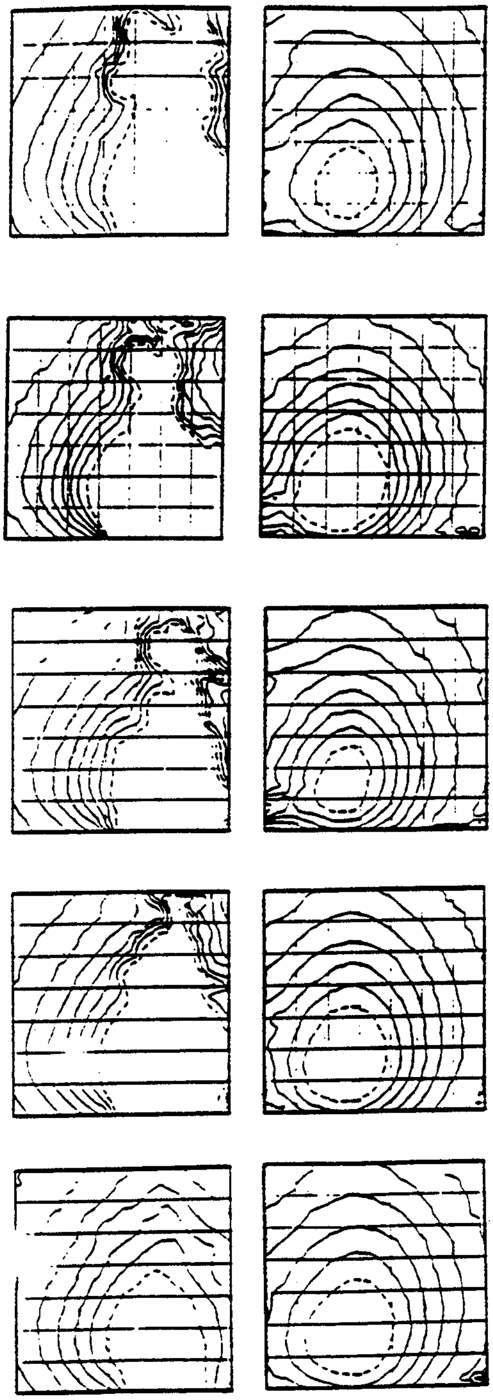

(a) Without filter

(b) Using 5.0 μm filter

(c) Using 6.0 μm filter

(d) Using 8.0 μm filter

(e) Using 10.6 μm filter

Figure 3-11 Wall temperature profiles measured using IR imaging system with and without band-pass filters; left column: results passing through a propane-air premixed flame; right column: results without passing through the flame.

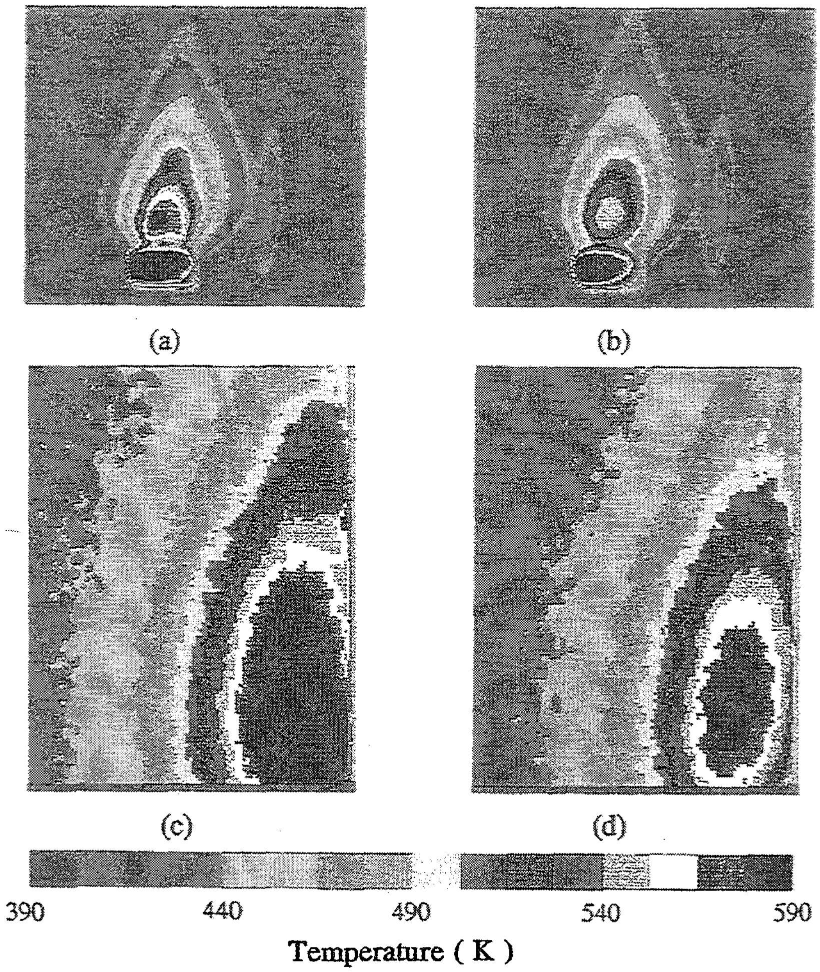

Figure 3-12 Color-coded infrared images of a fire-heated wall. Top: 18 kW blue methane-air premixed flame as a fire source. Bottom: a 10 cm diameter sooty and yellow hexane pool flame as a fire source. The images (a) and (c) are at a steady condition, and were obtained through the flame using the 10.6 μm bandpass filter, (b) is 1 s after the burner was turned off and (d) is 4 s after the flame was quenched.

Heat Flux = 20 W/cm² Stand-off Dist. = 5 cm

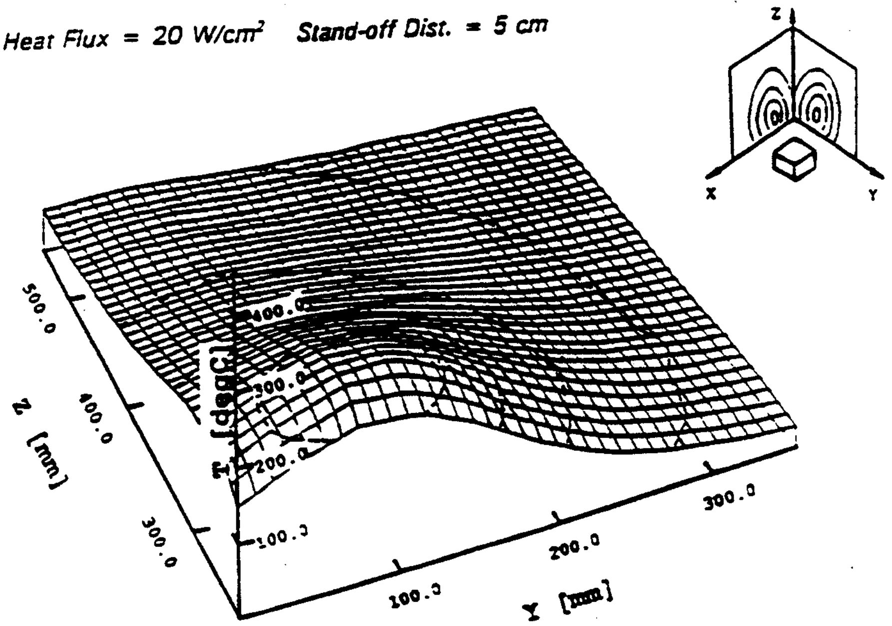

Heat Flux = 80 W/cm² Stand-off Dist. = 5 cm

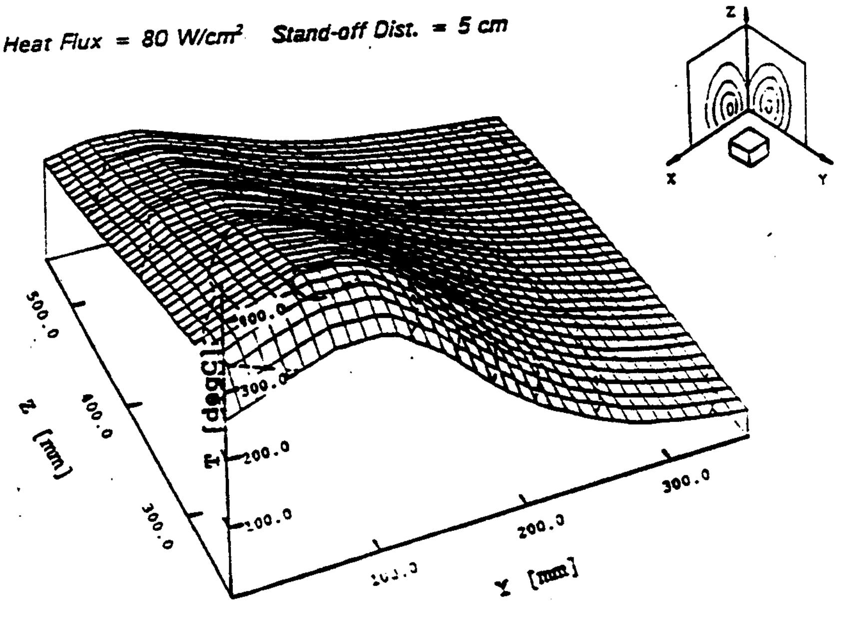

Figure 3-13 Three-dimensional perspective of the thermal images from gas burner heated wall. Burner stand-off distance is 5.0 cm. Burner heat flux is 20 (top) and 80 (bottom) W/cm ^{2}

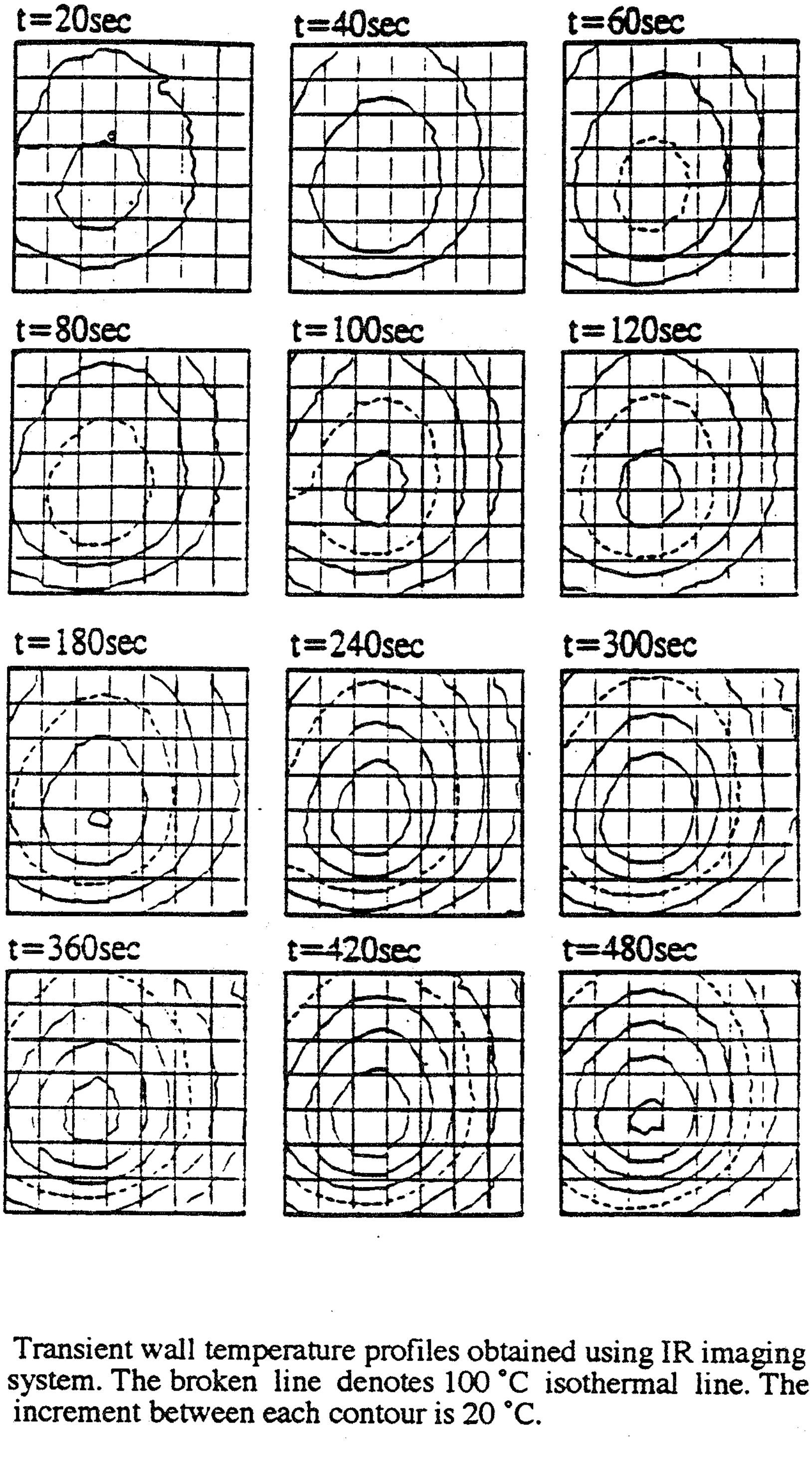

Figure 3-14 Transient wall temperature profiles obtained using IR imaging system. The broken line denotes 100 °C isothermal line. The increment between each contour is 20 °C.

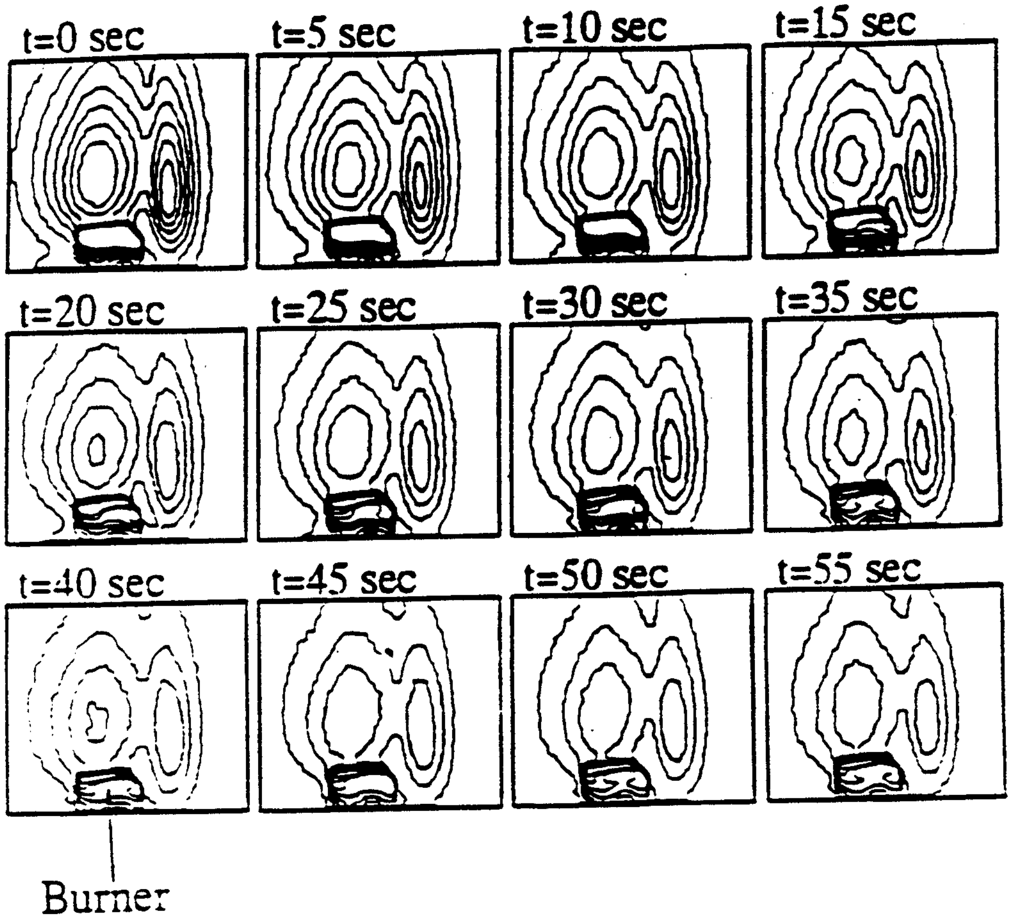

Figure 3-15 Isothermal contours of the cooling corner walls obtained by the IR maging system. Outmost contour: 60 °C, Increment: 20 °C.

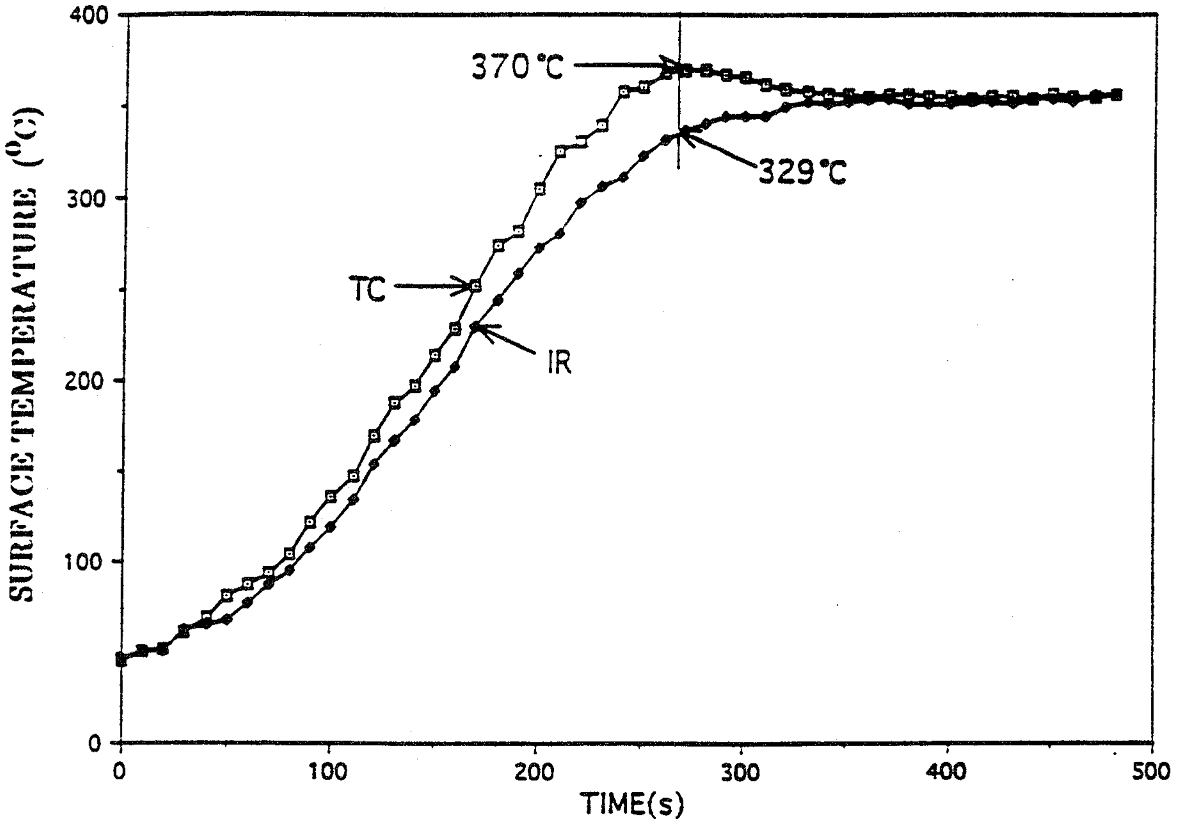

Figure 3-16 A PMMA surface temperature history during flame spread measured with a 0.07 mm diameter chromega-alomega thermocouple (TC) and IR camera (IR). Emissivity setup for the IR camera is one.

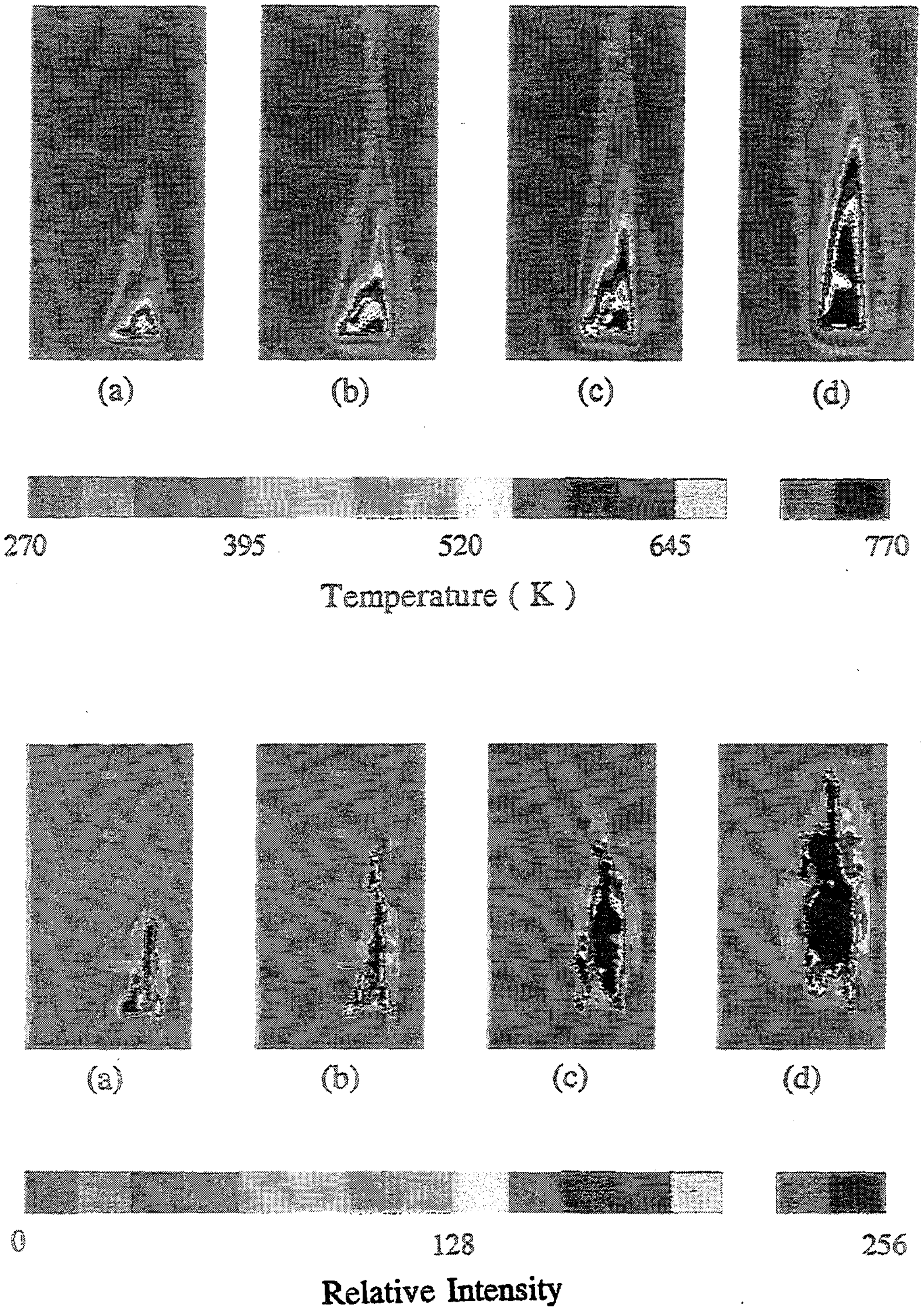

Figure 3-17 Color-coded infrared images for upward flame spread along vertical corner walls made of black cardboard. Top: infrared images obtained using IR camera with a bandpass filter 10.6 ± 0.5 μm every 10 s after ignition. Bottom: video camera images recorded at the corresponding time periods to the infrared images.

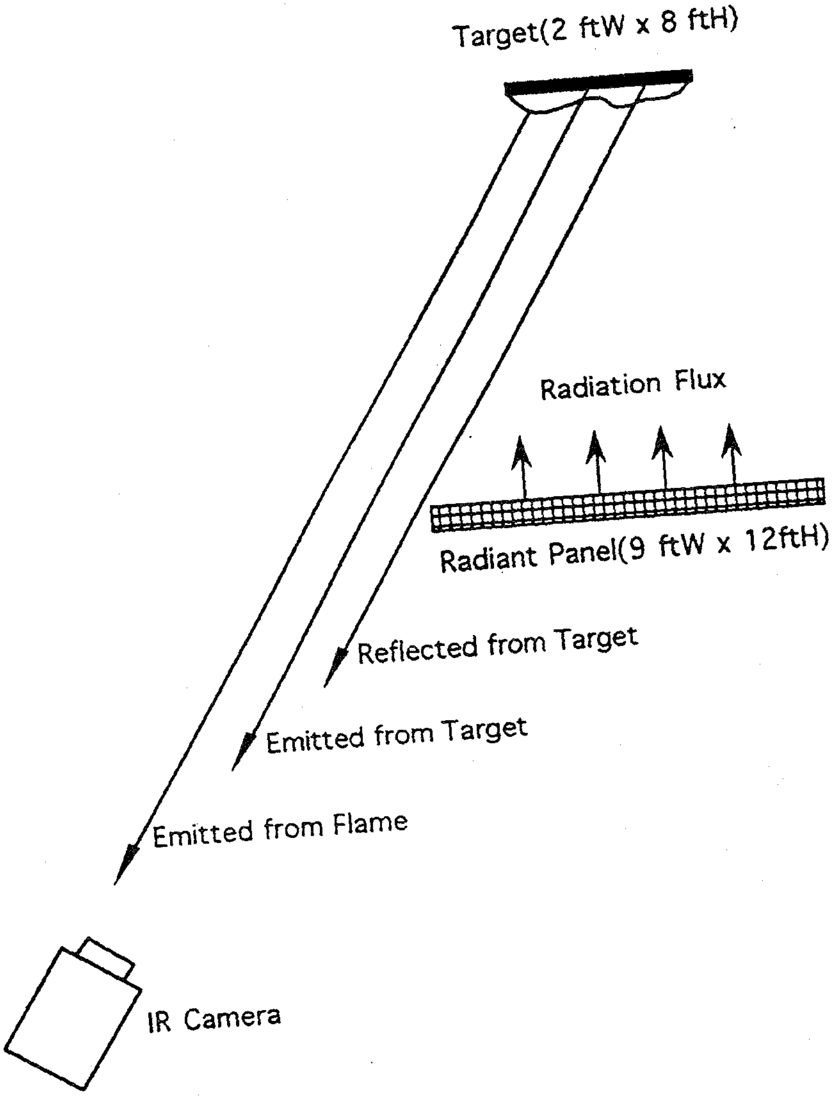

Figure 3-18 Experimental set-up and target radiosity.

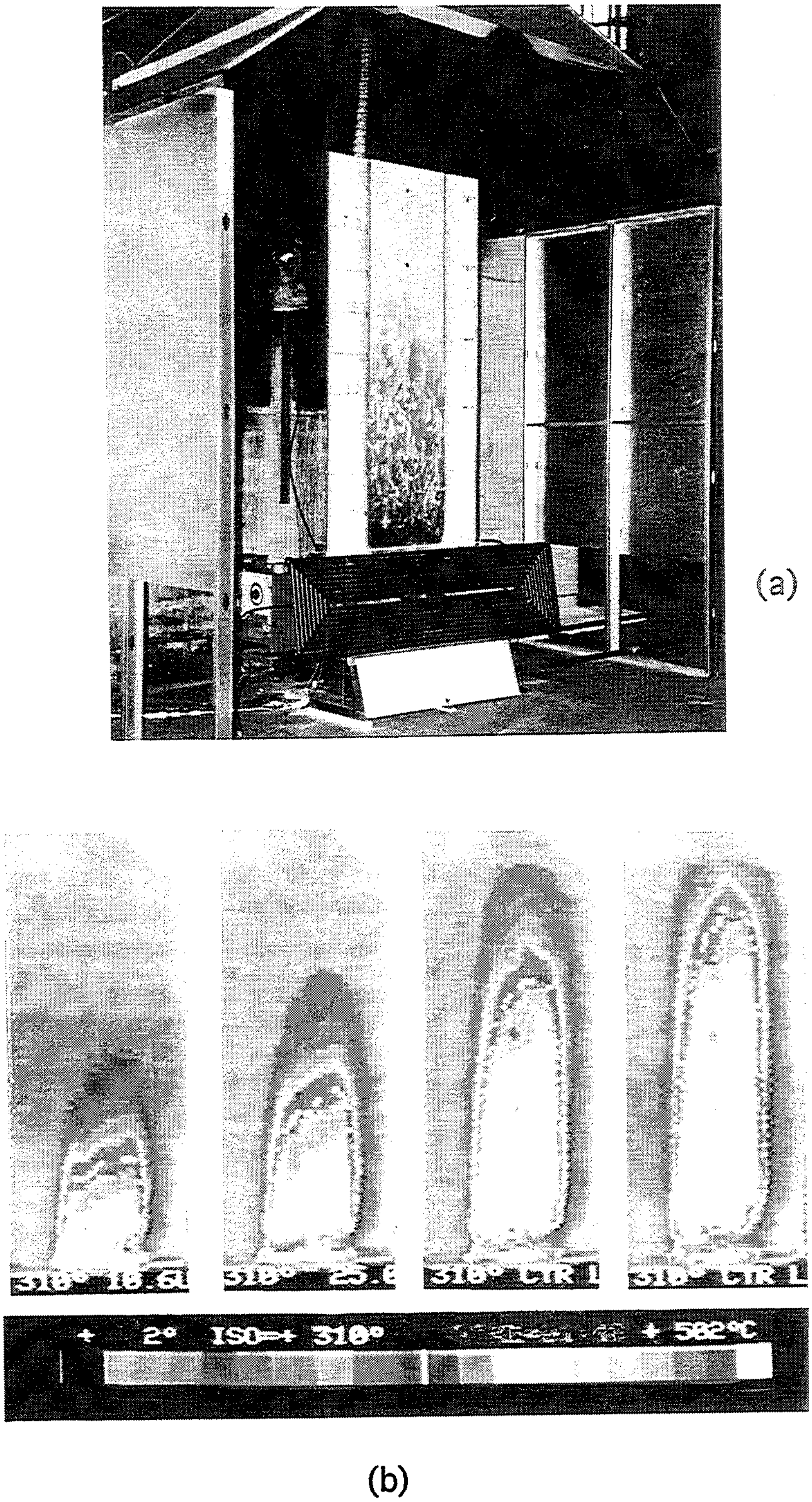

Figure 3-19 Flame spread on large scale plywood with external heat flux: (a) a direct photograph of the flame and the experiment setup; (b) The digital infrared images of the burning surface. In these images, pyrolysis fronts were high lighted by fine white spots.

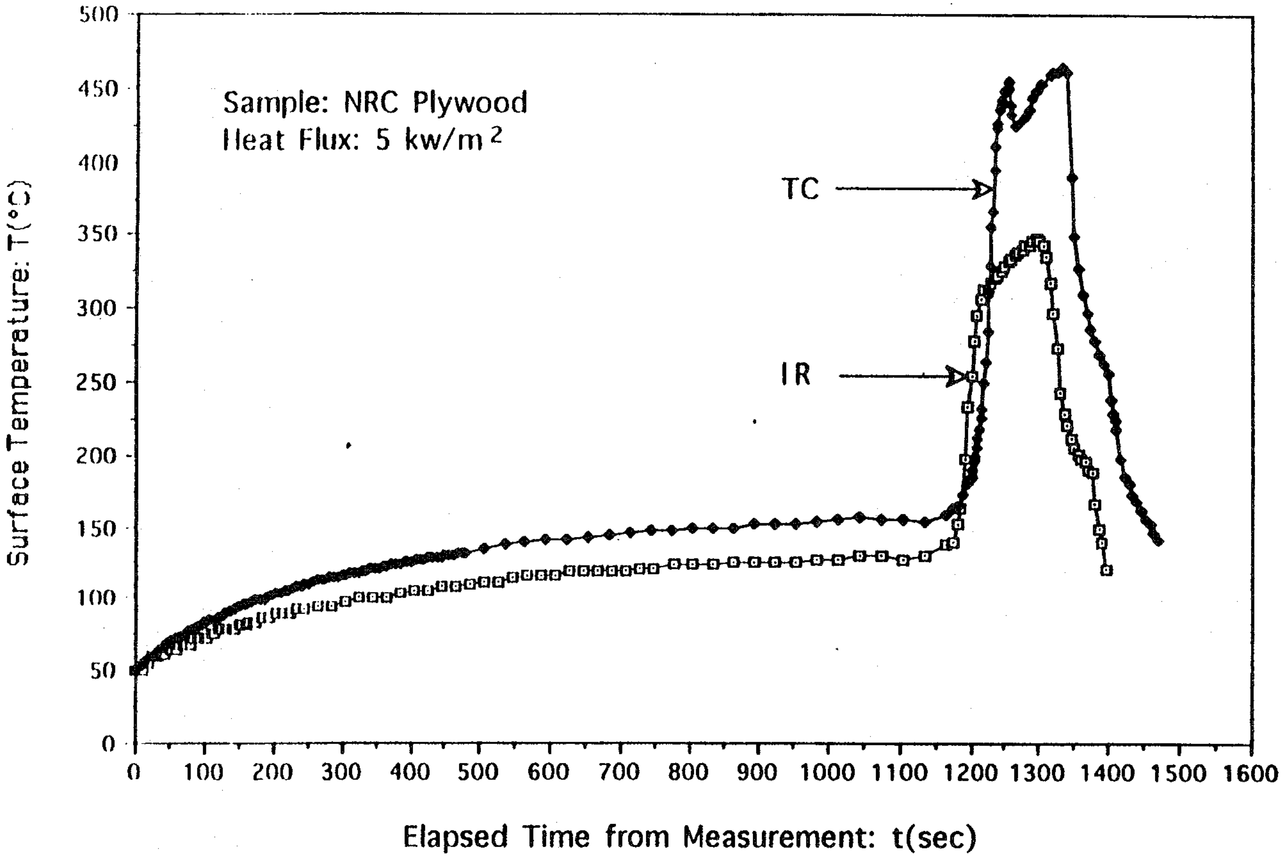

Figure 3-20 Comparison of the surface temperature histories at reference point measured by thermocouple and IR camera

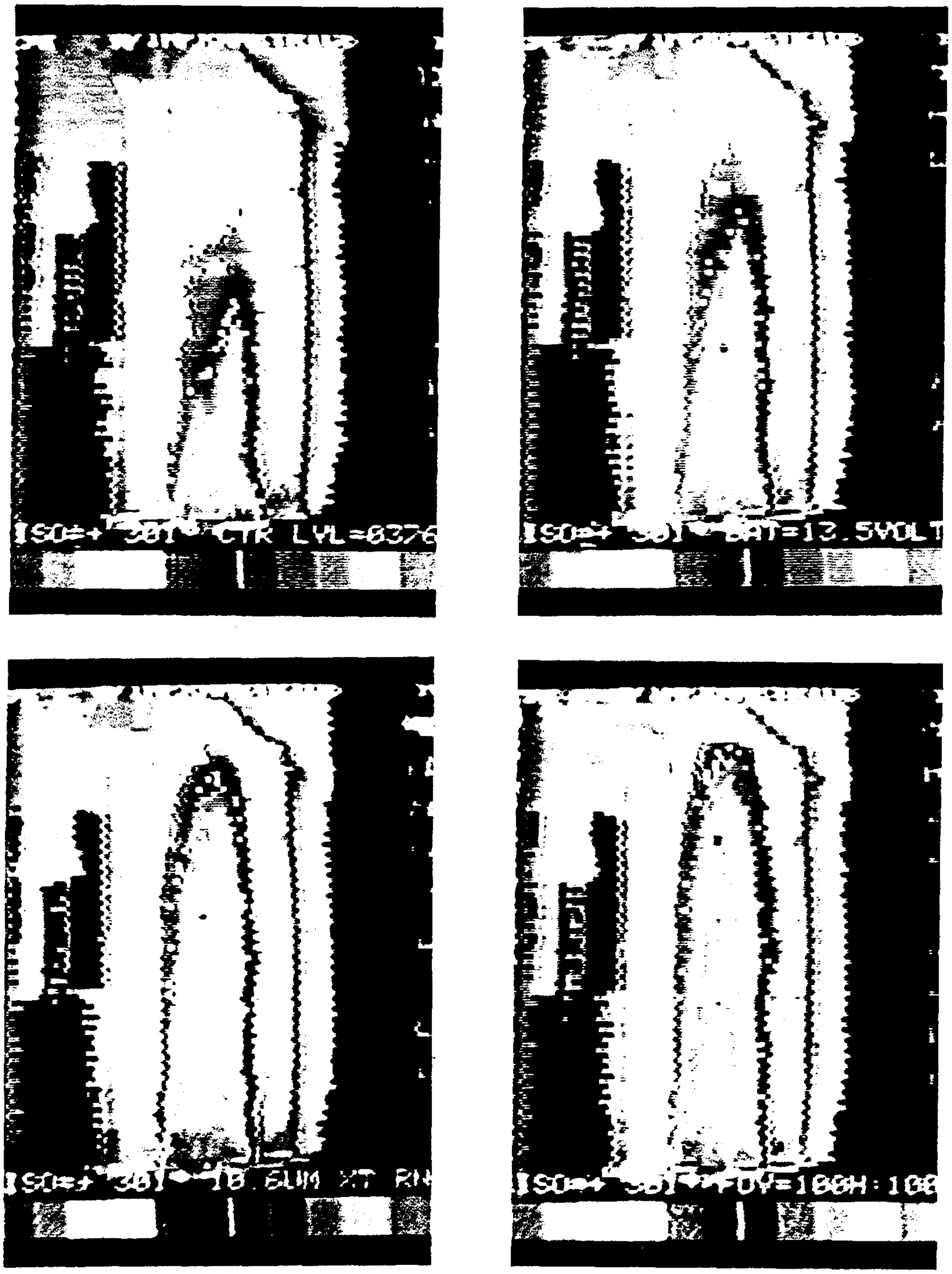

Figure 3-21 Pyrolysis front measured by infrared imaging system. In these pictures, the pyrolysis fronts are displyed by the fine white spots. It can be seen there is a very strong edge effect which produces a sharp pyrolysis front.

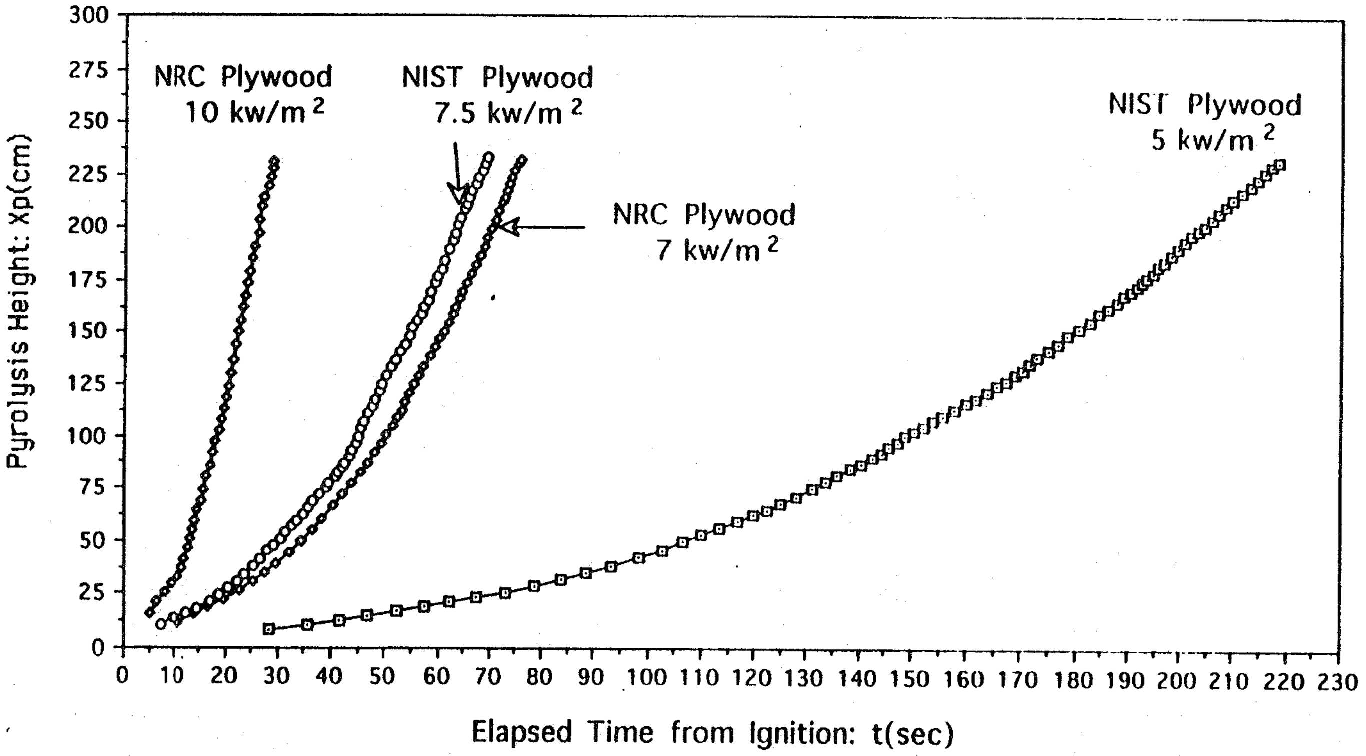

Figure 3-22 Pyrolysis height measured by IR camera as a function of time under different external radiation levels

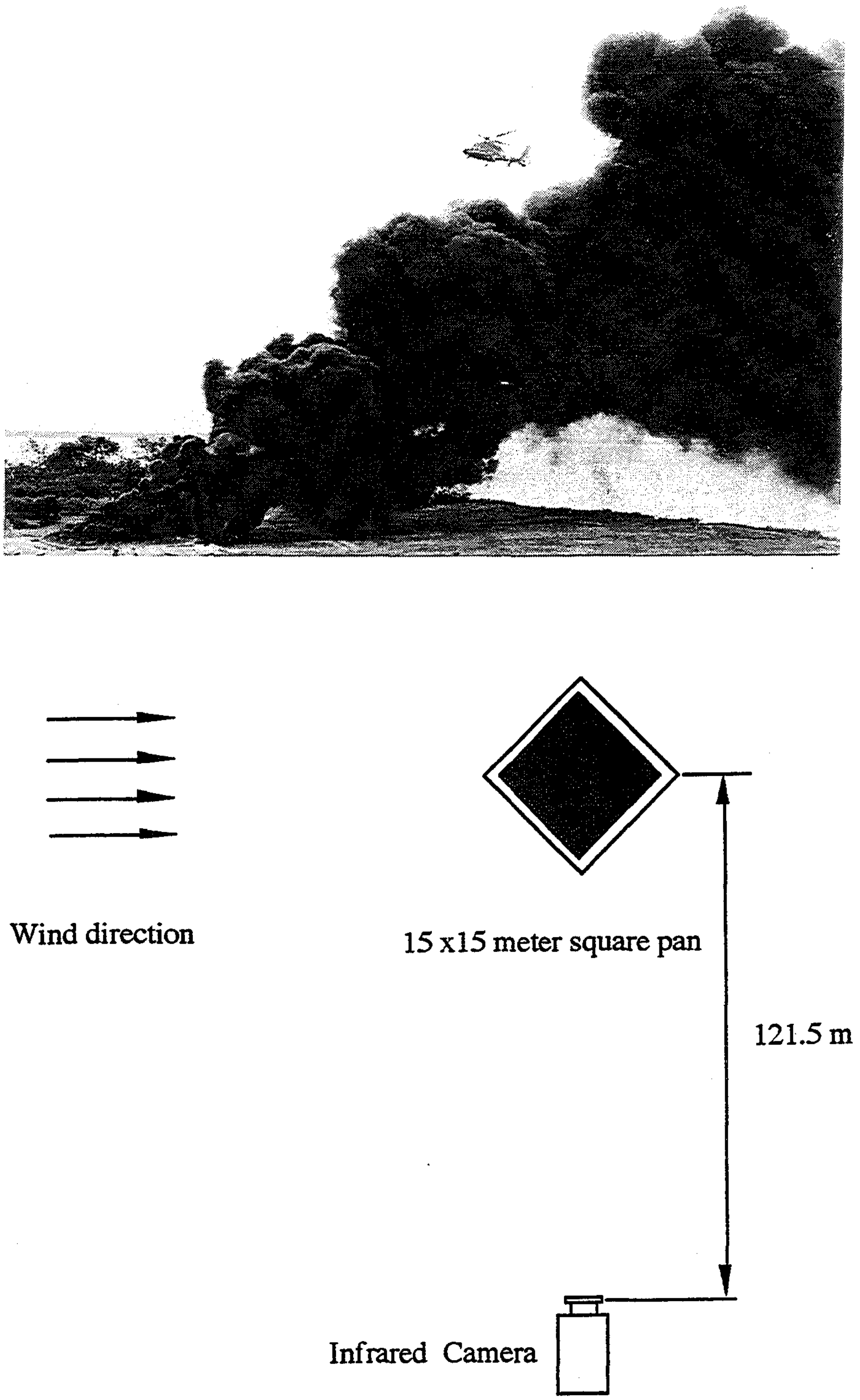

Figure 3-23 Above: The diesel pool fire experiment using a 15m aquare pool; Below: Schematic of flame temperature measurement using infrared camera (by NIST and U.S. Coast Guard in Mobile, Alabama).

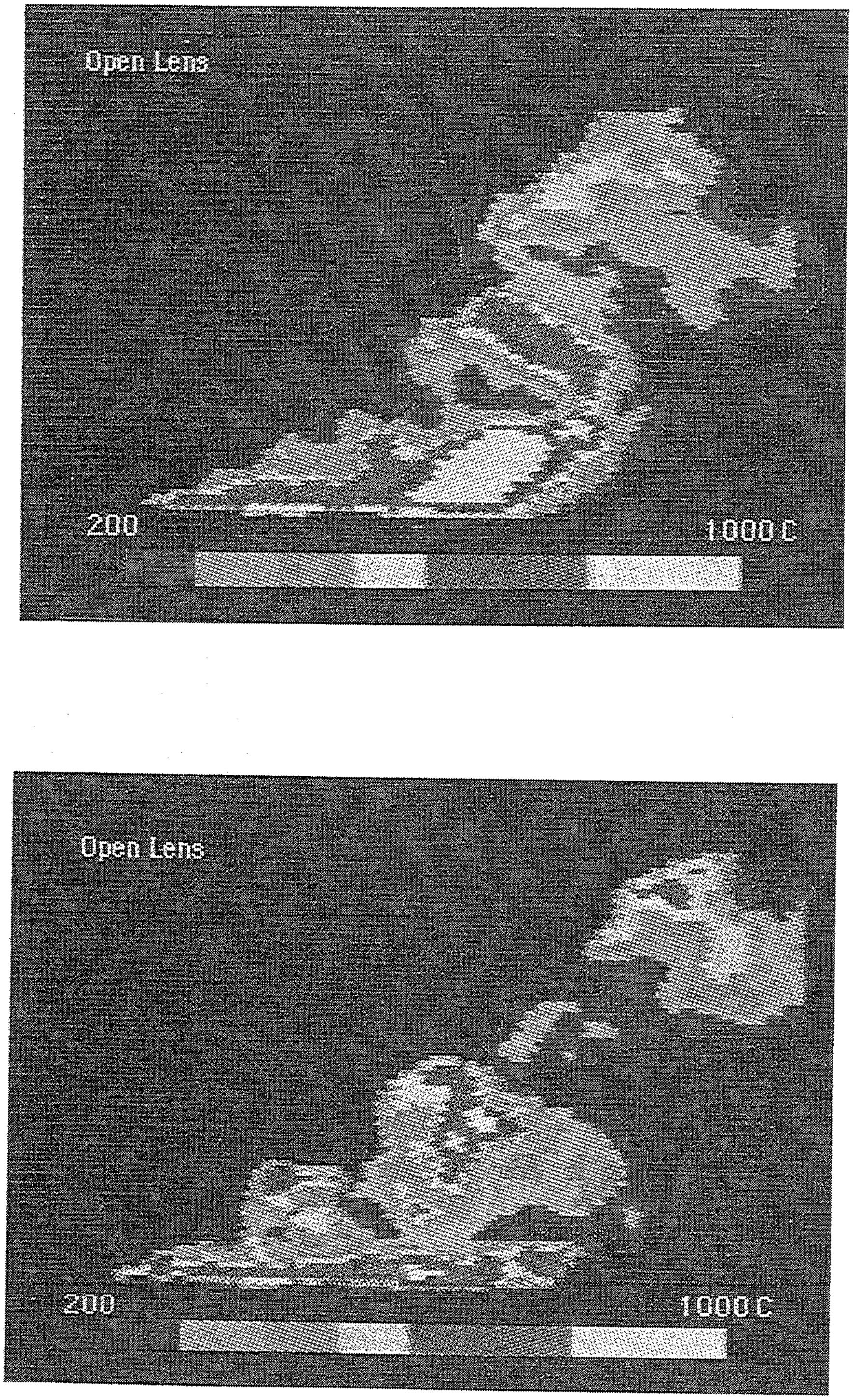

Figuer 3-24 The infrared thermal images of the large scale pool fire. The two pictures were taken at different moments.

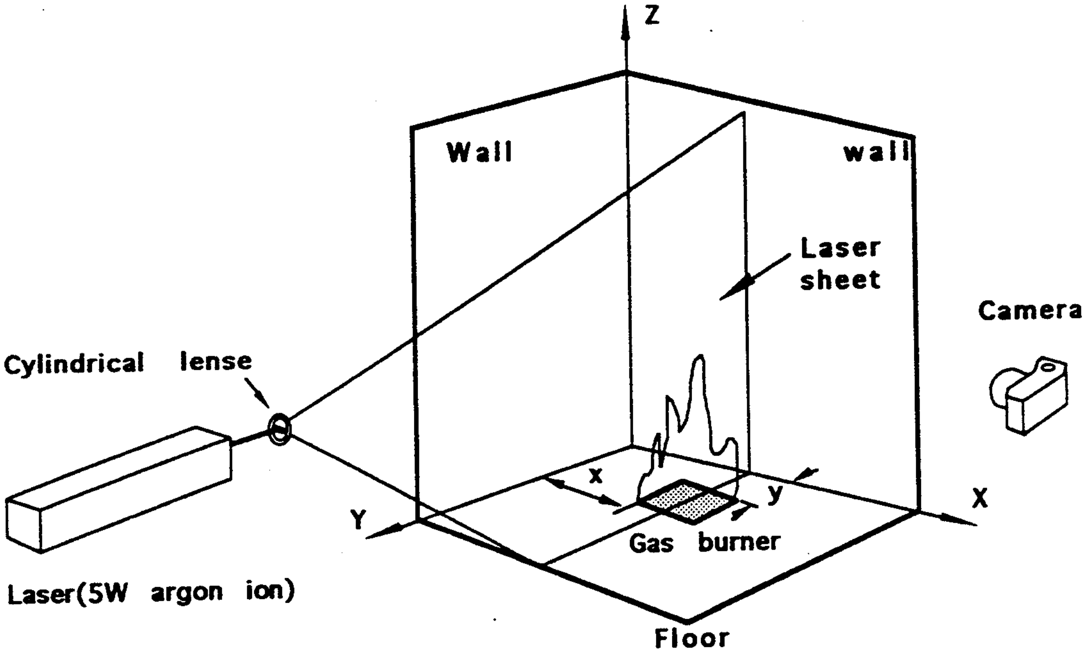

Figure 4-1 Schematic of the illumination and coordinate system for the flow visualization experiment

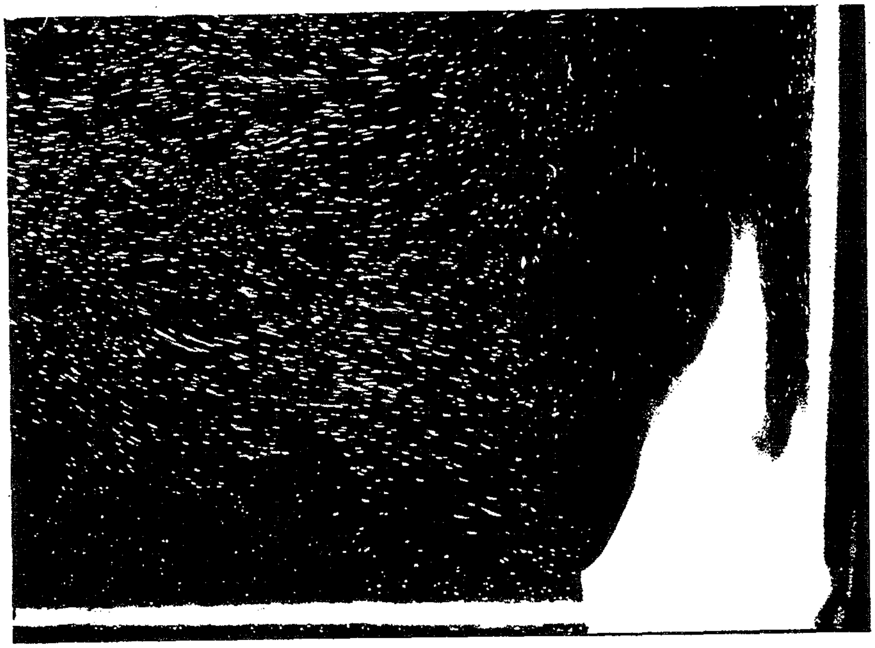

(a)

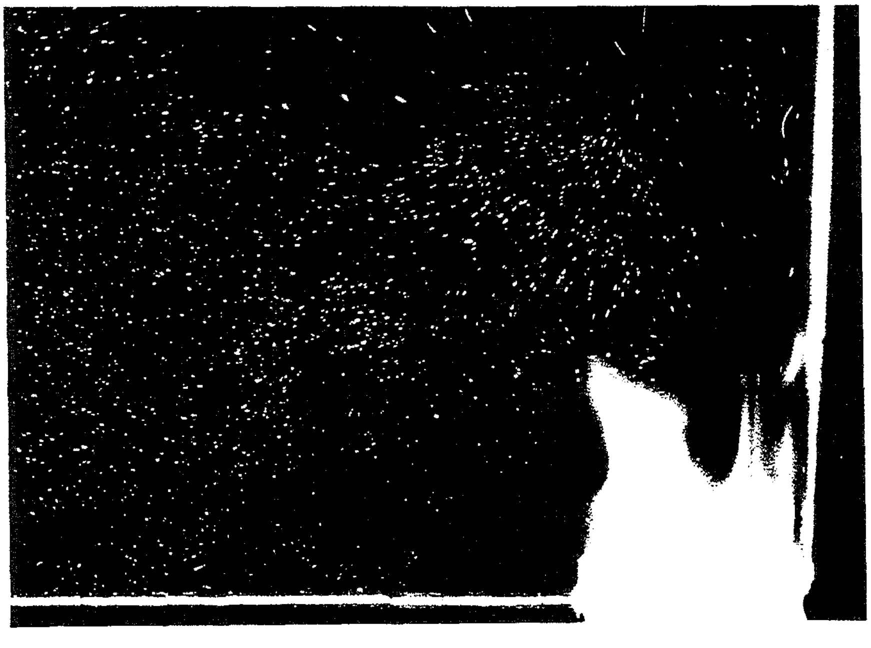

(b)

Figure 4-2 Instantaneous stream lines visualized by particle tracers. (a), (b), (c): the burner is just in the corner, the illuminated section is in the plane of x = 7.5 cm; (continue on next page)

(c)

(d)

Figure 4-2 (cont.) (d): the stand-off distances, x = 0.2, y = 0; and the illuminated section is in the plane of y = 7.5 cm. These pictures show the air puffing induced by the pulsation of the flame in a wide range.

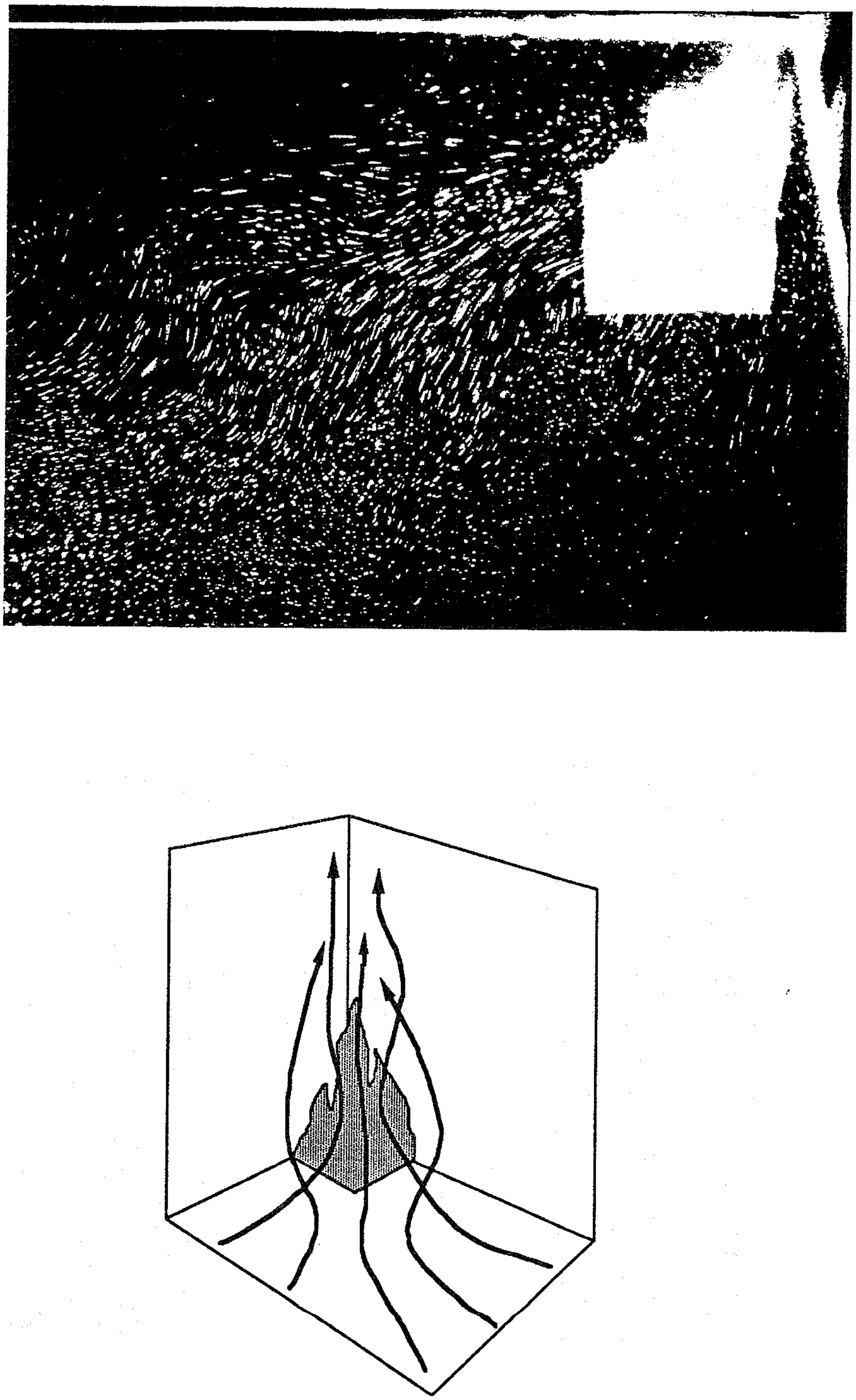

Figure 4-3 Fire-induced flow entrainment into the corner wall. Top: Flow visualization picture, the burner is just in the corner, illuminated section is in the plane of z = 15 cm; Bottom: the flow patterns.

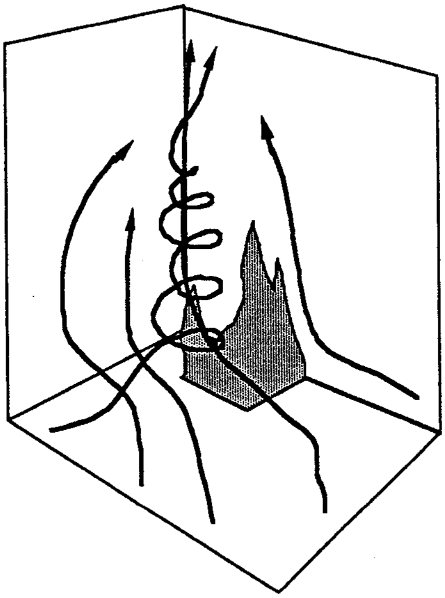

Figure 4-4 Fire-induced flow with a concentrate vortex. Top: flow visualization picture, stand-off 20 cm from one side wall, illuminated plane: z = 15 cm. It can be seen the main flame body was detached by the vortex axial flow; Bottom: the sketch of flow pattern.

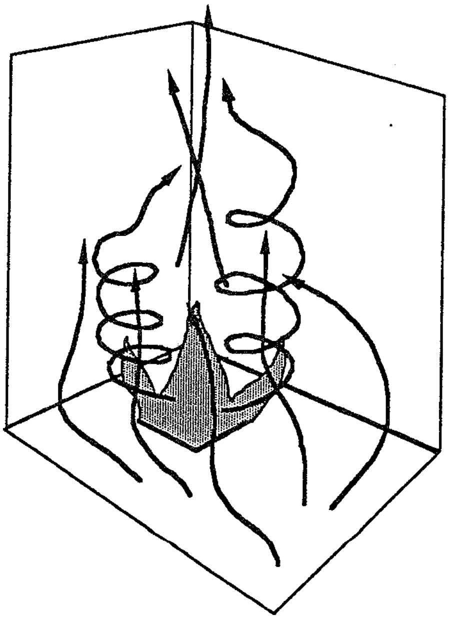

Figure 4-5 Fire-induced flow with a vortex couple. Top: flow visualization picture, the stand-off distance is 10 cm from both sides of wall, illuminated plane: z = 15 cm; Bottom: the sketch flow patterns.

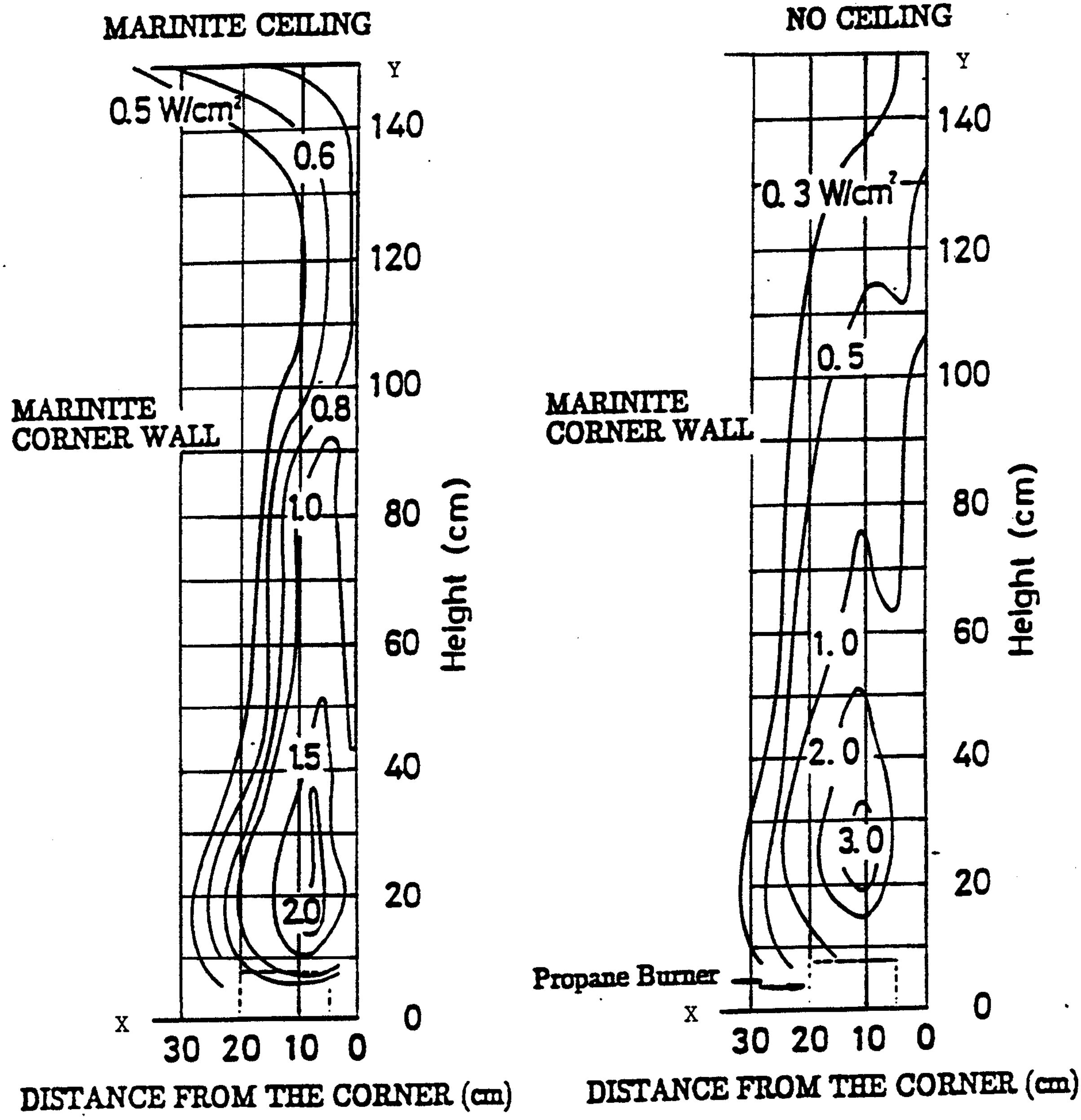

(A) (B)

Figure 4-6 Total heat flux distribution on a fire-heated Marinite corner wall. Burner heat release rate: 18 kW, burner stand-off distance: 5 cm. A: with a Marinite ceiling; B: with no ceiling.

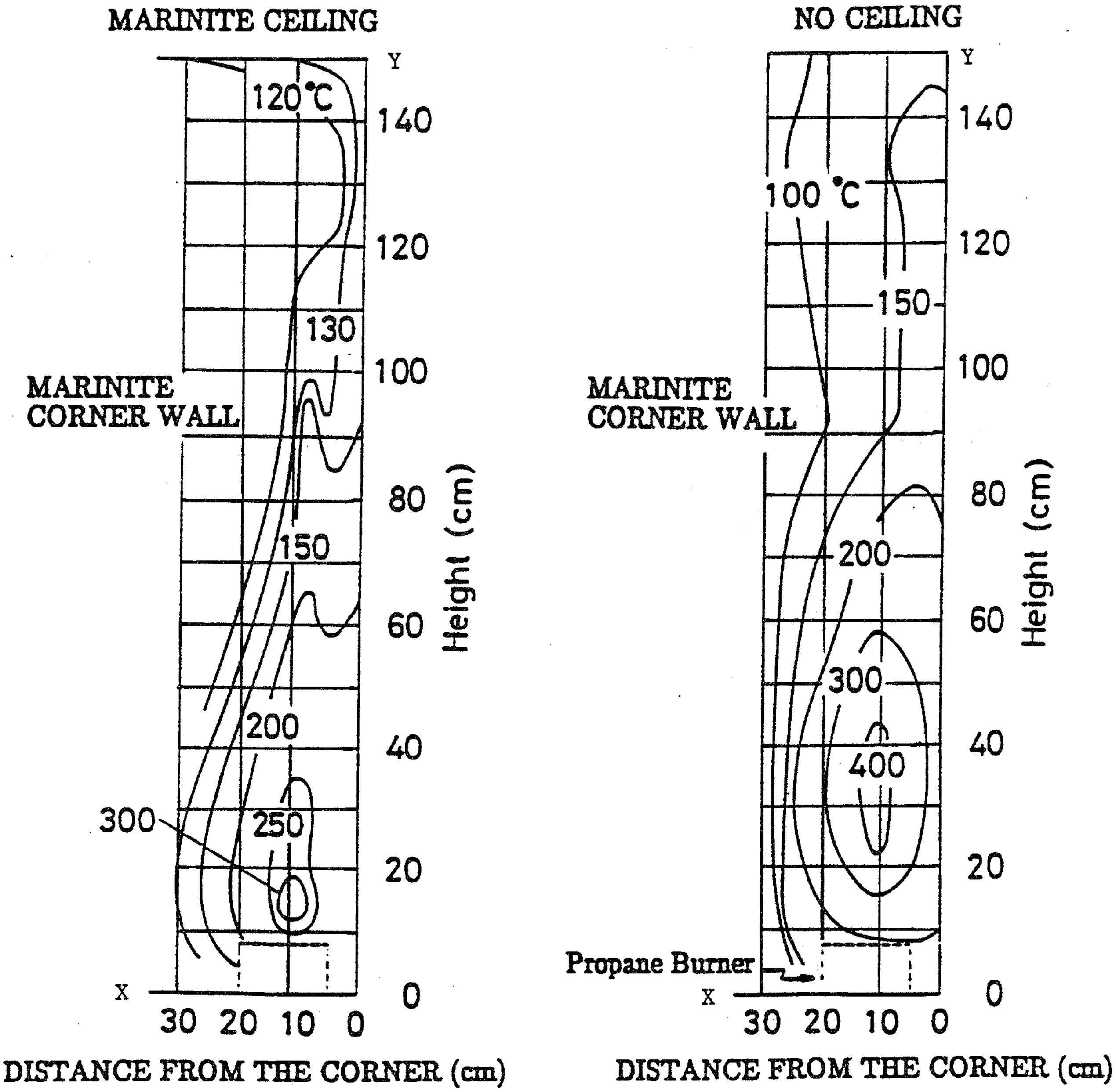

(A)

(B)

Figure 4-7 Temperature profiles on a fire-heated Marinite corner wall. Burner heat release rate: 18 kW, burner stand-off distance: 5 cm. A: with a Marinite ceiling; B: with no ceiling.

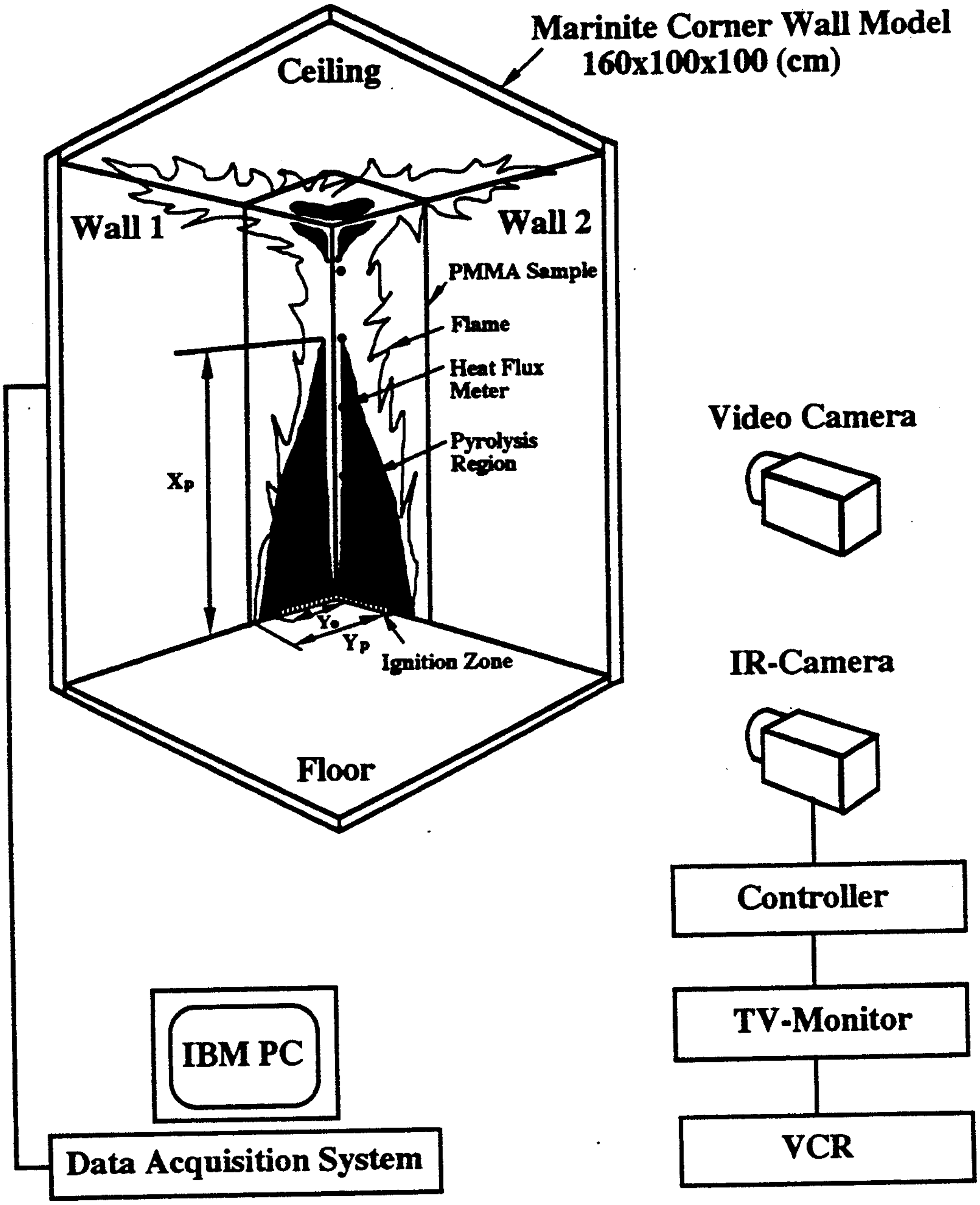

Figure 5-1 A schematic of experimental apparatus, flame shape and pyrolysis region visualized by IR imaging system. X_p is the pyrolysis height, Y_p is the pyrolysis width, and Y_o is the ignition length.

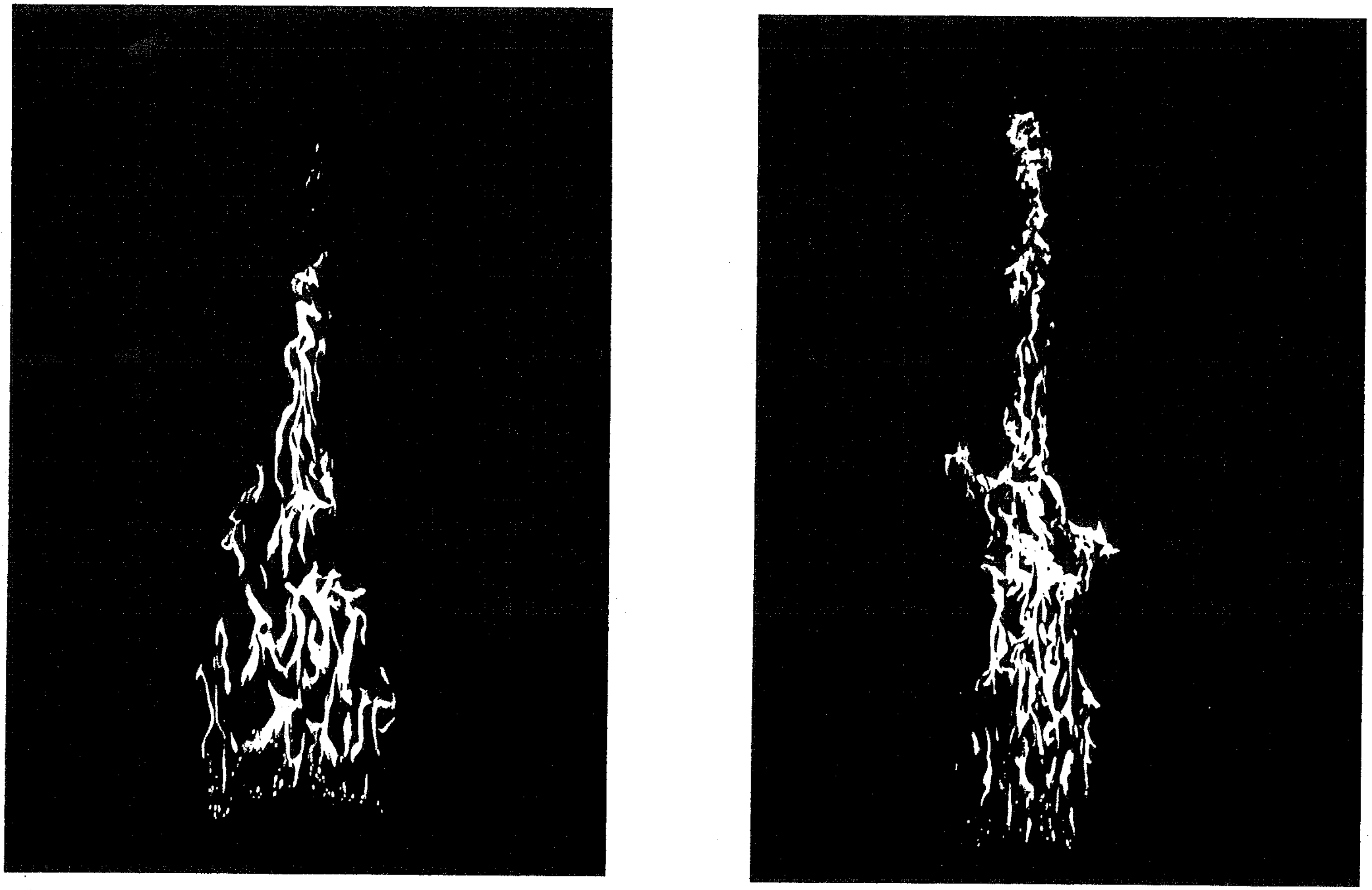

(a)

(b)

Figure 5-2 (a, b) Photographs of the flame along the corner walls: (a) a triangle flame at the begining of spread, (b) the flame reaching the ceiling.

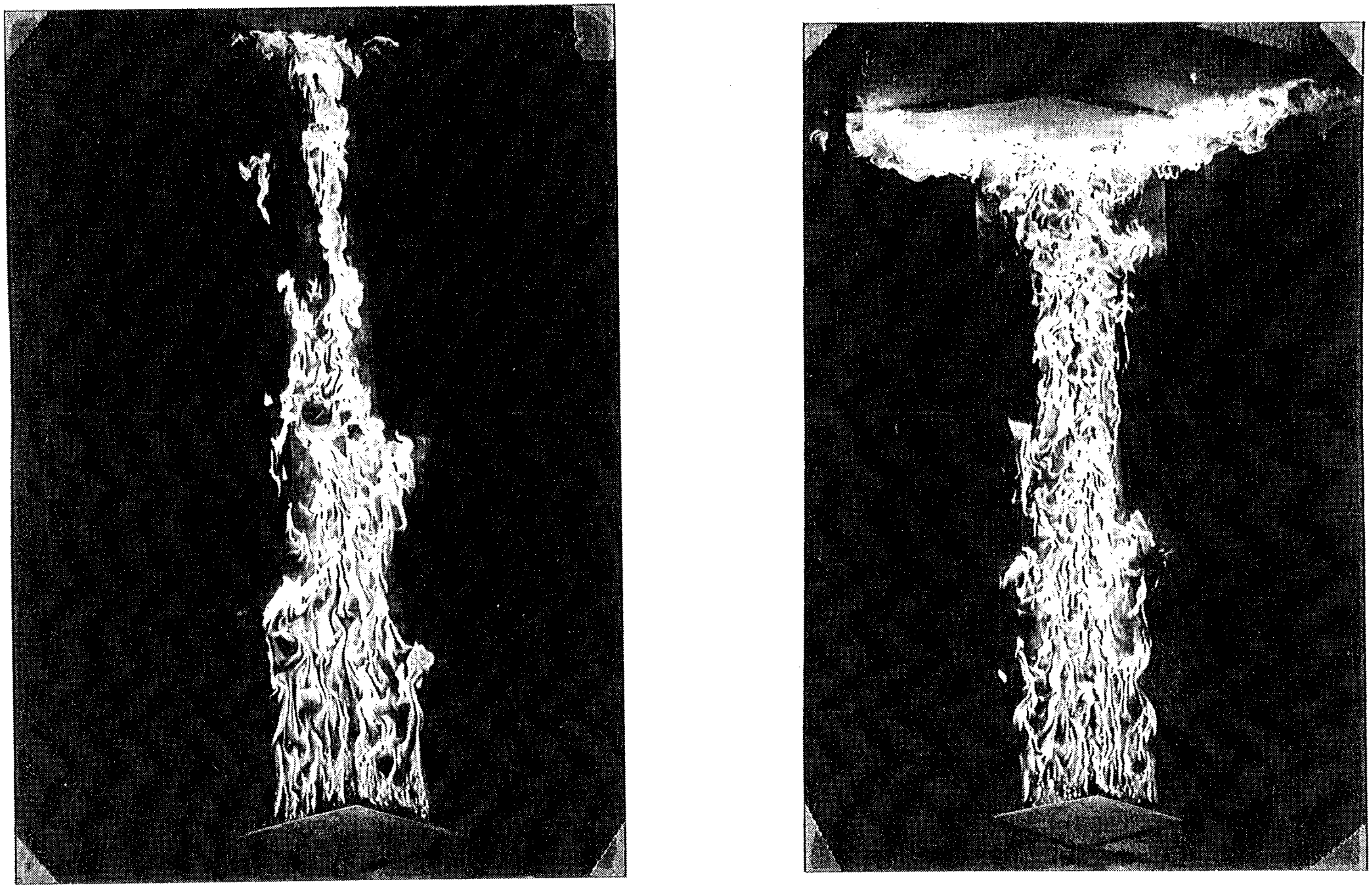

(c)

(d)

Figure 5-2 (c, d) Photographs of the flame along the corner walls: (c) ceiling is ignited, (d) the fully developed corner wall flame.

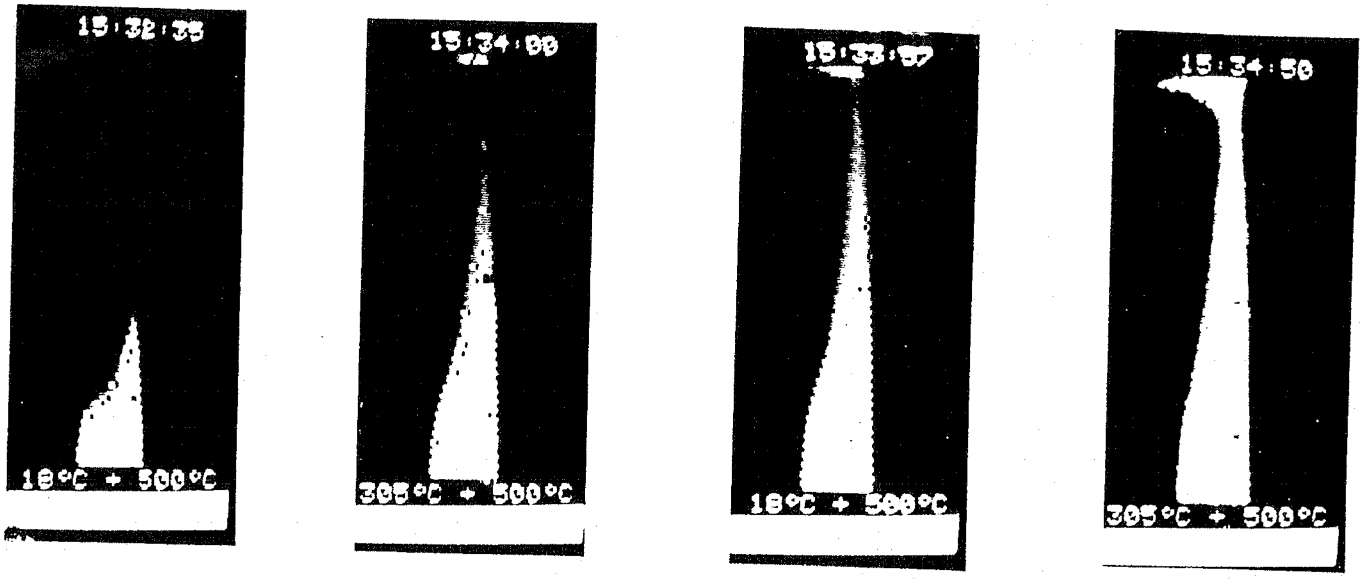

(a) (b) (c) (d)

Figure 5-3 Pyrolysis zone detected by the IR imaging system, the pyrolysis front is high lighted by fine white spots which is the contour of 329°C.

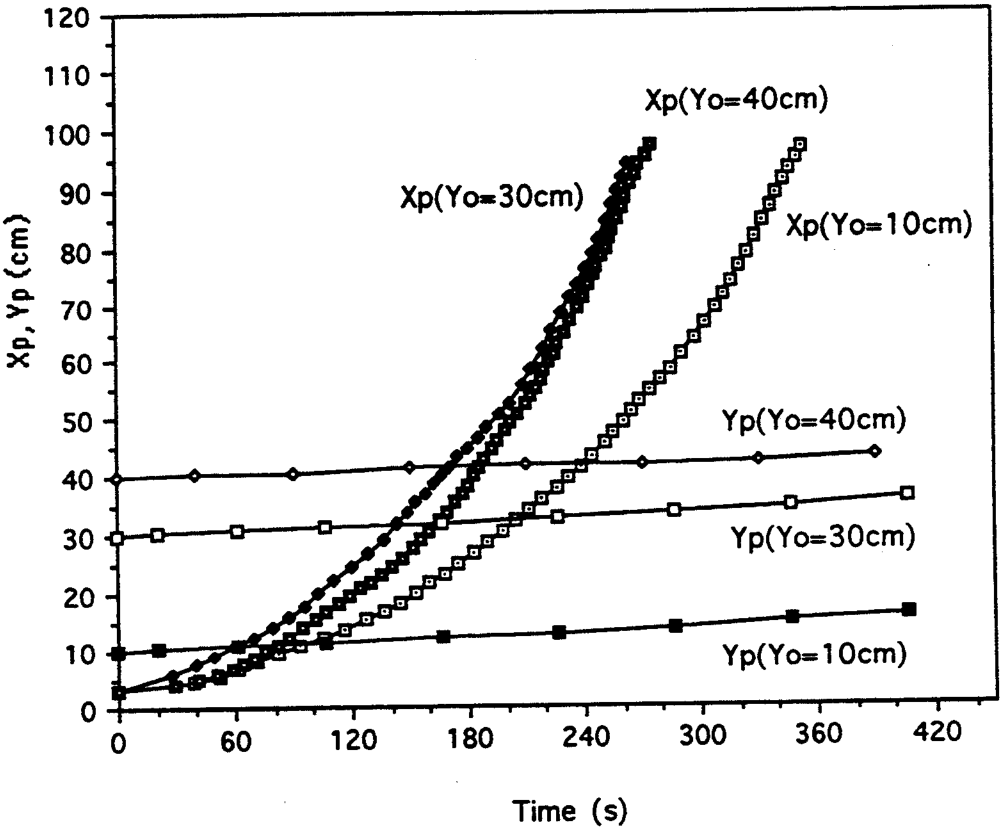

Figure 5-4 Pyrolysis height and pyrolysis width as functions of time for three different ignition lengths

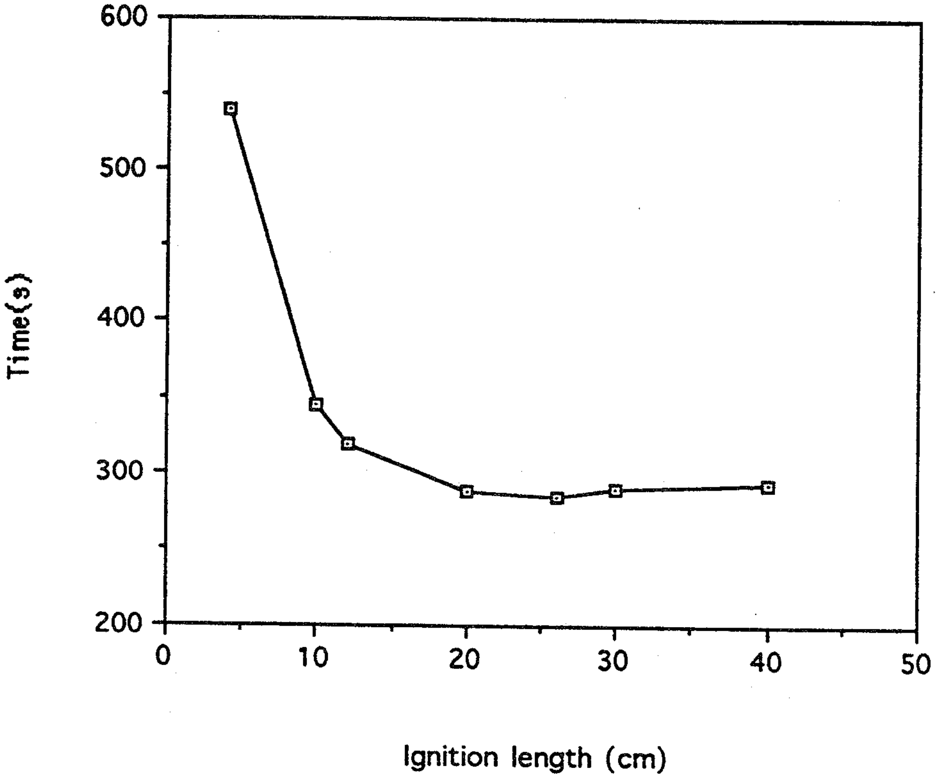

Figure 5-5 Time elapsed after ignition when the pyrolysis front reaches the samlpe top with different ignition lengths

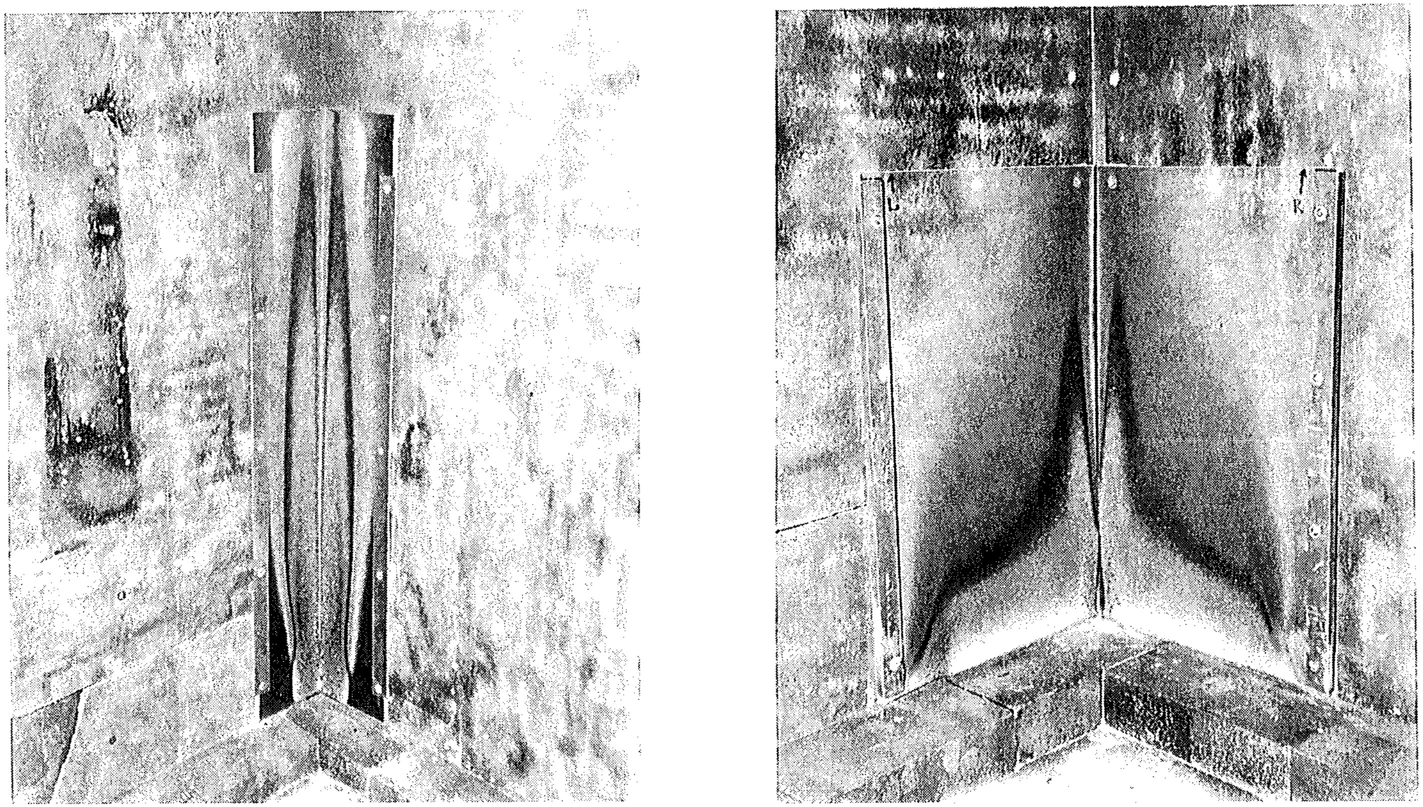

(a) (b)

Figure 5-6 Photographs of pyrolysis regions which were taken after the fire was extinguished: (a) pyrolysis geometry from a spot ignition, ø30 mm; (b) from a line ignition, 300 x 30 mm each side.

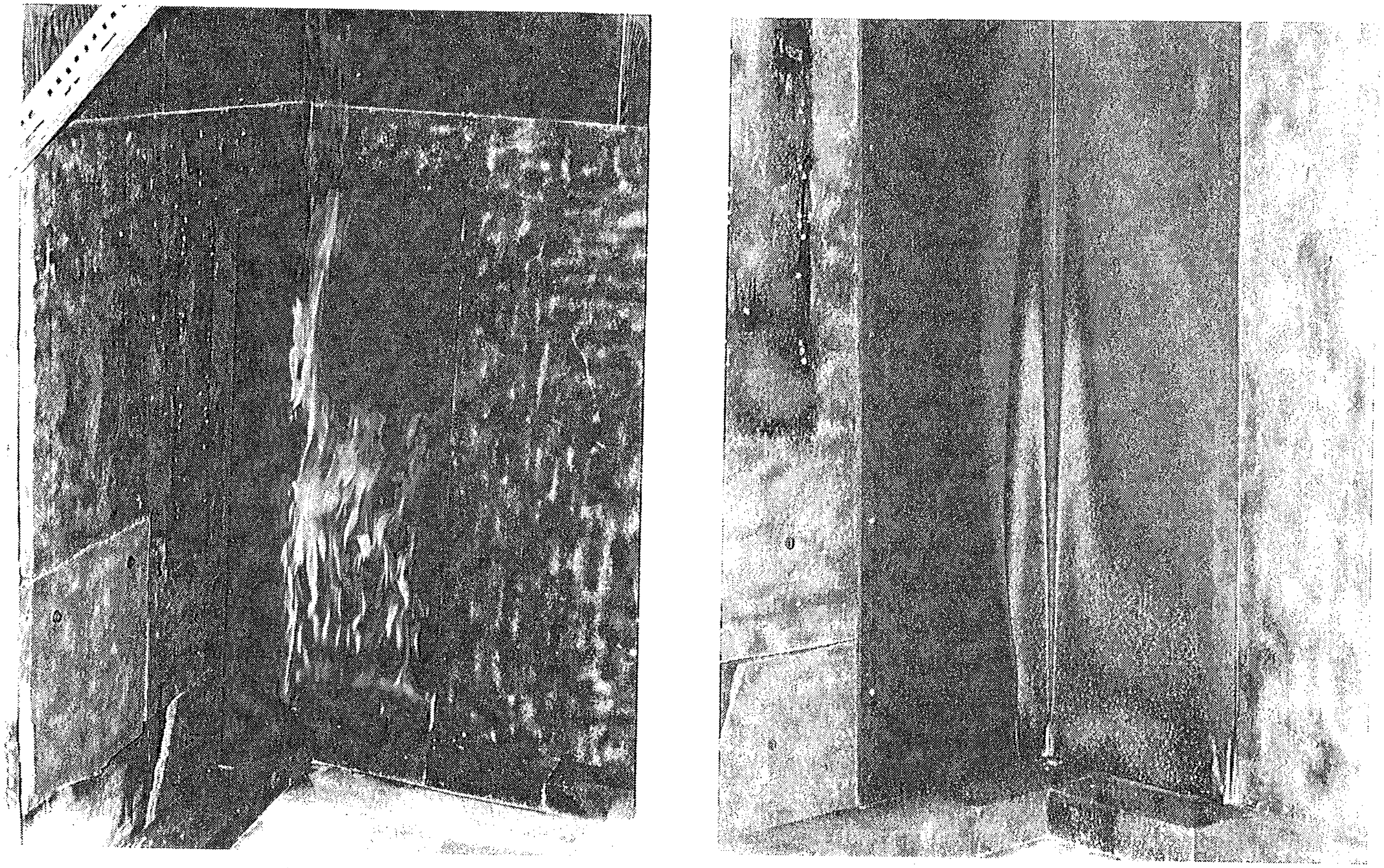

(a) (b)

Figure 5-7 (a) A photograph of flame shape after one side of PMMA wall bottom was ignited, and (b) A photograph of pyrolysis region geometry after the fire was extinguished.

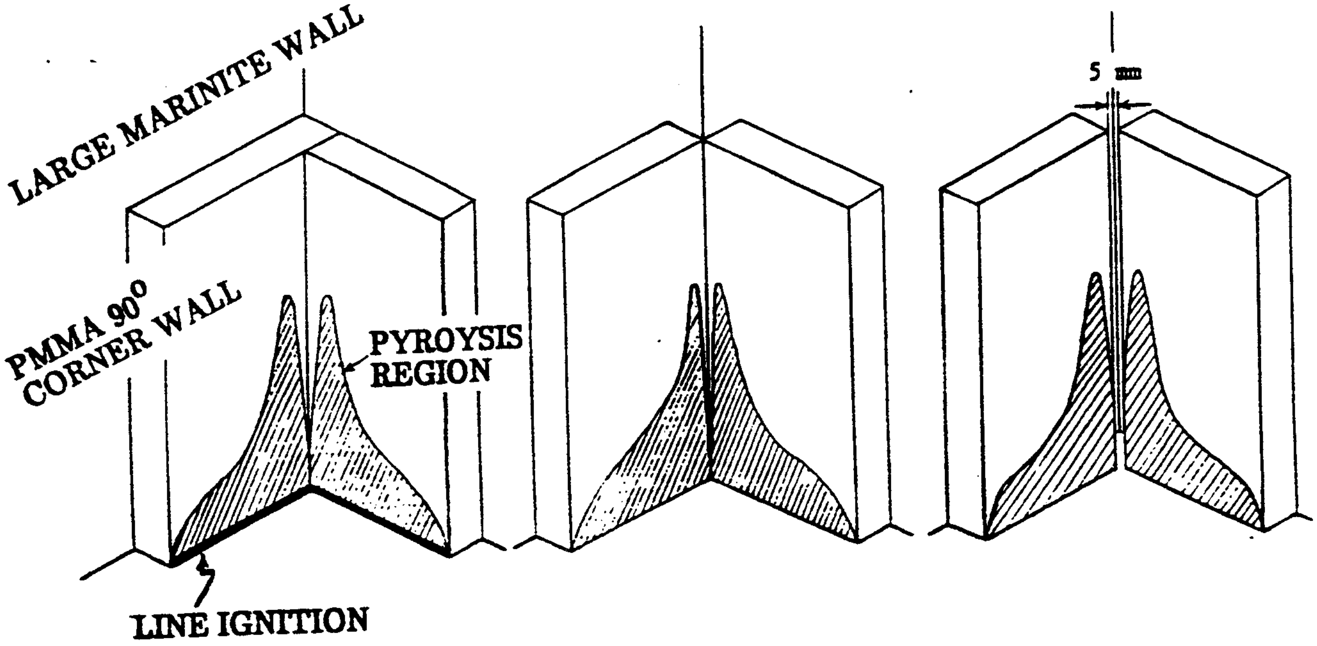

CASE I

CASE II

CASE III

Figure 5-8 Schematics of pyrolysis front shape on three different PMMA corner models (CASE I- III)

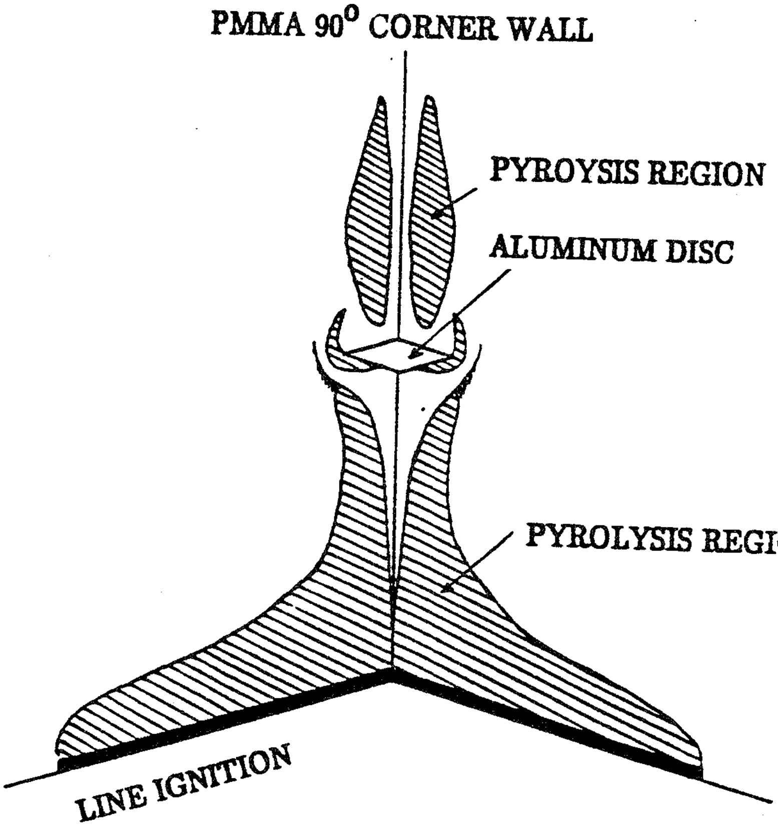

Figure 5-9 A schematic of pyrolysis front shape on a PMMA corner wall model with an aluminum square disc, 5 cm long x 5 cm wide x 0.2 cm thick.

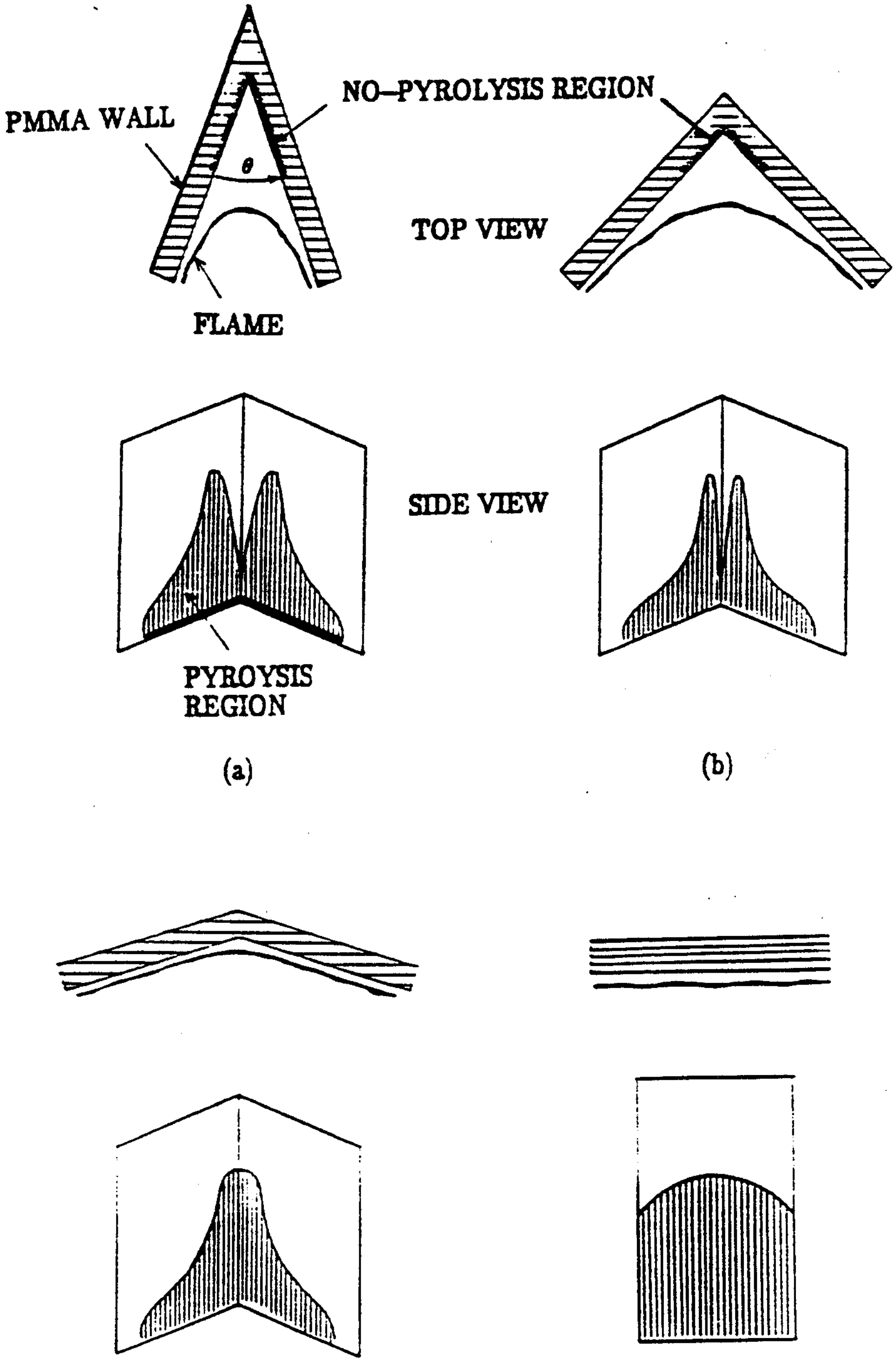

Figure 5-10 Schematics of flame sheet location relative to corner wall surface (top view) and pyrolysis front shape on PMMA samples with four different corner angles. (a) θ = 45°, (b) θ = 90°, (c) θ = 135°, and (d) θ = 180°.

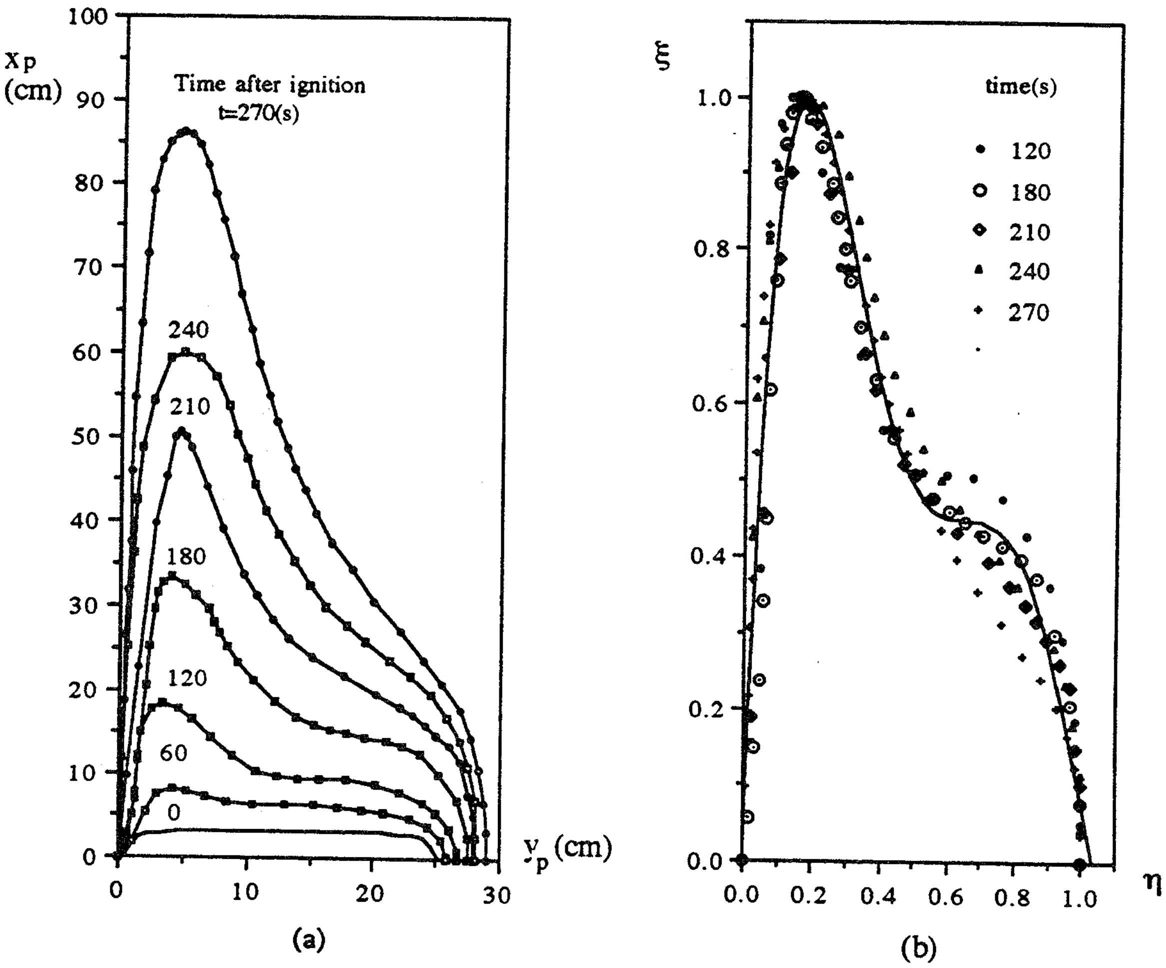

Figure 5-11 (a) Spreading pyrolysis front measured by IR imaging system at six different ime periods after ignition, and (b) a similarity correlation of normalized pyrolysis front

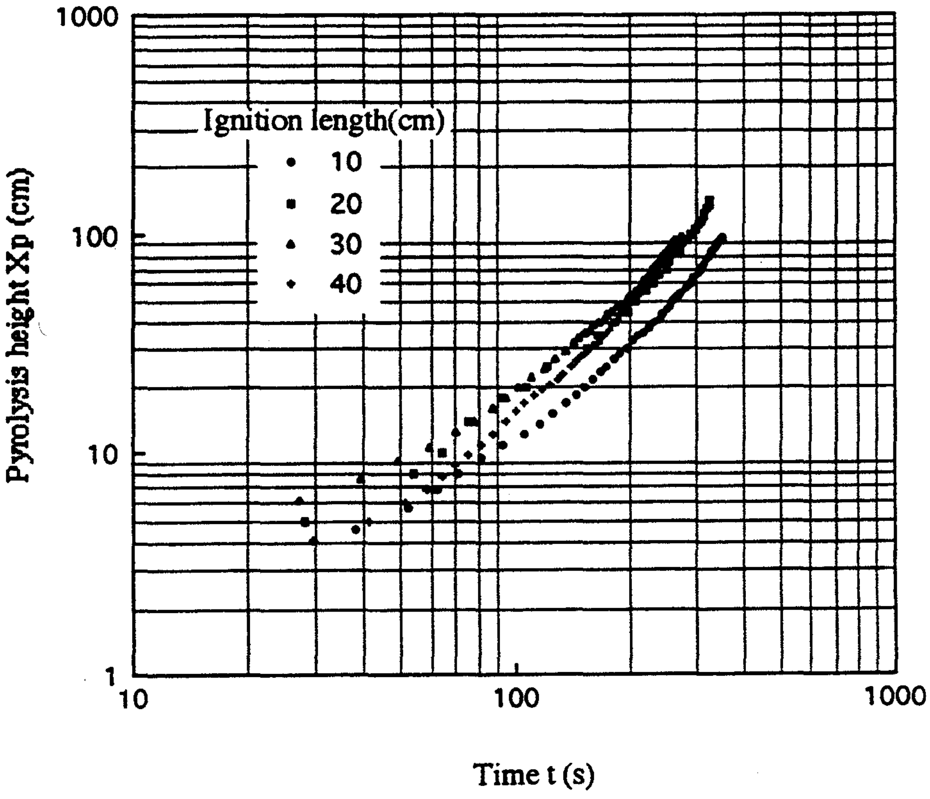

Figure 5-12 Measured pyrolysis height as a function of time for different ignition lengths

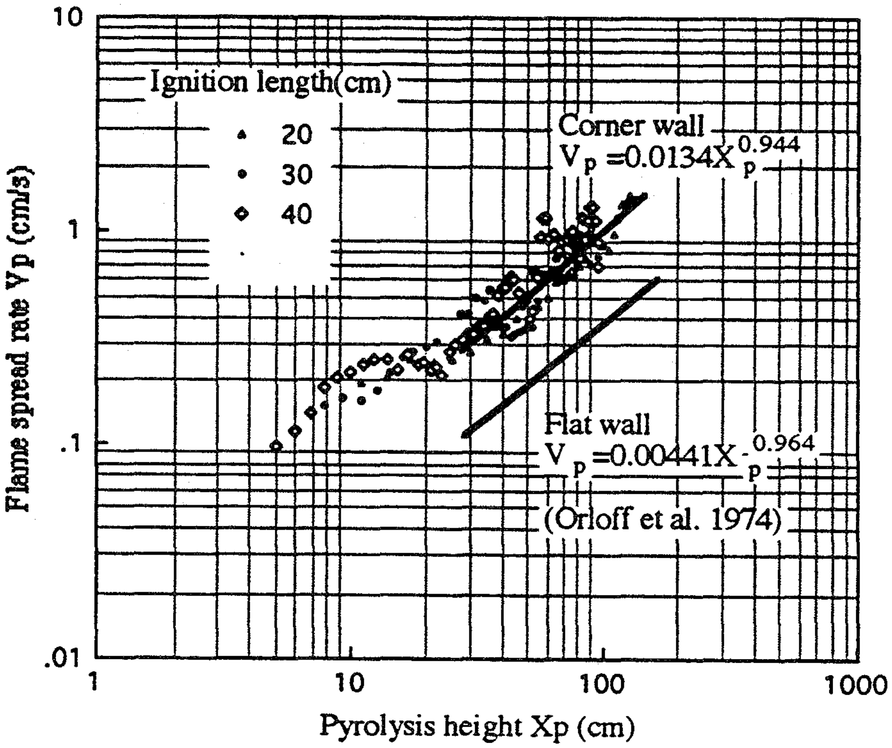

Figure 5-13 Flame spread rate correlations with pyrolysis height

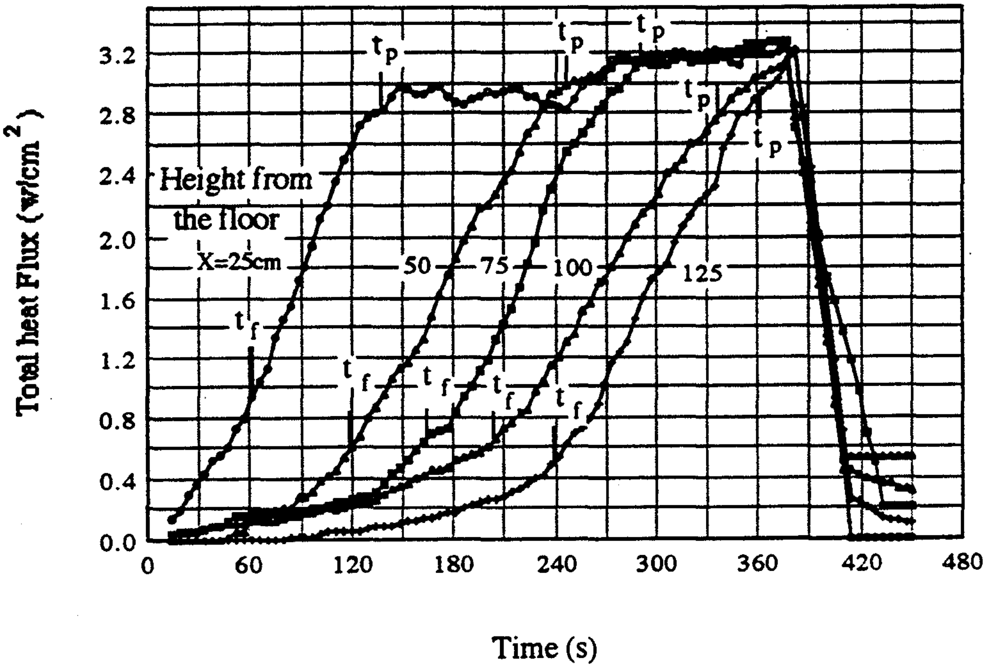

Figure 5-14 Histories of total heat flux received at five different heights along the PMMA corner wall for a spreading fire

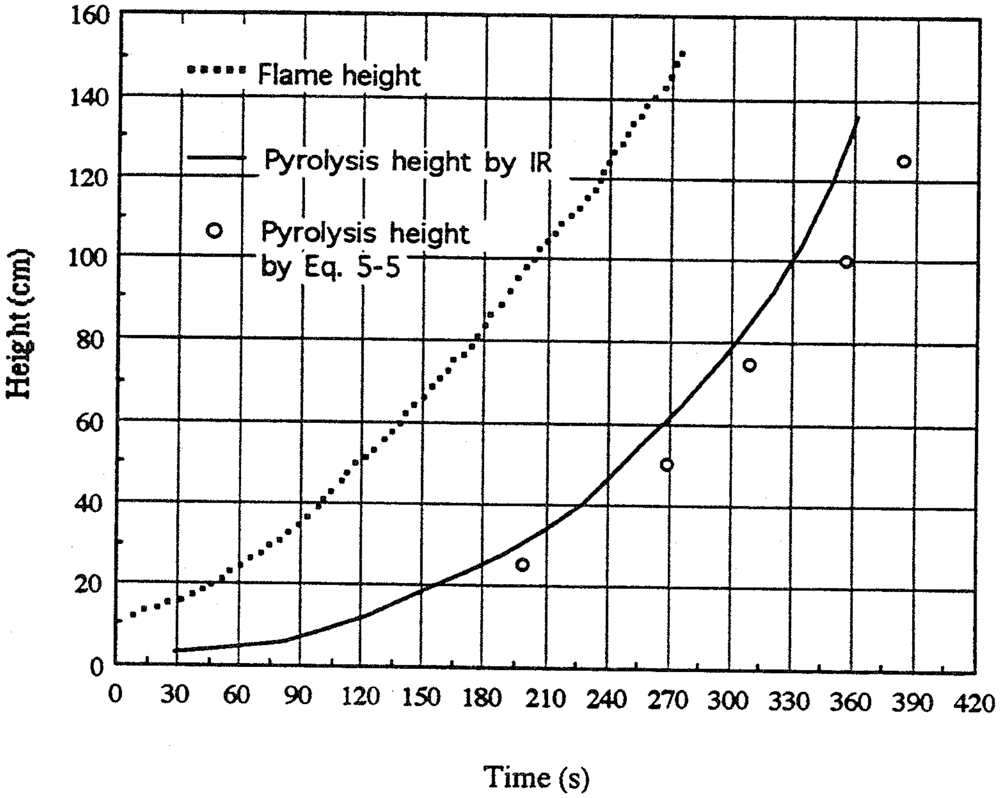

Figure 5-15 Comparison of one-dimensional heat transfer model prediction by (Eq.5-5) with experimental measurements

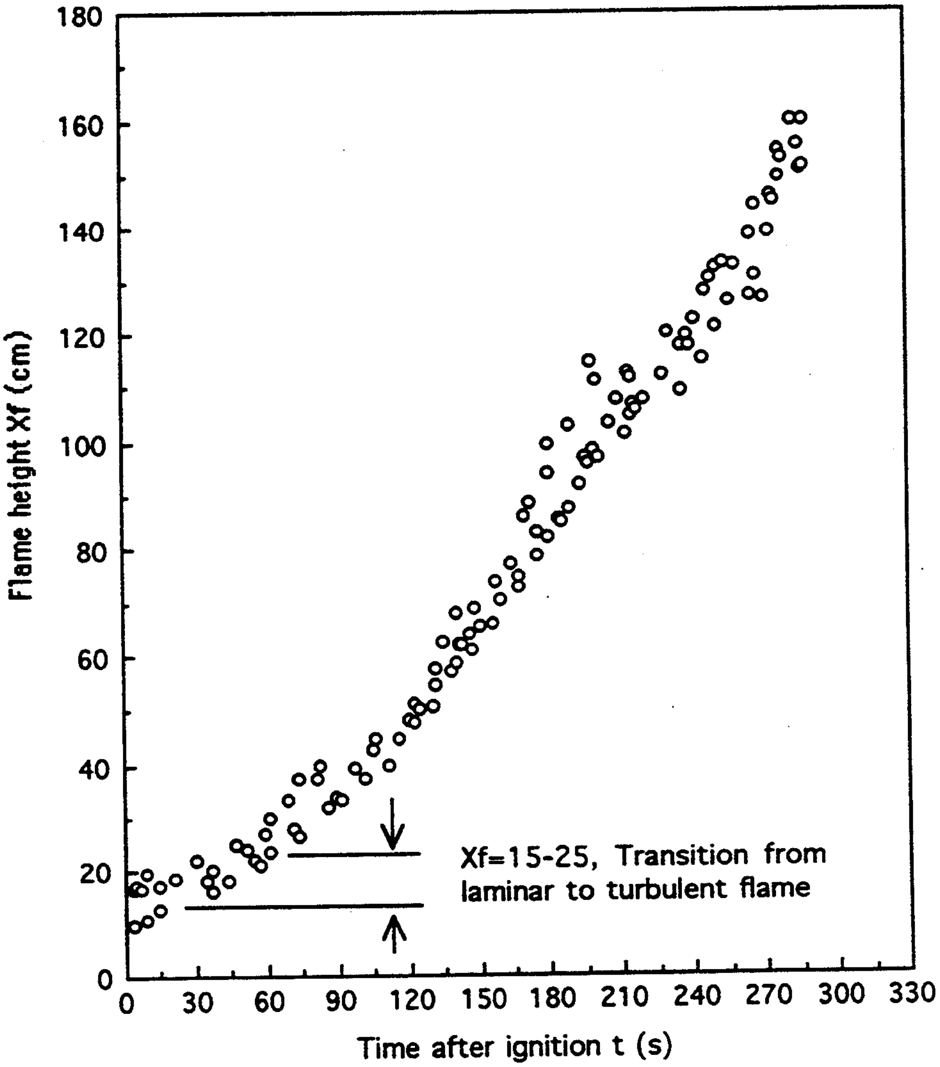

Figure 6-1 Flame height as a function of time measured in flame spread along vertical corner walls

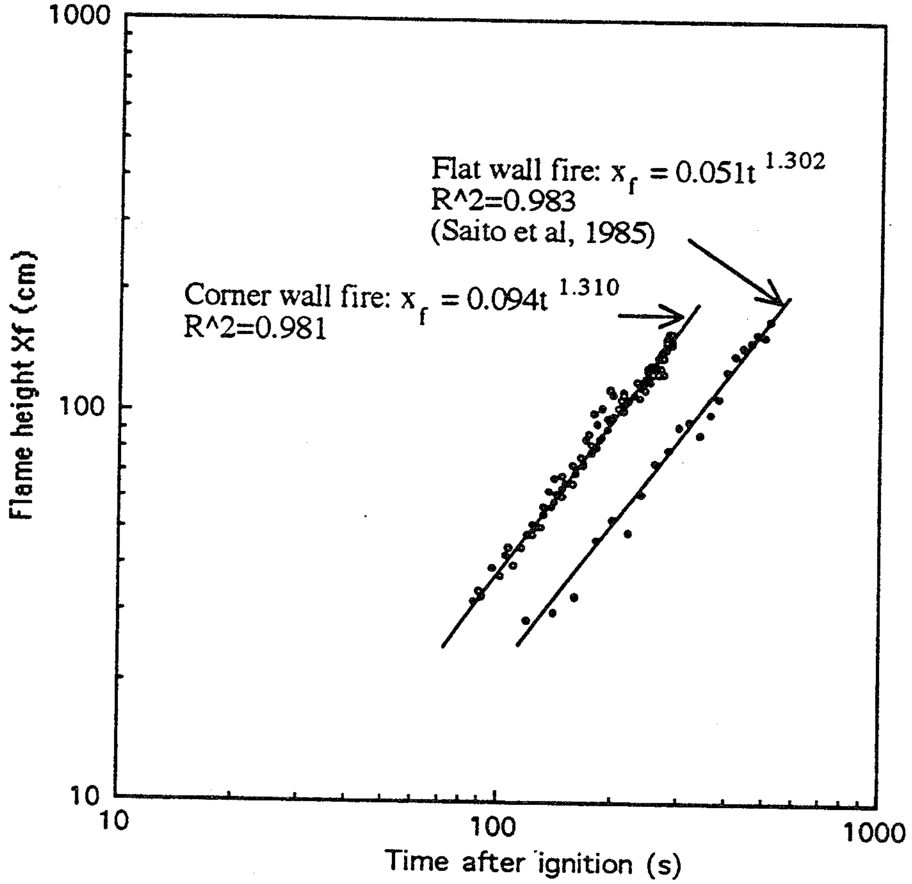

Figure 6-2 Flame height as a function of time. Solid line is the least squares fit to data higher than 25 cm

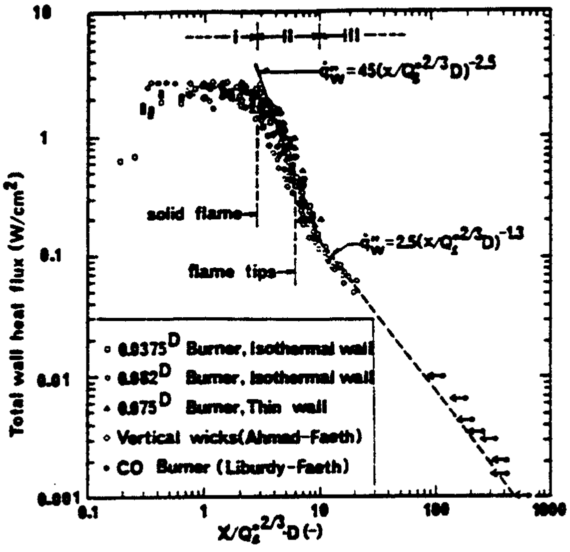

Figure 6-3 Total wall heat flux vs. normalized height from Hasemi (1984)

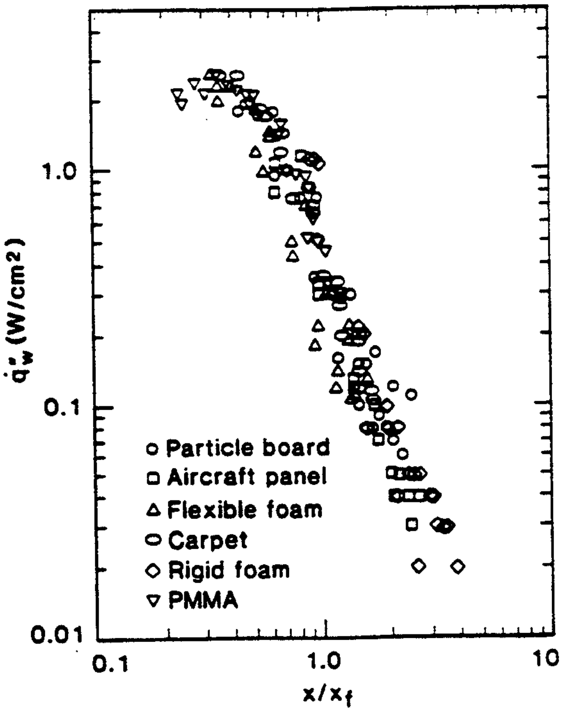

Figure 6-4 Wall heat flux correlated using flame height from Quintere (1986)

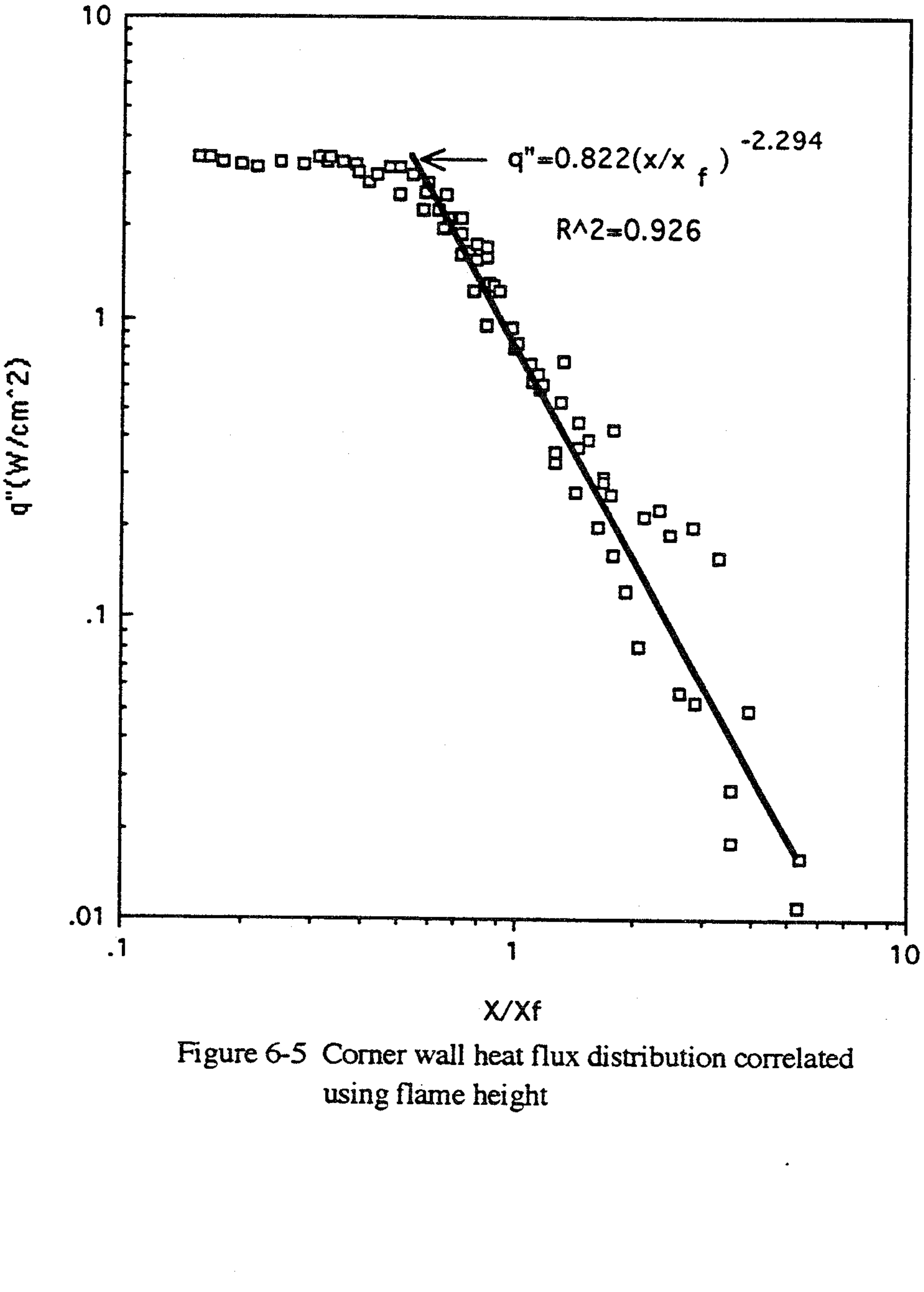

Figure 6-5 Corner wall heat flux distribution correlated using flame height

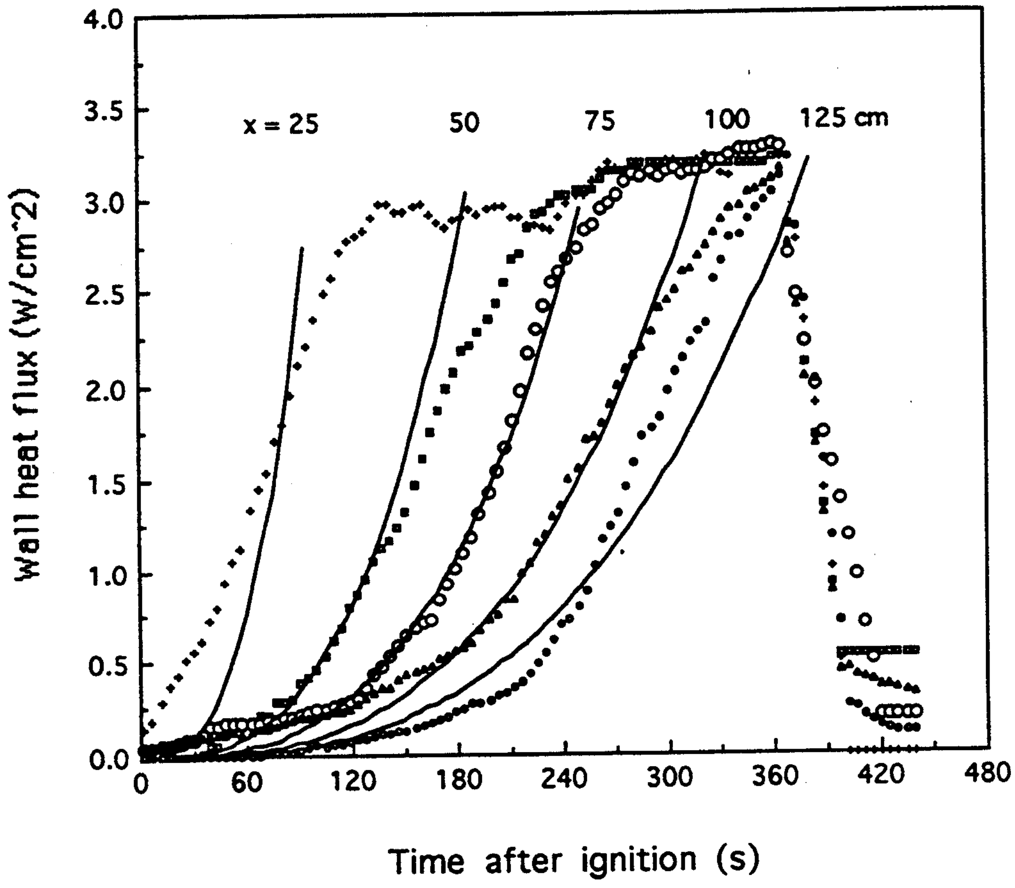

Figure 6-6 Comparison of the heat flux model with the experimental data. Solid lines are calculated from the model at five different heights. This model was developed only for the preheat period.

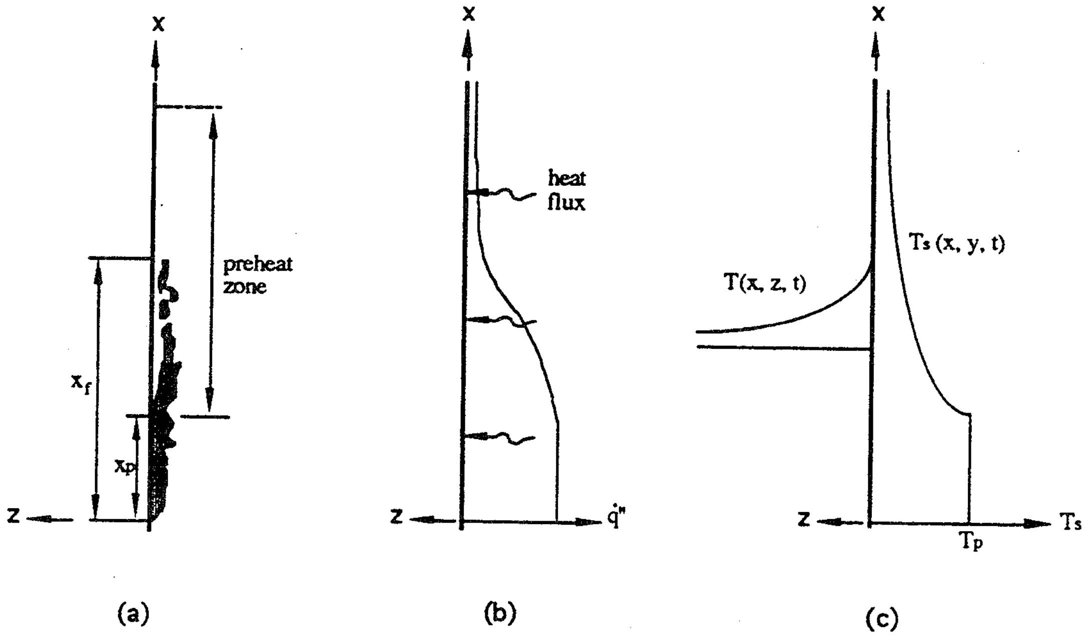

Figure 6-7 Schematic diagram of flame spread on corner walls
(a) Flame configuration;
(b) Heat flux distribution;
(c) Wall surface and internal temperature.

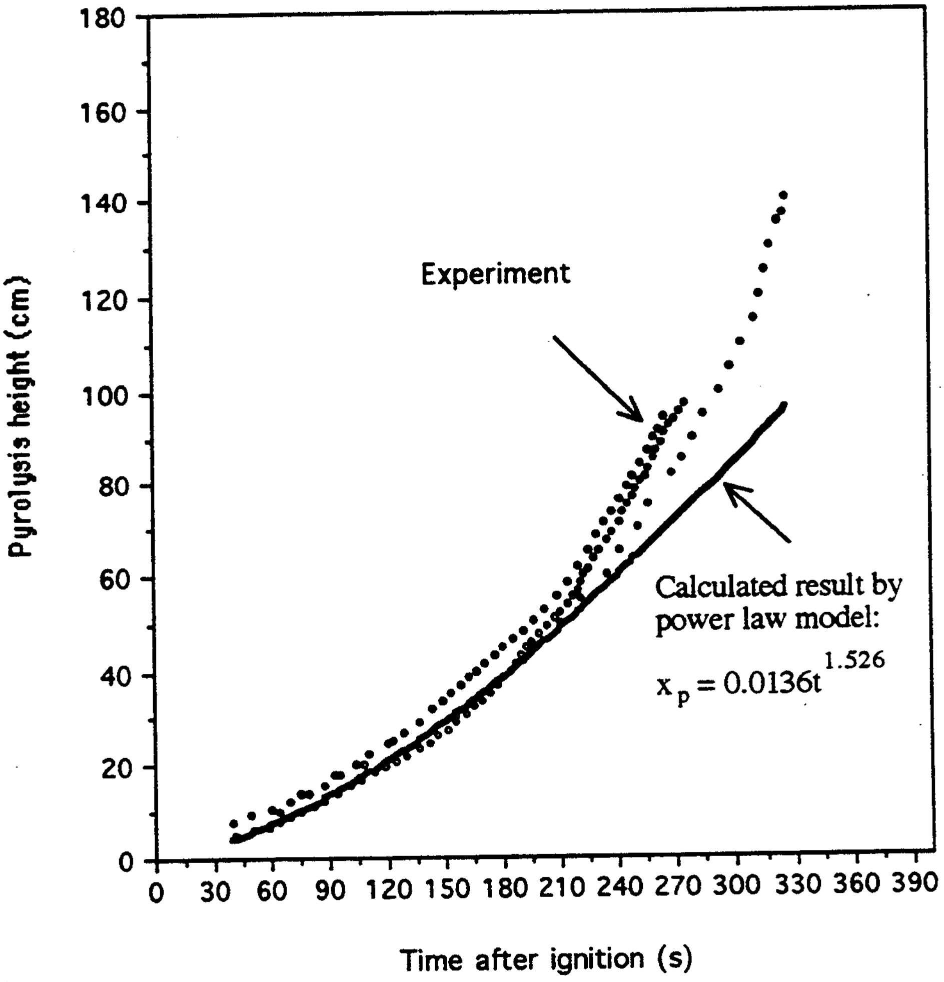

Figure 6-8 Comparison of the present model with the experimental data

Nomenclature

English symbols

A	Constant coefficient in pyrolysis height correlation	
B	Constant coefficient in spread rate correlation	
C	Constant coefficient in flame height correlation	J/(g·°C)
C_e	Entrainment coefficient	
C_s	Specific heat of solid	
C_p	Specific heat at constant pressure	cal/(g·°C)
c	Specific heat	cal/(g·°C)
D	Constant coefficient in heat flux correlation	
E	Constant, $D/C^{1.3}$	
E'	Energy release rate per unit width	W/cm
F	Constant, $0.962(D^{0.435}/C^{0.566})$	
g	Gravity acceleration	cm/s^2
k	Heat conductivity	cal/(s·cm^2·°C)
L_p	Gasification heat of fuel material	J/g
m	The exponent in pyrolysis height correlation	
n	The exponent in spread rate correlation	
r	Stoichiometric oxygen to fuel ratio	
T	Temperature	°C
T_o	Initial temperature	°C
T_a	Ambient temperature	°C
T_{ig}	Ignition temperature	°C
T_p	Pyrolysis temperature	°C
T_s	Surface temperature	°C
t	Time	s

v	Air flow velocity	cm/s
V_p, v_p	Vertical flame spread rate	cm/s
x	Vertical coordinate	cm
X_p, x_p	Pyrolysis height	cm
x_f	Flame height	cm
Y_o	The length of the ignition zone	cm
Y_p	Width of the pyrolysis zone	cm
$Y_{ox,\infty}$	Oxygen concentration	

Greek letter

ΔH_{ox}	Heat of reaction per mass of oxygen	
ΔH_g	Heat of gasification	cal/g
ε	Emissivity	
λ	Fuel and air mixing factor	
ρ	Density of the solid fuel material	g/cm^3
ρ_∞	Air density	g/cm^3
τ	Time, integration variable, or characteristic ignition time	s
ϕ	Heat transfer parameter	$(kW)^2/m^3$

Appendix A: Specifications of Inframetrics Model 600 IR Imaging Radiometer

NOTE: Addition of filters, especially narrow bandpass filters, will affect system performance.

Spectral Bandpass (Nominal)	8-12 um, 3-5 um or 3-12 um
Detector	Mercury/Cadmium/Telluride (HgCdTe); @ 77 K
Detector Coolant	Liquid Nitrogen
Dewar Hold Time	More than 3 Hours
Typical Minimum Detectable Temperature Difference	
@ 30C (8-12 um, 3-12 um)	0.1C
@ 30C (3-5 um)	0.2C
Noise Equivalent Temperature Difference (typical)	
@ 30C (8-12, 3-12 um)	less than 0.2C
@ 30C (8-12, 3-12 um with optional image averager, 16 fields)	less than 0.05C
@ 30C (3-5 um)	less than 0.4C
@ 30C (3-5 um with optional image averager, 16 fields)	less than 0.1C
Scan Rate:	
USA	8 KHz Horizontal; 60 Hz Vertical
International	8 KHz Horizontal; 50 Hz Vertical
Output Rate:	
USA	15,750 Hz Horizontal; 60 Hz Vertical
International	15,750 Hz Horizontal; 50 Hz Vertical
Field of View (FOV)	15 Deg Vertical x 20 Deg Horizontal 8X Continuously Adjustable E-O Zoom
Horizontal Resolution at 50% Slit Contrast (typical):	
USA and International (8-12 um)	1.8 mRad, 197 IFOVs/Line 256 Pixels/Line
USA and International (3-5 um)	3.5 mRad, 100 IFOVs/Line 256 Pixels/Line

Output Format	
USA	RS-170, NTSC & RGB
International	CCIR, PAL & RGB
Dynamic Range	7 Bit, 128 Levels, 42 dB 8 Bit, 256 Levels (48 dB) with Image Averager
Temperature Reference	
USA	Internal Reference Sampled @ 60 Hz
International	Internal Reference Sampled @ 50 Hz
Temperature Spans	5, 10, 20, 50, 100, 200 Normal Range 50, 100, 200, 500 Extended Range
Temperature Measurement Range (for 8-12 um)	-20 to +400 C Normal Range 0 to +1500 C Extended Range
Temperature Readout Resolution	3 Digits
Power Requirements:	
System	11-17 VDC, 10 Watts
Monitor (5" Video Color)	11-15 VDC, 15 Watts
Image Averager (Optional)	5 Watts
AC Power Supplies	
USA	108-125 VAC, 60HZ
International	210-240 VAC, 50HZ
Ambient Operating Temperature	-15 to +45 C
Dimensions (l x w x h)/Weights:	
Scanner	8.1 x 4.9 x 4.8 in./6.5 lb.
Control/Electronics Unit	9.3 x 5.4 x 10.3 in./7.5 lb.
5 in. Video Monitor	
USA	12.7 x 4.9 x 6.3 in./8.5 lb.
International	13.6 x 5.5 x 8.7 in./9.0 lb.

Appendix B: Heat Flux and Temperature Data tables

Table 1. Total heat flux distribution on a fire-heated Marinite vertical corner wall without ceiling (W/cm²)

Y\X(cm)	0	10	20	30
0	/	/	/	/
10	1.0	1.5	0.8	0.3
20	1.5	3.0	1.6	0.4
30	1.7	3.5	1.7	0.3
40	1.6	2.5	1.3	0.2
50	1.5	2.0	0.9	0.2
60	1.4	1.5	0.7	0.1
70	1.3	1.1	0.6	0.1
80	1.2	0.9	0.5	0.1
90	1.2	0.8	0.4	0.1
100	1.1	0.7	0.4	0.1
110	0.9	0.6	0.3	0.0
120	0.7	0.4	0.3	0.0
130	0.6	0.4	0.2	0.0
140	0.5	0.2	0.1	0.0
150	0.4	0.1	0.0	0.0

Table 2. Total heat flux distribution on a fire-heated Marinite vertical corner wall with ceiling (W/cm²)

Y\X(cm)	0	10	20	30
0	/	/	/	/
10	0.8	1.5	0.8	0.3
20	1.2	2.0	1.0	0.4
30	1.1	1.8	0.8	0.3
40	1.0	1.5	0.5	0.2
50	0.9	1.1	0.4	0.2
60	0.9	1.0	0.4	0.1
70	0.9	1.0	0.4	0.1
80	0.9	1.0	0.3	0.1
90	0.9	0.8	0.2	0.1
100	0.9	0.6	0.2	0.1
110	0.8	0.5	0.2	0.0
120	0.8	0.5	0.1	0.0
130	0.8	0.5	0.2	0.0
140	0.7	0.6	0.5	0.0
150	0.7	0.7	0.8	0.0

Table 3. Temperature distribution on a fire-heated Marinite vertical corner wall with ceiling (°C)

Y\X(cm)	0	10	20	30
0	/	/	/	/
10	235	250	200	130
20	240	290	205	130
30	235	275	200	125
40	230	245	170	120
50	215	225	140	110
60	210	210	125	95
70	190	165	115	90
80	170	150	110	85
90	160	155	100	80
100	155	125	95	75
110	150	120	90	70
120	145	115	100	70
130	140	110	110	60
140	135	120	115	90
150	135	130	125	120

Table 4. Temperature distribution on a fire-heated Marinite vertical corner wall without ceiling (°C)

Y\X(cm)	0	10	20	30
0	/	/	/	/
10	200	220	175	50
20	275	275	250	75
30	280	450	300	80
40	280	430	280	75
50	275	350	210	70
60	260	285	175	65
70	220	240	160	60
80	190	190	140	55
90	190	150	100	45
100	185	145	105	50
110	180	140	110	55
120	170	140	115	60
130	165	145	125	65
140	150	140	115	60
150	140	130	110	50

References

Abramovich, G. N., (1979) "Recent Development in Theoretical and Experimental Fluid Mechanics" Springer-Verlag, Berlin Heidelberg, New York, 476.

Ahmad, T., (1978), "Investigation of the Combustion Region of Fire-induced Plumes along Upright Surface" Ph. D. thesis, The Pennsylvania State University, University Park, PA.

Ahmad, T., and Faeth, G. M. (1978), "Turbulent Wall Fires" Seventeenth Symposium (International) on Combustion, The Combustion Institute, pp. 1149-1160.

Ahmad, T., and Faeth, G. M. (1978), "An Investigation of the Laminar Overfire Region along Upright Surface", J. of Heat Transfer, Vol. 100, No.1, pp. 112-119.

Annamala, K., and Sibulkin, M., (1979) "Flame Spread over Combustible Surfaces for Laminar Flow Systems, Part I: Excess Fuel and Heat Flux", Combustion Science and Technology, Vol. 19, pp. 167-183.

Annamala, K., and Sibulkin, M., (1979) "Flame Spread over Combustible Surfaces for Laminar Flow Systems, Part II: Flame Heights and Fire Spread Rates", Combustion Science and Technology, Vol. 19, pp. 1185-193

Arakawa, A., Saito, K., and Gruver W. A., (1993) "Automated Infrared Imaging Temperature Measurement with Application to Upward Flame Spread Studies, Part I", Combustion and Flame, Vol. 92, pp. 222-230.

Blackshear, Jr. P., and Kanury, A. M., (1970) "On the Combustion of Wood I: A Scale Effect in the Pyrolysis of Solids", Combustion Science and Technology, Vol. 2, pp. 1-9.

Chen, Y., Delichatsios, and Motevalli, V., (1993) "Material Pyrolysis Properties, Part I: An Integral Model for One-dimensional Transient Pyrolysis of Charring and Non-Charring Materials", Combustion Science and Technology, Vol. 88, pp. 309-328.

Daikoku, M., Lin, W., and Saito, K., (1991), "Flow Visualization of the Fire-induced Flow" The Central States Section, The Combustion Institute, Spring Meeting, Nashville, TN.

Delichatsios, M. A., (1987) "Burning and Upward Flame Spread on Charring Materials in Wall Fires: An outline of A Comprehensive Simulation Model and Simplified Correlations", Technical Report of Factory Mutual Research Corporation, Norwood, MA 02062.

Delichatsios, M. A., Orloff, L., and Delichatsios, M. M., "The Effects of Fuel Sooting Tendency and The Flow on Flame Radiation in Luminous Jet Flames", Combustion Science and Technology, Vol. 84, pp. 199-215.

DeRis, J. N., (1969) "Spread of A Laminar Diffusion Flame", Twelfth Symposium (International) on Combustion, The Combustion Institute, pp.241-252.

Dyke, M. V., (1982) "An Album of Fluid Motion", The Parabolic Press, Stanford, CA.

Emmons, H. W., (1965) "Fundamental Problems of the Free Burning Fire", Tenth Symposium (international) on Combustion, The Combustion Institute, pp. 951-964.

Fernandez-Pello, A. C., (1977) "Upward Laminar Flame Spread under Influence of Externally Applied Thermal Radiation", Combustion Science and Technology, Vol. 17, pp.87-98.

Fernandez-Pello, A. C., and Williams, F. A., (1976) "Experimental Techniques in the Study of Laminar Flame Spread over Solid Combustibles", Combustion Science and Technology, Vol. 14, pp. 155-167.

Hasemi, Y., (1986) "Thermal Modeling of Upward Wall Flame Spread", Fire Safety Science-The First International Symposium, Hemisphere Publishing Co., New York, NY pp. 87-96.

Hirano, T., Noreikis, S. E., and Waterman, T. E., (1974) "Measured Velocity and Temperature Profiles near Flames Spreading over A Thin Combustible Solid", Combustion and Flame, Vol. 23, pp. 83-96.

Hirano, T., and Saito, K., (1995) "Fire Spread Phenomena: The Role of the Observation in Experiment", Progress in Energy and Combustion Science (To appear).

Ishida, H., (1992), Fire Safety Journal, Vol. 18 No. 3, pp. 213-223.

Jain, A. K., (1981) "Image Data Compression: A Review", Proc. of IEEE, Vol. 69, No. 3, pp. 349 - 389.

Kulkarni, A. K., and Kim C. I., (1990) "Heat Loss to the Interior of A Free Burning Vertical Wall and Its Influence on Estimation of Effective Heat of Gasification", Combustion Science and Technology, Vol. 73, pp. 493-504.

Kulkarni, A. K., Kim C. I., and Kuo, C. K., (1990) "Heat Flux, Mass Loss Rate and Upward Flame Spread for Burning Vertical Walls", NIST-GCR-90-584, Building and Fire Research Laboratory, National Institute of Standards and Technology, Gaithersburg, MD 20899.

Liburdy, J. A., Groff, E. G., and Faeth, G. M., (1979) " Structure of A Turbulent Thermal Plume Rising along An Isothermal Wall" J. of Heat Transfer, Vol. 101, No.2, pp. 249-259.

Linan, A., and Williams, F. A., (1971) "Theory of Ignition of A Reactive Solid by Constant Energy Flux", Combustion Science and Technology, Vol. 3, pp. 91-98.

Mekki, K., Atreya, A., Agrawal and Wichman, I., (1990) "Wind-aided Flame Spread over Charring and Non-charring Solids: An Experimental Investigation", Twenty-Third Symposium (International) on Combustion, The Combustion Institute, pp. 1701-1707.

Mitler, H., (1990), "Predicting the Spread Rates of Fires on Vertical Surfaces", Twenty-Third Symposium (International) on Combustion, The Combustion Institute, pp. 1715-1721.

Milter, H., and Steckler, K. D., (1993) Comparison of Wall-Fire Behavior with and without A Ceiling", NISTIR 5830, Building and Fire Research Laboratory, National Institute of Standards and Technology, Gaithersburg, MD 20899.

Oka, Y., and Sugawa, O., (1989) "Temperature Visualization of Extended Flame from Opening Using Infrared Image Processor", Fire Science & Technology, Vol. 9, No. 2, pp. 15-22.

Orloff, L., deRis, J., and Markstein, G. H. (1975), "Upward Turbulent Fire Spread and Burning of Fuel Surface" Fifteenth Symposium (International) on Combustion, The Combustion Institute, Pittsburgh, pp. 183-192.

Orloff, L., Modak, A., T., and Alpert, R., L., (1976), "Burning of Large-scale Vertical Surfaces", Sixteenth Symposium (International) on Combustion, The Combustion Institute, pp.1345-1354,

Parker, W. J., (1972) "Flame Spread Model for Cellulosic Materials", J. of Fire and Flammability, Vol. 3, pp. 254-264.

Pyle, D. L., and Zaror, C. A., (1984) "Heat Transfer and Kinetics in the Flow Temperature Pyrolysis of Solids', Chemical Engineering Science, Vol. 39, No. 1, pp. 147-158.

Quintiere, J., (1981) "A Simplified Theory for Generalizing Results from A Radiant Panel Rate of Flame Spread apparatus", Fire and Materials, Vol. 5, No. 2, pp.52-60.

Quintiere, J., Harkleroad, M., and Hasemi, Y., (1986) "Wall Flames and Implications Upward Flame Spread" Combustion Science and Technology, Vol. 48, pp. 191-222.

Saito, K., Quintiere, J. G., and Williams, F. A. (1985), Upward Turbulent Flame Spread", Fire Safety Science - Proc. the First International Symposium, Hemisphere Publishing Corp., pp. 75-86.

Saito, K., Williams, F. A., Wichman, I. S., and Quintiere, J. G., (1989) "Upward Flame Spread on wood Under External Radiation" Journal of Heat Transfer, Vol.

111, pp.438-445.

Sibulkin, M., Kim, J., and Creeden, Jr., (1976) "The Dependence of Flame Propagation on Surface Heat Transfer II. Upward Burning", Combustion Science and Technology, Vol. 17, pp. 39-49.

Sibulkin, M., Kim, J., (1977) "The Dependence of Flame Propagation on Surface Heat Transfer I. Downward Burning", Combustion Science and Technology, Vol. 14, pp.43-56.

Spalding, D. B., (1976) "Mathematical Models of Turbulent Flames: A Review", Combustion Science and Technology, Vol. 13, pp.3-25.

West, J., Bhattacharjee, S., Altenkirch, R., (1992) "A Comparison of the Roles Played by Natural and Forced Convection in Opposed-Flow Flame Spreading", Combustion Science and Technology, Vol. 83, pp. 233-244.

Williams, F. A. (1982), "Urban and Wildland Fire Phenomenology" Prog. Energy Combust. Sci. 1982, Vol. 8, pp. 317-354.

Zhang, Y., Ronney, P., Roegner, E., and Greenberg, J., (1992) "Lewis Number Effects on Flame Spreading over Thin Solid Fuels", Combustion and Flame, Vol. 97, pp. 71-83.

Vita

Personal

Date and place of birth: Oct. 5, 1962; Shandong Province, China.

Education

Northwestern Polytechnical University, Xian, China

M. S. Aerodynamics, April, 1987

B. S. Aeronautical Engineering, July 1984

Professional position held

Combustion and Fire Research Laboratory, Mechanical Engineering Department, University of Kentucky

Research Assistant (Jan. 1991 - present)

Civil Aviation Administration of China (CAAC)

Airworthiness and Airplane Performance Engineer (Feb. 1987 - Oct. 1988)

Project Engineer: evaluation and selection of airplane, operation cost analysis and fleet planning (Nov. 1988 - Dec. 1989)

Papers and presentations

1. Qian, C. and Gao, J., "Analysis of the Maneuverability of F-7 (Mig-21) Fighter in High G Spin", Flight Dynamics Journal, Vol.3, pp. 25-32, 1985.

2. Qian, C. and Luo, S., " Design and Test of A Water Tunnel for Flow Visualization", Forth Fluid Mechanics Conference, Beijing, China, June 1988.

3. Qian, C. et al., "Feasibility Study of Y-7 (An-24) Powered by PW100 Turbopropeller Power Plant", CAAC Report with Pratt&Whitney Co., Aug. 1987.

4. Qian, C. et al., "Airworthiness Analysis of Boeing 757 to Fly in Tibetan Route",

CAAC Airworthness Division-Boeing Co. Report, May 1988.

5. Qian, C. et al., "Proposal for the Joint Assembling of MD-82s with McDonnell Douglas Corporation in Shanghai, Phase II", Research Report of CAAC and CATCH (China Aeronautical Technology Import-export Corporation), April 1989.

6. Qian, C., "Prospects for the Future of Commercial Aircraft Industry in China: Call for Asian's Airbus", the Ninth Midwest - American Chinese Science and Technology Conference, St. Louis, MI. June, 1991.

7 Qian, C. and Saito, K., "Fire-induced Flow along The Vertical Corner Wall", The First Asian Conference on Fire Science and Technology, pp. 257-262, China, Oct., 1992.

8. Qian, C., Isihda, H., and Saito, K., "Upward Flame Spread along The Vertical Corner Walls", Joint Technical Meeting by Central and Eastern States Sections, The Combustion Institute, pp. 616-620, New Orleans, LA, March 1993.

9. Qian, C. and Saito, K., "Turbulent Flame Spread on Corner Walls", Technical Meeting by The Eastern States Section of The Combustion Institute, pp. 338-341, Princeton University, Princeton, New Jersey, Oct., 1993.

10. Qian, C., Arakawa, A., Isihda, H., Saito, K., and Cremers, C., "Temperature Measurement by Infrared Imaging with Application to Fire Research" Twenty-Second International Conference on Thermal Conductivity, 1994.

11. Qian, C., Isihda, H., and Saito, K., "Upward Flame Spread along PMMA vertical

Corner Walls, Part II: Mechanism of M-shaped Pyrolysis Front Formation", Combustion and Flame Vol. 99, pp. 331-338(1994).

12. Delichatsios, M. M., Wu, P., Lougheed, G. D., Crampton, G. P., Qian, C., Ishida, H., and Saito, K., "Effect of External Radiant heat Flux on Upward Fire Spread: Measurements on Plywood and Numerical Prediction", The Fourth International Symposium on Fire Sciences, Ottawa, Canada, June 13 - 17, 1994.

13. Qian, C., Tashtoush, G., Ito, A., and Saito, K., "Structure of Large Scale Pool Fires", Fire Safety Conference, 1995, Orlando, FL.

14. Qian, C. and Saito, K.,"Measurements of Pool-fire Temperature Using IR Technique", Central States/Western States/Mexican National Sections of The Combustion Institute, Spring Meeting, April 1995, San Antonio, Texas.